Admittance Fluctuations in Nanostructures

Tiago De Jesus
Centre for the Physics of Materials
Department of Physics
McGill University
Montréal, Québec
Canada

A Thesis submitted to the
Faculty of Graduate Studies and Research
in partial fulfillment of the requirements for the degree of
Doctor of Philosophy

0-612-69999-4

CONTENTS

LIST OF FIGURES

Abstract

In this thesis, we develop a first principle technique to study linear AC and the nonlinear DC quantum transport in diffusive conductors. Starting from Büttiker's theory for AC and DC transport, the emittance and nonlinear DC conductance are found in terms of the scattering matrix and it's functional derivative. New theoretical tools are developed to compute the functional derivative of the scattering matrix, which would otherwise be unaccessible. These results allows us to compute the linear AC and the nonlinear DC conductance for a diffusive conductor from first principles, for the first time in literature. The sample-to-sample AC conductance fluctuations are computed for a diffusive conductor. In this regime the dynamic response of the conductor can either be capacitive or inductive, depending on impurity configuration. Our results also suggest a crossover for the AC conductance distribution, from a symmetric to a non symmetric distribution function as the number of impurities increases. A degree of generic behavior is discovered, in that the AC fluctuation amplitudes become independent of the strength of the impurities, although it depends on the impurity density. A sample-to-sample analysis of the nonlinear conductance fluctuations, in the diffusive regime, is also reported. In this situation the distribution function is found to be a symmetric Gaussian like function for small disorder and a symmetric exponentially decaying function for large disorder. An interesting result is that the conductance fluctuations increase in an exponential fashion with N, the number of impurities.

We also considered in this thesis the magneto-conductance fluctuations of a quasi-1D quantum wire with artificial impurities (antidots). This problem can only be solved numerically because of the finite size of the artificial impurities. We develop a novel transfer matrix technique to solve the quantum scattering problem by computing the scattering wave function, as a function of the external magnetic field. The Landauer-Büttiker equation is used to compute the magneto-conductance. This work is motivated by the experimental study [1], where several conductance fluctuations anomalies were reported. Our numerical results give good quantitative agreement with the experimental data and confirms the physical picture obtained from the experiment.

Résumé

Dans cette thèse on développe une technique à partir de principes fondamentaux pour l'étude du transport quantique linéaire AC et non linéaire DC dans des conducteurs diffusifs. En partant de la théorie de Büttiker pour le transport AC et DC, la conductivité linéaire AC et non linéaire DC sont exprimées en fonction de la matrice de diffusion et de sa dérivée fonctionnelle. Des nouveaux outils théoriques ont été développés pour calculer la dérivée fonctionnelle de la matrice de diffusion, sans lesquels celle-ci serait difficilement accessible. Ces résultats nous permettent de calculer la conductivité linéaire AC et non linéaire DC pour des conducteurs diffusifs à partir de principes fondamentaux et ceci pour la première fois dans la littérature. Les fluctuations d'un échantillon à l'autre de la conductivité AC sont calculées pour des conducteurs diffusifs. Dans ce régime, la réponse dynamique du conducteur peut être ou capacitive ou inductive, dépendant de la configuration des impuretés. Nos résultats suggèrent un changement de régime pour la fonction de distribution de la conductivité AC, d'une distribution symétrique à une distribution asymétrique avec l'augmentation du nombre d'impuretés. L'amplitude des fluctuations AC deviennent indépendantes de la force des impuretés mais dépendent de la densité des impuretés. Une analyse des fluctuations de la conductivité non linéaire, d'un échantillon à l'autre, dans le régime diffusif, est aussi étudié. Dans ce cas-ci la fonction de distribution se trouve à etre une fonction symétrique gaussienne quand le désordre est petit et une fonction symétrique qui décroit exponentiellement quand le désordre est grand. Un résultat intéressant qu'on a obtenu c'est que les fluctuations augmentent exponentiellement avec N, le nombre d'impuretés.

Nous avons aussi considéré dans cette thèse les fluctuations de la conductivité en fonction d'un champ magnétique dans un fil quantique quasi-1D avec des impuretés artificielles (antidots) . Ce problème ne peut etre résolu que numériquement à cause de la largeur finie des impuretés artificielles. Nous avons développé une nouvelle technique de transfert matricielle pour résoudre le problème de diffusion quantique en calculant la fonction d'onde de diffusion, en fonction d'un champ magnétique externe. L'équation de Landauer-Büttiker est utilisée pour calculer la conductivité en fonction du champ magnétique. Ce travail est motivé par l'étude expérimentale [1], ou plusieurs anomalies dans la conductivité ont été rapportées. Nos résultats numériques sont en accord avec les résultats expérimentaux.

Statement of Originality

In this thesis, I develop a novel theoretical technique for first principle studies of linear AC and nonlinear DC quantum transport, for mesoscopic conductors. In particular, for the first time in literature, I analyze the sample to sample fluctuations of the admittance and the first order nonlinear DC conductance, for a diffusive conductor in the regime where universal conductance fluctuations are observed. These studies are facilitated by a number of theoretical developments which I make. I also investigated the magneto-conductance fluctuations in a ballistic conductor with two artificial impurities, by developing a numerical transfer matrix technique.

Specifically, I made the following useful contributions:

- The derivation of an expression, from first principles, for the N-th order functional derivative of the scattering matrix. This quantity is crucial for analyzing AC and nonlinear DC transport coefficients.

- The derivation of a generalized Fisher-Lee relation which relates the scattering wave functions to the Green's function, and is applicable not only to general multi-probe conductors with jellium electrodes, but also to those with atomic electrodes.

- The derivation of exact expressions for the linear AC and nonlinear DC conductances which only require the scattering wave functions.

- The derivation of an exact expression for the N-delta impurity Green's function, wave function, scattering matrix, and relevant functional derivatives. These are expressed in terms of the impurity free Green's function and wave function, and valid for any potential, in the presence of a magnetic field and in any dimension.

- The study of linear AC and nonlinear DC conductances in the diffusive regime. Specifically, the distribution functions of these transport coefficients and their fluctuations.

- The analysis of the quasi-one dimensional ballistic conductor with artificial impurities inside a magnetic field to understand the experimentally observed magneto-conductance fluctuations.

Acknowledgments

I first want to thank my supervisor, Prof. Hong Guo, without him this thesis would not be what it is. His comments and suggestions were invaluable for the writing of this thesis. I also want to thank him for giving me the opportunity to visit Hong Kong and Beijing, an experience that I will never forget! Finally, I thank him for his encouragement and financial support, which helped to make my PhD experience quite enjoyable.

I also want to thank Dr. C.C. Wan, who helped me with my first PhD project, without him it would not have been possible. As for the members of our group, I thank them for the interesting conversations, which helped me to better understand the physics behind what we do all day. Special thanks goes to Jeremy, Hatem, and Brian for their insightful comments.

My time at McGill was unforgettable because of many people. Special thanks goes out to: Andre, Andrei, Andy, Brian, Christine, Claude, Colin, Declan, Graham, Hatem, Jeremy, Marko, May, Mikko, Mikko, Oleh, Tanvir, and Wai. A special thanks goes to C.W., without whom the last two months of my PhD would not have been so enjoyable. And let us not forget the kind people that have taken care of all those administrative forms for us. Thank you Paula, Joanne, and Diane for all your help over the years. Without you the physics department would come to a halt.

Finally, I want to thank my family for their unconditional love and support.

1

Introduction

1.1 Mesoscopic Physics

Historically condensed matter physics has primarily focused on the study of systems which are found in nature. It is only in the last two decades, with advances in semiconductor fabrication and lithography technologies, that the study of artificial nanometer scale systems has appeared [2, 3, 4, 5, 6, 7]. These artificial nanostructures include quantum wires [8, 9], quantum dots [10, 11, 12, 13, 14], and atomic wires [15, 16, 17, 18, 19, 20, 21, 22, 23], to just name a few. The ability to create and study these nanostructures is one of the great advances in condensed matter physics. The central feature of these new systems is that their size is typically in the sub-micron length scale, which leads to important quantum mechanical effects. A deep understanding of the behavior of electrons in these nanostructures cannot be accomplished without tackling the quantum mechanics of these systems. In particular, the nature of electronic conduction properties of nanostructures should be understood with a quantum transport theory [5]. On the other hand, the "designer" capability to construct such systems opens the door to exploring new quantum behavior. Indeed, these new systems are interesting candidates for future generations of electronic devices whose operational principles are based on quantum effects [7, 24, 25, 26, 27]. This new field of research is known as mesoscopic physics, a term first coined by van Kampen [28].

Mesoscopic physics, as the word indicates, lies somewhere between the microscopic and the macroscopic world. By microscopic we mean systems that are composed of only a few individual particles, like atoms or small molecules. As for macroscopic, it refers to systems which are composed of a great number of particles ($\overset{\sim}{>} 10^{23}$), which permits the application of the principles of statistical mechanics. The typical length scale of a mesoscopic system lies somewhere between $100\mathring{A}$ and $1\mu m$. Our working definition of a mesoscopic system, is one where the phase coherence length of the electronic carriers is greater than the sample size. Under such conditions quantum effects will play an important role in the electronic transport throught such systems. In these systems the classical Boltzmann equation is no longer be suited for understanding transport phenomena. The behavior of resistors and capacitors in series or parallel are changed because of quantum effects. One way to treat mesoscopic electronic devices is to view them as big quantum objects (large molecules), which are connected to leads. The leads are important because they connect the nanostructure to the macroscopic world. A transport theory for a mesoscopic system requires a fully quantum mechanical treatment of the dynamics of the electrons *inside* the device.

In these systems of reduced dimensionality there are many length scales that come into play. In particular, we have the Fermi wavelength, the mean free path, the phase coherence length, and the systems size. For a more complete description of all the relevant length scales which may play a role in quantum transport see [5]. Let us give a brief overview of the length scales which we are concerned with:

- The Fermi wavelength is given by $\lambda_F = 2\pi/k_F$, where k_F is the Fermi wave vector which depends on the electron density. For metals we typically find that $\lambda_F \sim 0.3nm$. As for 2D electron gases in semiconductors we have $\lambda_F \sim 40nm$.

- The elastic mean free path is defined by $l_m = v_F\tau_m$, where v_F is the Fermi velocity and τ_m is the momentum relaxation time. The mean free path represents the distance that the electron travels before it gets scattered elastically. By elastic scattering we mean a scattering event which changes the momentum but not the energy of the charge carrier.

- The phase coherence length is defined by $l_\phi = \sqrt{D\tau_\phi}$, where D is the diffusion constant and τ_ϕ is the phase relaxation time. The phase coherence length represents the distance traveled by an electron before encountering an inelastic scattering event. An inelastic scattering event is when the phase information of the wave function is lost, for example, by a scattering event which changes the energy of the carrier from one energy level to another. In contrast to elastic scattering, inelastic scattering destroys the phase information that the wave function was carrying before being scattered. The temperature dependence of l_ϕ is determined by the behavior of the inelastic relaxation time. One usually writes $\tau_\phi \sim T^{-p}$ $(p = 1 \sim 2)$ as $T \to 0$ [29]. As we approach the zero temperature limit the phase coherence length tends to infinity, $l_\phi \to \infty$ as $T \to 0$. However, this behavior has been challenged by the recent experiment of [30, 31]. Typically, when $T = 1K$ the phase coherence length is several microns. When $l_\phi > L$ the system is said to be phase coherent. This means that the electron travels through the system without loosing its phase. Phase coherence is a key ingredient to obtain interesting quantum phenomena.

- The systems size is represented by its linear dimensions in all three spatial directions: L_x, L_y, and L_z. From these three parameters we define four cases:
  - $\lambda_F \ll L_x \sim L_y \sim L_z$, usual bulk case
  - $\lambda_F \sim L_x \ll L_y \sim L_z$, two dimensional film
  - $\lambda_F \sim L_x \sim L_y \ll L_z$, quantum wire
  - $\lambda_F \sim L_x \sim L_y \sim L_z$, quantum dot

By fixing the above length scales we generate many interesting regimes. In this work we are interested in two particular physical situations. First, the diffusive regime which corresponds to a system where $\lambda_F \sim L_x < L_y \sim l_m \ll L_z < l_\phi$. In this situation the electron diffuses quantum mechanically through a quantum wire keeping its phase coherence. In other words, the electron suffers many elastic scattering events but it preserves its phase coherence.

The second situation of interest is the ballistic regime, where $\lambda_F \sim L_x < L_y \ll l_m \sim L_z < l_\phi$. In this case the electron goes through a quantum wire without, on average, suffering any impurity scattering while keeping its phase coherence. Most of the scattering in this regime comes from the boundaries of the device. In both cases the electrons maintain phase coherence which leads to interesting quantum interference effects.

One of the key developments that has led to the fabrication of exceptionally pure 2D electron systems is a technique known as modulation doping [32, 33]. This simple trick permits the spatial separation of charge carriers in the conducting channels from the dopant atoms in a semiconductor heterostructure. Using semiconductors of high purity and crystalline perfection, a thin layer of highly mobile electrons can be created. In this thin layer the motion of the electron is quantized in the perpendicular direction and thus the electrons are essentially constrained to live in a 2 dimensional system. Such a two dimensional electron gas (2DEG) has many interesting features, including a low electron density which can be varied with an electric field. The low density leads to a large Fermi wavelength, which is responsible for many interesting quantum transport phenomena. In contrast, thin metal films have a high electron density which is difficult to change because of the very small screening length for $e-e$ interactions. In a metal film the charge carriers have a very small Fermi wavelength.

A 2DEG can be constructed at the interface of a $GaAs/AlGaAs$ heterostructure. The electrons are confined to the $GaAs$ layer by a potential well created at the interface with $AlGaAs$. This potential well originates from the repulsive barrier which arises from the conduction band offset of the two semiconductors ($\sim 0.3eV$). Note that the band gap of $GaAs$ is $1.4eV$, whereas that of $Al_{0.3}Ga_{0.7}As$ is $1.7eV$. Therefore, electrons migrate to the $GaAs$ side because of the lower conduction band energy. This results in an accumulation of positive charges in the $AlGaAs$ side, which generates an attractive force that further confines the electrons in the $GaAs$ side of the interface. In order to reduce the boundary scattering due to the donors from the $AlGaAs$, a spacer layer of several hundred angstroms of undoped $AlGaAs$ is usually added at the interface. Because of the confinement of the electrons at the interface the motion perpendicular to the interface is quantized. This leaves us with a discrete series of 2D electronic states which are called "subbands". Typically, the potential well is sufficiently narrow (about $10nm$) that only one or two subbands are occupied. Due to this quantization, in one of the three directions, the transport is essentially two dimensional.

A central reason for using $GaAs/AlGaAs$ heterostructures is that $GaAs$ and $AlGaAs$ have approximately the same lattice constant and thermal expansion coefficient. This leads to a significant reduction of boundary roughness scattering at the interface, and thus an increase in the electrons mobility μ ($\mu = \partial v_d/\partial E$). For $GaAs/AlGaAs$ one typically finds $\mu \sim 10^6 cm^2/Vs$, as compared to $10^4 cm^2/Vs$ for silicon inversion layers. The electrons mobility is also high in $GaAs/AlGaAs$ because of the low effective mass of the charge carriers, $m_* = 0.067m_e$, as compared to $m_* = 0.19m_e$ for silicon inversion layers.

The degrees of freedom of the electrons in a 2DEG can be further constrained. We can create a narrow channel in the 2DEG such that a quasi-1D system is formed. This is accomplished by selectively depleting electrons in all the regions outside a 1D channel. A popular approach to create this lateral confinement is called the split gate technique [2, ?]. In this technique, a negative voltage is applied to a split metallic gate, fabricated on top of the 2DEG. The negative voltage repels (depletes) electrons under the gate area, leaving only a narrow channel undepleted in which the electrons are free to move. The most appealing feature of this approach is that the width of the quasi-1D channel can be varied continuously by changing the applied negative gate voltage, which is typically in the range of zero to one volt. The electron carrier density is also affected by changes in the gate voltage. The most well known application of the split-gate technique is in the fabrication of quantum point contacts [34, 9]. These are small constrictions which are used to control the current of carriers from one 2DEG to another 2DEG.

This new confinement leads to further quantization of the charge carriers: each of the 2D subbands of the 2DEG are split into 1D subbands. The bottom of the energy bands is denoted by E_n, where $n = 1, 2, \ldots$. The total energy of an electron in the quasi-1D channel in the n-th subband can be written as,

$$E = \frac{\hbar^2 k^2}{2m_*} + E_n \ , \tag{1.1}$$

where $\hbar$ is the reduced Planck constant, m_* the effective mass, and k the momentum along the free 1D direction. The energy E_n corresponds to one of the discrete energy levels created by the presence of the new transversal confinement potential. These energy levels depend on the details of the confinement. For instance, for hard wall confinement, the potential is infinite at the boundary of the quasi-1D channel, and the energy levels are simply $E_n = (n\pi\hbar)^2/(2m_*W^2)$, where W is the width of the quasi-1D channel. One may also consider a soft wall confinement, where a step potential with a finite height confines the charge carrier inside the wire. In this case, quantum mechanical effects allows the wavefunction of the charge carrier to leak into regions outside of the wire, but its amplitude decays exponentially in these regions which make the confinment effective. Another commonly used confinement is the parabolic potential, $V(x) = m_*\Omega^2x^2/2$, where Ω is the confinement parameter, and the energy levels are $E_n = (n + 1/2)\hbar\Omega$. From a theoretical calculation point of view, one major advantage of using hard wall confinement potential is that the corresponding transverse eigenfunction are simple sine functions which are mathematically convenient to deal with. Clearly, the detailed form of confinement potential of a real device depends on material properties and fabrication procedures of the system, and therefore is non universal. But for a qualitative analysis of the main features of quantum transport, which is the focus of this thesis, we will apply both hard wall and soft wall confinement potentials.

In the next section we review one of the most significant features of quantum transport in the mesoscopic regime, namely the phenomenon of universal conductance fluctuations (UCF). We outline the theoretical model used to analyze this interesting phenomenon. This was first carried out by Al'tshuler, Lee, Stone, and Fuckuyama [35, 36, 37, 38]. In their approach, the linear response theory is used to obtain the Kubo-formula for a diffusive conductor of infinite size for which the electrodes (leads) do not play a role. Feynman diagrams are then used to evaluate the expression for the conductance fluctuations. For a multi-probe conductor, where electrodes are very important, the transport analysis can be carried out using the Landauer-Büttiker scattering matrix theory[39, 40, 41, 42]. We will discuss scattering matrix theory and outline two of the main focus of this thesis: how to analyze the conductance fluctuation when the external driving force (bias voltage) is *time dependent*; and how to analyze DC conductance fluctuation at a *nonlinear* level. The linear DC conductance of a system is the zero frequency limit of the linear AC admittance $G_{\alpha\beta}(\omega)$, where ω is the frequency. Since for a diffusive conductor $G_{\alpha\beta}(0)$ exhibits UCF, it is very interesting and natural to ask: what are the statistical properties of the AC admittance? The same question can be asked for nonlinear DC conductance as well. These quantities are however very complicated so that the diagrammatic approach of Al'tshuler, Lee, Stone, and Fuckuyama [43] does not seem to be easily applicable. In this chapter we will also very briefly outline our investigation on an experimental situation where quantum transport in quasi-1D wires in which *artificial* scattering centers are introduced to control the flow of charges [1, 44, 45, 46]. With a uniform magnetic field, the transport properties can be tuned to produce very interesting conductance fluctuations. The understanding of this device forms the third topic of this thesis.

1.2 Universal Conductance Fluctuations

Perhaps the most striking phenomena of electron transport in the mesoscopic regime is the observed sample-to-sample universal conductance fluctuations [47, 48]. These fluctuations are not time dependent noise but are reproducible signatures of quantum interference. The physics of the sample-to-sample DC conductance fluctuations and its universal behavior have been the subject of active research for more than a decade [3] and is now well understood.

The UCF is completely a quantum phenomenon, because for classical systems the sample-to-sample conductance fluctuations are negligible. The root-mean-square of the classical conductance is given by $< (\Delta G_{classical})^2 > \approx l_m/L < G_{classical} >^2$, where

l_m is the elastic mean free path, L is the linear size of the sample, and $l_m \ll L$ for macroscopic conductors. This estimate is obtained by the following arguments. First, we split up the classical conductor into $N = L/l_m$ small independent conductors connected in series, each of which has some random value of conductance G_i, due to the random distribution of impurities inside. Applying the central limits theorem to these random numbers $\{G_i\}$, it follows that the fluctuations go as $< (\Delta G_i)^2 > / < G_i >^2 \approx 1/N$. This implies $< (\Delta G_{classical})^2 > / < G_{classical} >^2 \approx l_m/L$, therefore approaches zero as $L \rightarrow \infty$. An underlying assumption for the above arguments is that the phase coherence length l_ϕ of the conductor is smaller than l_m. If this condition is not satisfied, we cannot say that the small pieces of the conductor are independent classical conductors, since quantum coherence effects persist over distances that are greater than the size of each small conductor. In this situation, one can no longer break up the system into L/l_m independent classical conductors. It is, however, still possible to split up the conductor into L/l_ϕ small *quantum* pieces. Assuming that each of these quantum conductors has some random value $\{G_i\}$ for their conductance, we can apply the central limits theorem, once again, and find that the conductance fluctuations are given by $< (\Delta G_{quantum})^2 > \approx l_\phi/L < G_{quantum} >^2$. Therefore, the fluctuation vanishes when $L \rightarrow \infty$.

Now, consider the case where the phase coherence length is larger than the samples size, $L < l_\phi$: the above arguments break down. We can no longer split the system into small pieces that can be treated independently. Due to the quantum coherence over the entire sample, one must treat the conductor as a whole. For instance, a change in the position of a scattering center at one end of the device causes a change in the scattering wave function $\psi(\mathbf{r})$ at the other end. Thus, when $L < l_\phi$ the conductance fluctuations need not be negligible for large L, and the fluctuation can therefore contain information about the physics of the entire system.

Experimental measurements have shown that the conductance of a phase coherent conductor in the diffusive regime ($l_m \ll L < l_\phi$) fluctuates in a seemingly random but reproducible manner, as a function of external parameters such as bias voltage and magnetic field [47, 49, 50, 51, 52, 53]. Similar conductance fluctuations are observed from one sample to another. These fluctuations exhibit unexpected features, for example, as the temperature decreases ($T \rightarrow 0$) the conductance fluctuations increase. However, the central feature that has stimulated the most research is that these fluctuations seem to be universal, *i.e.* the value of the *rms* of conductance, ΔG, is independent of the value of the conductance itself, independent of systems size, and independent of the type of impurities — as long as the transport is in the mesoscopic diffusive regime. Moreover, the universal value of these conductance fluctuations are of the order $\Delta G \sim e^2/h$, at very low temperatures.

Since the universal fluctuations are found in the diffusive regime ($l_m \ll L < l_\phi$), one suspects that this effect is due to quantum interference. Recall that changes in magnetic field, bias voltage, or impurity configuration (positions of elastic scattering centers) lead to changes in the interference pattern of the wave function, because different quantum "paths" in a conductor are altered by these parameters. For example, the interference pattern is expected to be different from one sample to another due to the different positions of the impurities. This leads to a difference in the conductance between these samples. Why are the fluctuations universal? This is due to the fact that the conductance is not only affected but is actually dominated by quantum interference effects in this regime. Therefore, as long as the interference pattern is altered — regardless by what means, similar conductance fluctuations occur. This leads to an ergodic assumption [38], that fluctuations due to a change in the magnetic field, bias voltage, or impurity configuration, are all equivalent and lead to similar values for ΔG. It turns out that the actual value of ΔG depends on the time reversal symmetry (TRS) of the system [38, 54]. If TRS is broken then the value of ΔG is reduced by a factor $\sqrt{2}$, but the general physics of the fluctuations are still caused by quantum interference effects. Theoretical analysis of UCF has largely come from two directions. One is analytical work within the linear response theory [37, 38], and the other is by direct numerical simulations [54, 55, 56]. Both confirm the above physical picture.

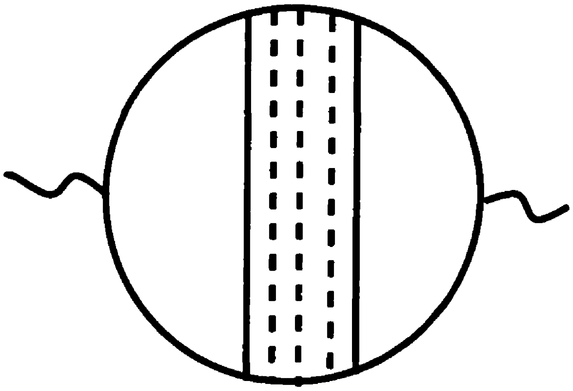

Figure 1.1: Single bubble diagram, which represents the impurity averaged conductance. The two vertical lines with the three dashed lines between them represent the contribution from the impurity averaging and is called the diffusion propagator.

The theory of Al'tshuler, Lee, Stone, and Fuckuyama [35, 36, 37, 38] is perhaps the most successful in understanding UCF. Their approach consists of using Feynman diagrams to evaluate the expression for $< (\Delta G)^2 >$ in the mesoscopic diffusive regime. Their results show that conductance fluctuations are independent of the impurity scattering strength and the impurity density, and depend only weakly on the geometry of the system. In the rest of this section, we briefly outline this theory, following its original development [38].

Consider an infinitely large diffusive conductor in the mesoscopic regime where localized impurities provide elastic scattering for the charge carriers. The impurity potential is chosen to be,

$$V(\mathbf{r}) = \sum_i \gamma\delta(\mathbf{r} - \mathbf{r}_i)\,, \tag{1.2}$$

where γ is the strength of the impurities, which are assumed to be the same for all impurities. The linear DC conductance is obtained from the conductivity, which is given by Kubo's formula:

$$\sigma_{zz}(\mathbf{r},\mathbf{r}') = -\frac{1}{4\pi}\left(\frac{e}{m}\right)^2 \left[G^R(\mathbf{r},\mathbf{r}') - G^A(\mathbf{r},\mathbf{r}')\right] (\overleftrightarrow{\nabla}_z)(\overleftrightarrow{\nabla}_{z'}) \left[G^R(\mathbf{r}',\mathbf{r}) - G^A(\mathbf{r}',\mathbf{r})\right]\ , \tag{1.3}$$

where $(\overleftrightarrow{\nabla}_z) \equiv 1/2(\vec{\nabla}_z - \overleftarrow{\nabla}_z)$ and the function $G^{R(A)}(\mathbf{r},\mathbf{r}')$ is the retarded (advantaged) Green's function. The average conductance is equal to, $< G >= 1/L^2 \int d\mathbf{r} \int d\mathbf{r}' < \sigma_{zz}(\mathbf{r},\mathbf{r}') >$, where $< ... >$ is an average over random impurity configurations. This

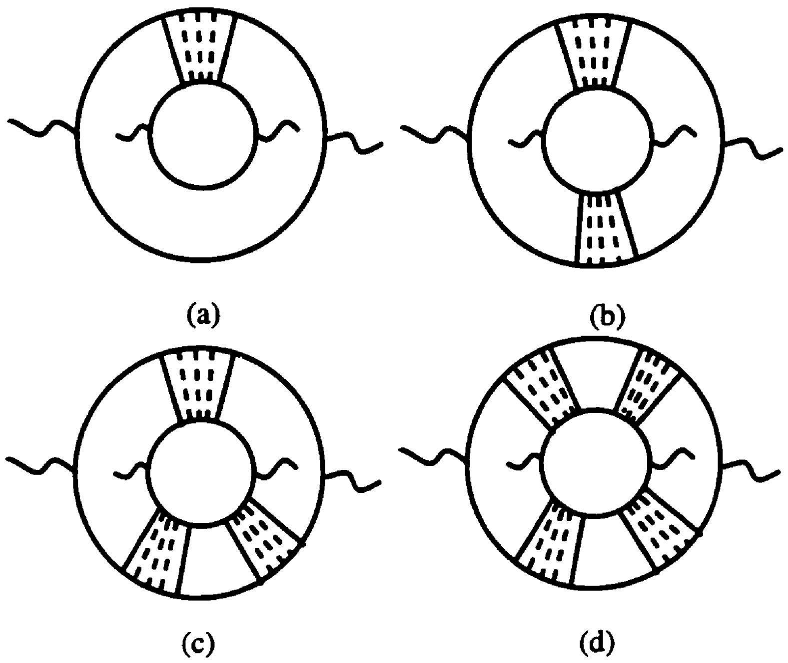

Figure 1.2: Conductance fluctuations diagrams, which include: (a) single, (b) double, (c) triple, and (d) quadruple, bubble-bubble diffusion connectors.

can be expressed in terms of Feynman diagrams [38], which are shown in Fig. 1.1. The diagram reads as follows: the wiggle lines represent the current vertices, the two lines connected to the two wiggles are Green's functions, and the rectangle with the dashed lines is the diffusive propagator which represents the averaged impurity scattering.

The conductance fluctuations are measured by:

$$< (\Delta G)^2 >=< G^2 > - < G >^2 \quad . \tag{1.4}$$

The Feynman diagrams which represent the *rms* of the conductance, $\Delta G \equiv \sqrt{< (\Delta G)^2 >}$, are of great complexity, but can still be evaluated using standard diagram techniques [57]. In the language of Feynman diagrams, $< GG >$ includes both connected and disconnected diagrams, but since the disconnected ones are canceled by the term $< G >< G >$ in Eq. (1.4), we only need to compute the connected ones.

Using Eq. (1.3), the expression for the conductance, and Fourier transforming the

Green's functions, we find [43]:

$$
\begin{aligned}
< GG >_{connected} = \left(\frac{e^2}{4\pi m^2 L^2}\right)^2 \int\int \frac{d\mathbf{p}}{(2\pi)^3}\frac{d\mathbf{p}'}{(2\pi)^3} p_z p_z p'_z p'_z \\
< \left[G^R(\mathbf{p}) - G^A(\mathbf{p})\right]\left[G^R(\mathbf{p}) - G^A(\mathbf{p})\right] \\
\left[G^R(\mathbf{p}') - G^A(\mathbf{p}')\right]\left[G^R(\mathbf{p}') - G^A(\mathbf{p}')\right] >_{connected} \ . \qquad (1.5)
\end{aligned}
$$

A typical term in the above expression is:

$$
\left(\frac{e^2}{4\pi m^2 L^2}\right)^2 \int\int \frac{d\mathbf{p}}{(2\pi)^3}\frac{d\mathbf{p}'}{(2\pi)^3} p_z p_z p'_z p'_z < G^R(\mathbf{p})G^R(\mathbf{p})G^R(\mathbf{p}')G^A(\mathbf{p}') >_{connected} \ . \qquad (1.6)
$$

From a Feynman diagram point of view, these expressions correspond to all the possible ways to connect two conductivity diagrams using one, two, three or four impurity diffusion propagators, which are represented by the ladders connecting the two conduction bubbles (see Fig. 1.2). The first, diagram in Fig. 1.2(a), can be shown to be negligible in the weak scattering limit [38]. This leaves us with the task of evaluating the last three Feynman diagrams in order to compute the total conductance fluctuations. We give a brief review of how to compute these diagrams by evaluating the diagrams corresponding to Fig. 1.2(b).

The expression for Fig. 1.2(b), which we denote by F_a, is given by:

$$
F_a = \left(\frac{1}{m^2 L^2}\right)^2 \int d\mathbf{r} \int d\mathbf{r}' \int d\mathbf{r}'' \int d\mathbf{r}''' P(\mathbf{r}''', \mathbf{r}'') P(\mathbf{r}', \mathbf{r}) J(\mathbf{r}, \mathbf{r}''') J(\mathbf{r}', \mathbf{r}'') \ , \qquad (1.7)
$$

where the two $P(\mathbf{r}, \mathbf{r}')$ represent the two ladders connecting the conductivity bubbles and the two $J(\mathbf{r}, \mathbf{r}')$ are the current functions which connect the two ladders together. Let us evaluate this expression.

The current contribution for this diagram, which represents one of the term obtained from Eq. (1.6), is given by,

$$
J(\mathbf{r}, \mathbf{r}') = \int d\mathbf{r}'' \int d\mathbf{r}''' (p_z)^2 G^R(\mathbf{r}'', \mathbf{r}) G^R(\mathbf{r}''', \mathbf{r}'') G^R(\mathbf{r}', \mathbf{r}''') G^A(\mathbf{r}, \mathbf{r}') \ . \qquad (1.8)
$$

To evaluate the current function $J(\mathbf{r}, \mathbf{r}')$ we note that $< G^R(\mathbf{r}, \mathbf{r}') >$ decays exponentially on the length scale of the mean free path l_m in the diffusive regime. Since this is the shortest length in our system and $l_m \ll L$, we may approximate the current function with its totally localized form,

$$J(\mathbf{r},\mathbf{r}') = J_0\delta(\mathbf{r}-\mathbf{r}') = \left(\frac{1}{V}\int d\mathbf{r}\int d\mathbf{r}' J(\mathbf{r},\mathbf{r}')\right)\delta(\mathbf{r}-\mathbf{r}') \ , \tag{1.9}$$

where V is the volume of the sample. After tedious manipulations [43], we find the following expression for J_0:

$$J_0 = \frac{\pi m v_F^2 N_E}{6\delta^3} \ , \tag{1.10}$$

where δ is the imaginary part of the self-energy, N_E is the total density of states at energy E, v_F is the Fermi velocity, and m the mass of the charge carriers.

The diffuse propagator, which we denote by $P(\mathbf{r},\mathbf{r}')$, satisfies the following partial differential equation [43],

$$-D\nabla^2 P(\mathbf{r},\mathbf{r}') = 2\delta N_i \gamma^2 \delta(\mathbf{r}-\mathbf{r}') \ , \tag{1.11}$$

where N_i is the impurity density and $D \equiv v_F^2\hbar/(2\delta)$ is the diffusion constant. This equation has a general solution given by

$$P(\mathbf{r},\mathbf{r}') = \sum_m \frac{Q_m^*(\mathbf{r}')Q_m(\mathbf{r})}{\lambda_m} \ , \tag{1.12}$$

where $Q_m(\mathbf{r})$ are the eigenfunctions and λ_m are the eigenvalues obtained from the eigenvalue equation,

$$-\frac{D}{2\delta N_i \gamma^2}\nabla^2 Q_m(\mathbf{r}) = \lambda_m Q_m(\mathbf{r}) \ . \tag{1.13}$$

The boundary conditions are hard wall in the transverse directions x and y, and periodic in the direction of propagation z. This leads to the following expression for $Q_m(\mathbf{r})$:

$$Q_m(\mathbf{r}) = \sqrt{\frac{L_x L_y L_z}{8}}\cos(\frac{m_z \pi z}{L_z})\sin(\frac{m_x \pi x}{L_x})\sin(\frac{m_y \pi y}{L_y}) \ , \tag{1.14}$$

with the eigenvalues:

$$\lambda_m = \frac{D}{2\delta N_i \gamma^2}\left(\frac{\pi}{L_z}\right)^2\left[m_z^2 + m_x^2\frac{L_z^2}{L_x^2} + m_y^2\frac{L_z^2}{L_y^2}\right] \ . \tag{1.15}$$

To evaluate F_a we substitute Eq. (1.9), Eq. (1.10), Eq. (1.12), Eq. (1.14), and Eq. (1.15), into Eq. (1.7). This leads to an expression, where the integrals are easily evaluated using the orthonormality conditions of $Q_m(\mathbf{r})$. The final result is,

$$F_a = \frac{1}{L_z^4}\left(\frac{D}{\delta}\right)^2 \sum_m \frac{1}{\lambda_m^2} \ . \tag{1.16}$$

This expression represents the contribution from one of the diagrams that is topologically represented by Fig. 1.2(b). Evaluating all diagrams that are topologically equivalent to Fig. 1.2(b), we find that the total contribution from this type of Feynman diagram to be [43],

$$F_a = 2\frac{1}{L_z^4}\left(\frac{D}{\delta}\right)^2 \sum_{m_z=1}^{\infty} \sum_{m_x=0}^{\infty} \sum_{m_y=0}^{\infty} \left(Re(\frac{1}{\lambda_m})\right)^2 \ . \tag{1.17}$$

Similarly, the contributions from the other Feynman diagrams, Fig. 1.2(c) and Fig. 1.2(d), which are denoted by F_b and F_c, respectively, are given by [43],

$$F_b = -8\frac{1}{L_z^4}\left(\frac{D}{\delta}\right)^2 Re\left[\sum_{m_x=0}^{\infty} \sum_{m_y=0}^{\infty} \sum_{m_z=1}^{\infty} \sum_{n_z=1}^{\infty} \frac{f_{mn}^2}{\lambda_m \lambda_n}\left(\frac{1}{\lambda_m} + \frac{1}{\lambda_n}\right)\right] \ , \tag{1.18}$$

and

$$F_b = 24\frac{1}{L_z^4}\left(\frac{D}{\delta}\right)^2 Re\left[\sum_{m_x=0}^{\infty} \sum_{m_y=0}^{\infty} \sum_{m_z,l_z=1}^{\infty} \sum_{n_z,j_z=2}^{\infty} \frac{f_{mn} f_{nl} f_{lj} f_{jm}}{\lambda_m \lambda_n \lambda_l \lambda_j}\right] \ , \tag{1.19}$$

where $f_{nm} = 4mn/\pi(m^2 - n^2)$. The total conductance fluctuations are given by,

$$\Delta G = 2\left(F_a + F_b + F_c\right) \ , \tag{1.20}$$

where the factor 2 is to account for the particle-hole channels which have the exact same contribution as the particle-particle channels [38]. All that is left is to evaluate numerically the summations in Eq. (1.17), Eq. (1.18), and Eq. (1.19). For a 2D square conductor, $L_x \ll L_y \sim L_z$, one finds that the value of the conductance fluctuations is $\Delta G = 0.86e^2/h$, where e is the electron charge and h the Planck constant. Notice that the impurity density and the scattering strength γ of the impurities do not appear in ΔG (see Eq. (3.52)): these non universal parameters are canceled out. One therefore use the term *universal* to describe these conductance fluctuations.

As already mentioned above, we are interested in analyzing conductance fluctuations *beyond* ΔG in the mesoscopic diffusive regime. However, as we will discuss in the next section, the AC and nonlinear DC transport coefficients are more difficult to analyze due to several factors, the most prominent one is the role played by electrodynamics. While the diagrammatic technique reviewed above can be *formally* applied to these situations [58], it is extremely difficult to obtain concrete predictions even for the dynamic conductance itself, let alone its fluctuations. In the following section we discuss the basic considerations for AC and nonlinear DC transport.

1.3 General considerations of quantum transport

In the last section we have reviewed linear response analysis of UCF, using Kubo's formula, for infinitely large mesoscopic diffusive conductors. Another approach to quantum transport, equivalent to the linear response theory, but much more convenient to apply when the electrodes of a conductor must be considered, was proposed by Landauer in 1957[39]. The idea is that since conduction measures how easy (or how difficult) it is for an electron to traverse a system, the conductance should be related to the probability of the electron to go from one side of the conductor to the other. In other words, conductance should be expressed in terms of the transmission and reflection coefficients of a conductor. The Landauer formula expresses this point of view,

$$G_{\alpha\beta} = \frac{2e^2}{h} T_{\alpha\beta} , \tag{1.21}$$

where $G_{\alpha\beta}$ is the linear DC conductance for a two-lead conductor, with the leads labelled by α, β, and $T_{\alpha\beta}$ is the transmission coefficient from lead β to α. For example, if a conductor is classical, one can calculate its conductance by solving a drift-diffusion equation for the transmission coefficient $T_{\alpha\beta}$, while for quantum coherent conductors one can obtain $T_{\alpha\beta}$ by solving the quantum scattering problem. Landauer's approach has given a clear view and a very simple way to understand conduction of a two-lead conductor. Inspired by Landauer's idea, Büttiker in 1986 derived a result for linear DC conductance for general phase coherent multi-leads device [42], using scattering matrices. In this section, we discuss some general considerations of quantum transport in AC and nonlinear DC situations using the scattering matrix approach. It will become clear why the diagrammatic approach reviewed in the last section does not seem to be applicable.

So far the Landauer-Büttiker formalism has been successfully applied to understand a wide variety of experimental observations [5]. In particular, it has been applied to study weak localization phenomenon in a diffusive conductor [59], the Aharonov-Bohm effect in metallic rings [60, 61], and universal conductance fluctuations [43]. All these systems were studied at equilibrium. Very recently, it has it become possible to measure linear AC and nonlinear DC conductance coefficients in nanostructures [62]. These new experimental investigations have demanded that the theoretical approaches be extended to these new and complicated situations. Indeed, in clear contrast to the linear DC transport theory where, the Landauer-Büttiker formalism has been very successful, the status of AC and nonlinear DC theory is far from satisfying. For example, it was only until recently that some fundamental issues of AC and nonlinear DC quantum transport theory have been identified [63, 64, 65, 66] and only very few have been solved [67, 68, 69, 70].

For a multi-probe coherent conductor, the transport coefficients are defined by the current-voltage $(I - V)$ curve:

$$I_\alpha(\omega) = \sum_\beta G_{\alpha\beta}(\omega) V_\beta + \sum_{\beta,\gamma} G_{\alpha\beta\gamma}(\omega) V_\beta V_\gamma + \dots \ , \tag{1.22}$$

where the subscripts $\{\alpha\}$ indicates lead α, $G_{\alpha\beta}(\omega)$ is the linear frequency dependent conductance, $G_{\alpha\beta\gamma}(\omega)$ is the second order nonlinear conductance, and so on. So far, there is no first principles theory which can predict the general nonlinear coefficients, unless $\omega \to 0$. From a theoretical point of view, there are two fundamental principles which are very important. First, the total current flowing through all the leads must be conserved. Therefore, from Eq. (1.22), we must have

$$\sum_\alpha I_\alpha(\omega) = 0 \ . \tag{1.23}$$

This gives rise to the sum rules, such as:

$$\sum_\alpha G_{\alpha\beta}(\omega) = \sum_\alpha G_{\alpha\beta\gamma}(\omega) = 0 \ . \tag{1.24}$$

The sum rules put severe constraints on the form of these transport coefficients. Second, a theory must be gauge invariant, meaning that the predicted current cannot change if the potential at all the leads are shifted by the same constant amount. This is simply the statement that the definition of the potentials zero cannot change physics. Therefore, setting $\{V_\alpha\} \rightarrow \{V_\alpha + \Delta\}$, where Δ is a constant, we find from Eq. (1.22) the sums rules:

$$\sum_\beta G_{\alpha\beta}(\omega) = \sum_\beta G_{\alpha\beta\gamma}(\omega) = \sum_\gamma G_{\alpha\beta\gamma}(\omega) = 0 \ . \tag{1.25}$$

Again, these further sum rules constrain the form of the transport coefficients. It turns out that the linear DC conductance coefficient $G_{\alpha\beta}(0)$, given by Eq. (1.21) satisfies these sum rules automatically.

However, a difficulty for AC transport theory, even at the linear order, is the current conservation Eq. (1.24), *i.e.* how to guarantee $\sum_\alpha G_{\alpha\beta}(\omega) = 0$. As shown by Büttiker [64, 65, 66, 71], current is not conserved unless the displacement current, which is induced by the AC field, is taken into account. Displacement current arises because of induction by electrodynamics, therefore it is related to interactions. Therefore, a correct AC theory must include interactions at some level, usually at the Hartree level [72], but this complicates matters significantly. For a nonlinear DC theory, the difficulty is to make sure that gauge invariance is satisfied, for example the second order nonlinear coefficient $\sum_\beta G_{\alpha\beta\gamma}(0)$ must be made to satisfy Eq. (1.25). Again, one can prove that gauge invariance is not satisfied unless interactions are included [73]. Therefore, to correctly analyze AC and nonlinear DC transport coefficients, a necessary condition is to solve quantum scattering problem self-consistently, including electrodynamics [58], which is, unfortunately, a very difficult problem. Recall the analysis of last section: no interaction is necessary in understand the basic physics of UCF, because it is a result of linear DC transport. In addition, it seems very difficult to generalize the diagrammatic approach of the last section by adding the self-consistent electrodynamics, in order to investigate AC and nonlinear DC transport coefficients. Clearly, these coefficients are important physical quantities as they help to provide a general and more complete picture of quantum transport in nanostructures.

1.4 *Outline of thesis*

In this thesis we use both exact analytical techniques [74] and a numerical transfer matrix approach [75] to solve quantum scattering problems in mesoscopic conductors.

First, we develop new theoretical tools that will allows us to compute the functional derivative of the scattering matrix in terms of the scattering wave function: these derivatives appear naturally in AC and nonlinear DC theory. This is a very important step which allows us to compute the linear AC and the nonlinear DC conductance for a diffusive conductor from first principles, for the first time in literature. Second, we will investigate the zero temperature linear AC conductance fluctuations, and discover that the sample-to-sample fluctuations indicate the fact that a diffusive conductor can have a capacitive or a inductive dynamic response, which is sensitive to the impurity configuration. Our results also suggest a crossover for the AC conductance distribution, from a symmetric to a non symmetric distribution as the impurity density increases. A degree of generic behavior is discovered in that the AC fluctuation amplitudes become independent of the scattering strength, although depends on the impurity density. Third, we report an analysis of the sample-to-sample fluctuations of the nonlinear DC transport coefficient, in the conventional UCF regime. Very interesting behavior is discovered for the first time in literature as well.

The final topic of this thesis considers a seemingly simpler situation where magnetoconductance fluctuations occur in a quasi-1D quantum wire where artificial impurities (anti-dots) are placed. However, this problem can only be solved numerically because of the finite size of the artificial impurities. This drastically complicates the scattering analysis and renders the analytical approach non applicable. We therefore developed a novel numerical transfer matrix technique to solve the quantum scattering problem by calculating the transmission coefficients as a function of the external magnetic field. We apply the Landauer's formula Eq. (1.21) to predict the conductance. Our work is motivated by the experimental study of the same system, where several conductance fluctuation anomalies were reported [1]. Our numerical results give good quantitative agreement with the experimental data and we confirm the physical understanding inspired by the experiment.

The rest of the thesis is organized in the following way. In chapter 2 we review the scattering matrix theory for quantum transport. We derive expressions for the emittance $E_{\alpha\beta}$, which is defined by $G_{\alpha\beta}(\omega) = G_{\alpha\beta}(0) - ie^2\omega E_{\alpha\beta}$, and the nonlinear DC conductance $G_{\alpha\beta\gamma}(0)$. All three of these transport coefficients, $G_{\alpha\beta}$, $E_{\alpha\beta}$, and $G_{\alpha\beta\gamma}$, are expressed in terms of the scattering matrix $s_{\alpha n,\beta m}$, its functional derivative $\delta s_{\alpha n,\beta m}/\delta U(r)$, and the internal response potential $u_\alpha(r)$, also known as the characteristic potential. In chapter 3 we derive a series of new theoretical results which greatly simplify our computation of the emittance and the nonlinear conductance, including a general formula for the N-th order functional derivative of the scattering matrix. We also derive the Generalized Fisher-Lee relation, which relates the scattering wave function to the Green's function for multi-probe conductors. Such a relationship is expected but, to the best of our knowledge, we do not know of any such formula in literature. required These results combined, greatly reduce the computational effort required when we calculate the linear AC and nonlinear DC transport coefficients. In chapter 4 we derive an exact expression for the N-delta impurity Green's function, $G^{(N)}(\mathbf{r}, \mathbf{r}')$, in terms of the impurity free Green's function, $G^{(0)}(\mathbf{r}, \mathbf{r}')$. Using this result we obtain an analogous result for the wave function $\psi_\alpha^{(N)}(r)$, the scattering matrix $s^{(N)}_{\alpha n,\beta m}$, and its functional derivative $\delta s^{(N)}_{\alpha n,\beta m}/\delta U(\mathbf{r})$. Using our general formulas we reproduce the exact analytical results found in [76] and [77], which were obtained for the case of a single impurity. In the latter part of chapter 4 we study the UCF regime for the usual linear DC conductance, $G_{\alpha\beta}(0)$, using our formalism. We then study the emittance and nonlinear DC conductance fluctuations in the UCF regime. In chapter 5 we develop an extended transfer matrix technique to study the effects of artificial impurities in a magnetic field on the linear DC conductance, in the ballistic regime. These numerical simulations are used to explain recent experimental results [1, 44, 45]. Finally, in chapter 6 we summarize our work and provide a brief outlook for future research.

2

Gauge invariant transport theory

In the last decade quantum transport under a time dependent field has been the subject of many studies [78, 79, 80]. The problem of nonlinear DC quantum transport has also, in recent years, been a subject of new experimental and theoretical work [62, 63, 64, 65, 66, 69, 70, 81]. A great theoretical challenge is to predict, for a general phase coherent conductor, the transport coefficients as a function of the AC field frequency ω and the bias potentials $\{V_\gamma\}$. In particular, one desires to obtain general expressions for the emittance, $E_{\alpha\beta}$, and the first nonlinear DC conductance, $G_{\alpha\beta\gamma}$, as defined in Eq. (1.22).

A system which is subjected to a time dependent field, provided by an AC bias voltage, produces a total current composed of two parts: a particle current and a displacement current. The displacement current is an essential ingredient in AC transport since without it the total current is not conserved. Therefore, any realistic theory for AC transport must contain a displacement current. The origin of the displacement current is electrodynamic induction, which is related to electron-electron interactions. Hence, $e-e$ interactions are at the heart of any physically plausible theory of time dependent transport.

Similarly, nonlinear DC transport requires gauge invariance: the physics of the system does not change when the electrostatic potential is changed everywhere by the same constant amount. This requirement put severe restrictions on any theory of nonlinear quantum transport, as discussed in the last chapter. In particular, any realistic theory needs to contain information about the internal potential distribution in order to preserve gauge invariance. Thus, AC and nonlinear DC transport contain more ingredients than the familiar linear DC theory.

The original scattering matrix theory for quantum transport was developed to study the linear DC transport, i.e. the first term of Eq. (1.22) at $\omega = 0$. The approach consists of computing the particle current using the scattering matrix. Büttiker and his co-workers have developed an extended scattering matrix theory which deals with linear AC transport and nonlinear DC transport [29, 64, 65, 66, 69, 70, 71, 73]. To solve the AC problem the scattering matrix approach is applied in two steps. First, the particle current is calculated and one finds that the current is not conserved in the AC regime. Second, the $e-e$ interactions are considered which change the potential landscape, and thus generates an internal response (induction) that cancels exactly the non-conserved piece. Similar considerations are applied to the nonlinear DC transport problem, which leads to a gauge invariant scattering matrix theory of nonlinear transport at the 2nd order.

A new ingredient that is found in the linear AC and nonlinear DC transport theory is the characteristic potentials. The characteristic potentials describe the changes of the electrostatic potential inside the quantum conductor during transport, i.e. when the electro-chemical potentials of the electron reservoirs are changed externally. In particular, the first order characteristic potential, u_γ, describes the change of the electrostatic potential to first order in the bias potentials $\{V_\gamma\}$. It is the first order characteristic potential which enters into the expressions of the emittance, $E_{\alpha\beta}$, and the 2nd order nonlinear DC conductance $G_{\alpha\beta\gamma}$. Higher order transport coefficients require the knowledge of higher order characteristic potentials, $u_{\gamma\alpha}, u_{\gamma\alpha\beta}, \ldots$.

In this chapter, we follow [82] to review these concepts, and to develop the necessary theoretical framework for our work. Let us once again emphasize that our theory of quantum transport respects current conservation and gauge invariance.

2.1 Expansion of the current operator

In this section we derive an expansion for Büttiker's current operator [73]. The current operator is defined in terms of creation and annihilation operators, which

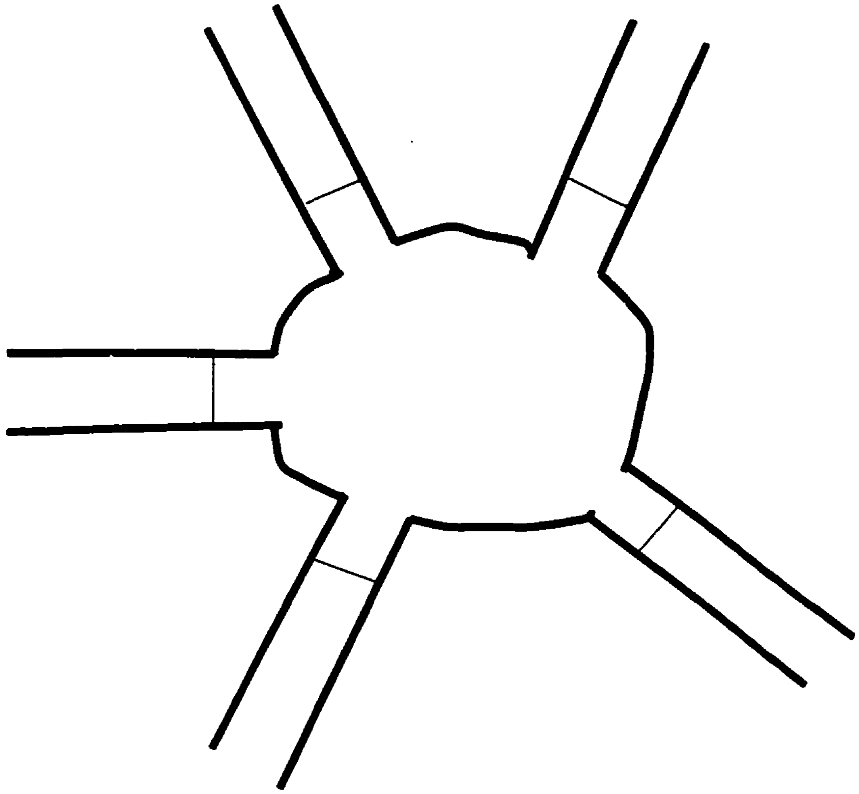

Figure 2.1: Schematic drawing of a general quantum conductor. In this situation we have 5 leads that connect the device to the externally controlled electron reservoirs. We chose the scattering region such that it extends into the lead regions.

are denoted by $\tilde{a}^{\dagger}_{\alpha n}(E)$ and $\tilde{a}_{\alpha n}(E)$, where these operators represent the creation and the annihilation of an incoming mode in the n-th subband from the α-th lead with incoming energy E. We also define the creation and annihilation operators $\tilde{b}^{\dagger}_{\alpha n}(E)$ and $\tilde{b}_{\alpha n}(E)$ for outgoing charge carriers in the n-th subband leaving from the α-th lead with energy E.

The operators for incoming and outgoing modes are related by the scattering matrix:

$$\tilde{b}^{\dagger}_{\alpha n}(E) = \sum_{\beta,m} s_{\alpha n,\beta m}\tilde{a}^{\dagger}_{\beta m}(E) \ . \tag{2.1}$$

This relation simply states that the probability amplitude that a charge carrier leaves the device (see Fig. 2.1) through the α-th lead in the n-th mode is given by the sum over incoming all incoming modes $\tilde{a}^{\dagger}_{\beta m}(E)$ multiplied by the scattering matrix. Recall that the scattering matrix $s_{\alpha n,\beta m}$ is the probability amplitude that an incoming mode from the β-th lead in the m-th subband leaves in the α-th lead in the n-th subband. The above relation gives the partitioning of the outgoing states in terms of the incoming states.

Using these operators it can be shown that the total current operator to first order in ω is given by [73]:

$$\hat{I}_\alpha(t) = \frac{e}{h}\sum_n \int dEdE' \left[\tilde{a}^\dagger_{\alpha n}(E)\tilde{a}_{\alpha n}(E') - \tilde{b}^\dagger_{\alpha n}(E)\tilde{b}_{\alpha n}(E')\right] e^{i(E-E')t/\hbar} \quad . \qquad (2.2)$$

This equation states that the total current going through the α-th lead at time t is given by the sum over all incoming modes from the α-th lead minus the sum over all outgoing modes leaving through the α-th lead, with the appropriate averaging.

Typically one assumes that the operators $\tilde{a}^\dagger_{\alpha n}(E)$ and $\tilde{a}_{\alpha n}(E)$ are time independent, which is correct for a DC bias potential. But for an AC potential the creation and annihilation operators are no longer time independent. In general they have a non trivial time dependence because of the oscillating external bias. They are the solutions to the equations of motion generated from the time dependent Hamiltonian, which includes the AC external potential as a perturbation. In order to obtain a current conserving expression for the operator Eq. (2.2) we need expressions for $\tilde{a}^\dagger_{\alpha n}(E)$ and $\tilde{a}_{\alpha n}(E)$ which take into account the internal potential $U(\mathbf{r}, \{V_\gamma\})$.

We now follow the work of [82]. The model Hamiltonian for a system in the presence of an external oscillating potential is given by,

$$\hat{H} = \sum_{\alpha m} \left(\bar{E}_{\alpha m} + eV_\alpha \cos\omega t\right) \hat{a}^\dagger_{\alpha m}(\bar{E}_{\alpha m}, t)\hat{a}_{\alpha m}(\bar{E}_{\alpha m}, t) \quad . \qquad (2.3)$$

In this equation $\hat{a}_{\alpha m}(\bar{E}_{\alpha m}, t)$ is the time dependent annihilation operator for an incoming carrier from region α in mode m. $eV_\alpha \cos\omega t$ is the shift in the electro-chemical potential away from equilibrium, i.e. $\mu_\alpha(t) = \mu_{eq} + eV_\alpha \cos\omega t$, where μ_{eq} is the equilibrium electro-chemical potential of the leads. The eigen-energy levels $\bar{E}_{\alpha m}$ have a functional dependence on the internal potential landscape $U(\mathbf{r}, \{V_\alpha\})$. The potential U includes the internal response to the external perturbation which generates the displacement current. Note that the potential U should also be a function of time but since we are only interested in the response to first order in ω we can neglect this dependence.

The creation operator $\hat{a}_{\alpha m}(\bar{E}_{\alpha m}, t)$ represent the incoming electrons which are "dressed" by the oscillating bias potential. The operators $\tilde{a}^{\dagger}_{\alpha n}(E)$ in Eq. (2.2) are the Fourier transform of $\hat{a}^{\dagger}_{\alpha m}(\bar{E}_{\alpha m}, t)$. Usually, the operators in Eq. (2.2) are taken to be the "bare" creation and annihilation operators, i.e. the creation and annihilation operators for incoming modes in the presence of a *static* infinitesimal bias potential. When bare operators are used for AC transport, current conservation is violated [64]. To obtain current conserving AC transport coefficients, Büttiker [64, 66, 71] added an extra term to Eq. (2.1) which is a functional of the internal potential U. Instead of using this approach we follow [82] to derive an expression for the dressed operators by solving their equations of motion to the desired order in the bias potential and AC frequency.

Expanding the total energy in terms of the external perturbation potential $\{V_\gamma\}$ we find,

$$\bar{E}_{\alpha m} + eV_\alpha \cos\omega t = E_{\alpha m} + \hat{O}^{(1)}_\alpha \cos\omega t + \hat{O}^{(2)}_\alpha (\cos\omega t)^2 + \dots \ , \tag{2.4}$$

where the operators $\hat{O}^{(i)}_\alpha$ are given by the spatial integration of the i-th characteristic potential folded with the i-th order functional derivative of $\bar{E}_{\alpha m}$ with respect to the internal potential. In particular, we have that

$$\hat{O}^{(1)}_\alpha \equiv \sum_\beta \left(\delta_{\alpha\beta} + \partial_{V_\beta} E_{\alpha m}\right) V_\beta \ , \tag{2.5}$$

where

$$\partial_{V_\beta} \bar{E}_{\alpha m} = \int d\mathbf{r} u_\beta(\mathbf{r}) \frac{\delta \bar{E}_{\alpha m}}{\delta U(\mathbf{r})} \ , \tag{2.6}$$

and $u_\beta(\mathbf{r}) = \frac{\partial U(\mathbf{r})}{\partial V_\beta}$ is the first order characteristic potential. We can now use the expansion Eq. (2.4) to rewrite the Hamiltonian in the following way,

$$\hat{H} = \sum_{\alpha m} \left(E_{\alpha m} + \sum_i \hat{O}^{(i)}_\alpha (\cos\omega t)^i \right) \hat{a}^{\dagger}_{\alpha m}(\bar{E}_{\alpha m}, t) \hat{a}_{\alpha m}(\bar{E}_{\alpha m}, t) \ . \tag{2.7}$$

The dressed annihilation operators $\hat{a}_{\alpha m}(\bar{E}_{\alpha m}, t)$ satisfy the equation of motion:

$$\frac{d\hat{a}_{\alpha m}}{dt}(\bar{E}_{\alpha m}, t) = \left[\hat{a}_{\alpha m}(\bar{E}_{\alpha m}, t), \hat{H}\right] \ . \tag{2.8}$$

Since the time dependence of the Hamiltonian is simple, direct integration can be performed. Up to linear order in voltage we only need to keep the term $\hat{O}^{(1)}_{\alpha}$ in the Hamiltonian. This leads us to the following solution for $\hat{a}_{\alpha m}(\bar{E}_{\alpha m}, t)$:

$$\hat{a}_{\alpha m}(\bar{E}_{\alpha m}, t) = \hat{a}_{\alpha m}(\bar{E}_{\alpha m}) exp\left(-\frac{i}{\hbar}\left[E_{\alpha m}t + \frac{e\hat{O}^{(1)}}{\omega}\sin\omega t\right]\right) \ , \tag{2.9}$$

The operator $\hat{a}_{\alpha m}(\bar{E}_{\alpha m})$ is essentially the bare annihilation operator at an energy level $\bar{E}_{\alpha m}$. Eq. (2.9) provides an explicit expression for the dressed annihilation operators in terms of the bare operator as a function of time. To obtain the dressed operators in energy space we perform a Fourier transform:

$$\begin{aligned}
\tilde{a}_{\alpha m}(E) &= \int dt \ \hat{a}_{\alpha m}(\bar{E}_{\alpha m}, t) e^{iEt/\hbar} \\
&= \hat{a}_{\alpha m}(E) \\
&- \frac{e}{2\hbar\omega}\hat{O}^{(1)}_{\alpha}\left[\hat{a}_{\alpha m}(E+\hbar\omega) - \hat{a}_{\alpha m}(E-\hbar\omega)\right] \\
&+ \frac{e^2}{8\hbar^2\omega^2}\left(\hat{O}^{(1)}_{\alpha}\right)^2\left[\hat{a}_{\alpha m}(E+2\hbar\omega) - \hat{a}_{\alpha m}(E-2\hbar\omega)\right] + \ldots \\
&= \sum_n \frac{1}{n!}\left(\frac{-e\hat{O}^{(1)}_{\alpha}}{2\hbar\omega}\right)^n \left[e^{\hbar\omega\partial_E} - e^{-\hbar\omega\partial_E}\right]^n \hat{a}_{\alpha m}(E) \ .
\end{aligned} \tag{2.10}$$

To obtain this expression the continuum limit was taken, i.e. we transformed the discrete energy levels $\bar{E}_{\alpha m}$ into a continuum of energy states labeled by E. The first term in this expression corresponds to the *zero*-th order response of the system in ω. This corresponds to the usual DC transport regime. To obtain the linear and non linear DC conductances we must put the first term of the above expansion into the expression for the current Eq. (2.2) and then expand in terms of the bias potentials, V_{γ}. Similarly, the second term in Eq. (2.10) represents the first order response in ω to the oscillating AC potential. To obtain the linear AC conductance we put this term into Eq. (2.2) and expand to first order in V_{γ}. Let us now compute $G_{\alpha\beta}$, $G_{\alpha\beta\gamma}$, and $E_{\alpha\beta}$.

2.2 *Transport*

In this section we compute the linear and nonlinear DC transport coefficients. To obtain an expression for the DC current operator we put the first term from the expansion Eq. (2.10) into Eq. (2.2). Taking the ensemble average of the DC current operator leads us to an expression for the DC current in terms of the bias potentials. Expanding this expression in terms of the bias potentials $\{V_\alpha\}$ leads us to the transport coefficients $G_{\alpha\beta}$ and $G_{\alpha\beta\gamma}$.

Putting the first term from Eq. (2.10) into Eq. (2.2) and using Eq. (2.1) we find,

$$\begin{aligned}\hat{I}_\alpha(t) &= \frac{e}{h}\sum_n \int dEdE' \\ &\quad \left[\hat{a}^\dagger_{\alpha n}(E)\hat{a}_{\alpha n}(E') - \left(\sum_{\beta m} s^\dagger_{\alpha n,\beta m}(E)\hat{a}^\dagger_{\beta m}(E)\right)\left(\sum_{\gamma l} s_{\alpha n,\gamma l}(E')\hat{a}_{\gamma l}(E')\right)\right] e^{i(E-E')t/\hbar} \\ &= \frac{e}{h}\sum_n\sum_{\beta m}\sum_{\gamma l}\int dEdE'\hat{a}^\dagger_{\beta m}(E)\left[\delta_{\alpha\beta}\delta_{\alpha\gamma}\delta_{nm}\delta_{nl} - s^\dagger_{\alpha n,\beta m}(E)s_{\alpha n,\gamma l}(E')\right]\hat{a}_{\gamma l}(E')e^{i(E-E')t/\hbar} \\ &= \frac{e}{h}\int dEdE' \sum_{\beta\gamma lmn} \hat{a}^\dagger_{\beta m}(E)A_{\beta m\gamma l}(\alpha, n, E, E')\hat{a}_{\gamma l}(E')e^{i(E-E')t/\hbar} \;, \qquad (2.11)\end{aligned}$$

where

$$A_{\beta m\gamma l}(\alpha, n, E, E') = \delta_{\alpha\beta}\delta_{\alpha\gamma}\delta_{nm}\delta_{nl} - s^\dagger_{\alpha n,\beta m}(E)s_{\alpha n,\gamma l}(E') \;. \qquad (2.12)$$

To obtain the physical current we take the quantum statistical ensemble average of the current operator. The ensemble average, at temperature T, of the creation and annihilation operators deep in the leads is given by,

$$< \hat{a}^\dagger_{\alpha n}(E)\hat{a}^\dagger_{\beta m}(E') >_{eq} \;=\; \delta_{nm}\delta_{\alpha\beta}\delta(E-E')f_\alpha(E) \;, \qquad (2.13)$$

where $f_\alpha(E)$ is the Fermi function for reservoir α. Taking the ensemble average of the DC current operator Eq. (2.11) we find,

$$\begin{aligned}< I_\alpha > &= \frac{e}{h}\int dEdE' \sum_{\beta\gamma lmn} A_{\beta m\gamma l}(\alpha, n, E, E') < \hat{a}^\dagger_{\beta m}(E)\hat{a}_{\gamma l}(E') > e^{i(E-E')t/\hbar} \\ &= \frac{e}{h}\int dEdE' \sum_{\beta\gamma lmn} A_{\beta m\gamma l}(\alpha, n, E, E')\delta_{ml}\delta_{\beta\gamma}\delta(E-E')f_\beta(E)e^{i(E-E')t/\hbar} \\ &= \frac{e}{h}\int dE \sum_{\beta mn} A_{\beta m\beta m}(\alpha, n, E, E)f_\beta(E) \\ &= \frac{e}{h}\int dE \sum_{\beta mn}\left[\delta_{\alpha\beta}\delta_{nm} - s^\dagger_{\alpha n,\beta m}(E,\{V_\gamma\})s_{\alpha n,\beta m}(E,\{V_\gamma\})\right] f_\beta(E) \\ &= \frac{e}{h}\int dE \sum_\beta f_\beta(E)A_{\alpha\beta}(E,\{V_\gamma\}) \;, \qquad (2.14)\end{aligned}$$

where the transmission function $A_{\alpha\beta}(E,\{V_\gamma\})$ is defined by:

$$A_{\alpha\beta}(E,\{V_\gamma\}) \equiv \sum_{mn} \left[\delta_{\alpha\beta}\delta_{nm} - s^{\dagger}_{\alpha n,\beta m}(E,\{V_\gamma\}) s_{\alpha n,\beta m}(E,\{V_\gamma\})\right] \ . \tag{2.15}$$

Notice that we have explicitly included the scattering matrix dependence on the bias potentials $\{V_\gamma\}$. Notice that, the time dependence has dropped out of Eq. (2.14), as it should for DC transport.

The DC transport coefficients are formally obtained by Taylor expanding the current function in terms of the bias potential $\{V_\gamma\}$:

$$< I_\alpha > \equiv \sum_{\beta} G_{\alpha\beta} V_\beta + \sum_{\beta\gamma} G_{\alpha\beta\gamma} V_\beta V_\gamma + \dots \ . \tag{2.16}$$

To accomplish this we expand the Fermi function, $f_\alpha(E) = f(E - \mu_{eq} - eV_\alpha/k_B T)$, and $A_{\alpha\beta}(E,\{V_\gamma\})$ in terms of $\{V_\gamma\}$:

$$f_\alpha = f + (\partial_E f)(-eV_\beta) + \frac{1}{2}(\partial_{EE} f)(-eV_\beta)^2 + \dots \ , \tag{2.17}$$

and

$$A_{\alpha\beta}(E,\{V_\gamma\}) = A_{\alpha\beta}(E) + \sum_{\gamma} \partial_{V_\gamma} A_{\alpha\beta}(E) V_\gamma + \frac{1}{2}\sum_{\gamma,\mu} \partial_{V_\gamma}\partial_{V_\mu} A_{\alpha\beta}(E) V_\mu V_\gamma + \dots \ . \tag{2.18}$$

Putting these expressions into Eq. (2.14) we find, to 2nd order in the bias,

$$\begin{aligned}
< I_\alpha > &= \frac{e}{h}\int dE f_\alpha(E) \sum_{\beta} A_{\alpha\beta}(E,\{V_\gamma\}) \qquad (2.19)\\
&= \frac{e}{h}\int dE \sum_{\beta}\left(f + (\partial_E f)(-eV_\beta) + \frac{1}{2}(\partial_{EE} f)(eV_\beta)^2\right)\\
&\quad \left(A_{\alpha\beta}(E) + \sum_{\gamma} \partial_{V_\gamma} A_{\alpha\beta}(E) V_\gamma + \frac{1}{2}\sum_{\gamma\mu} \partial_{V_\gamma}\partial_{V_\mu} A_{\alpha\beta}(E) V_\mu V_\gamma\right)\\
&= \frac{e}{h}\int dE f(E) \sum_{\beta} A_{\alpha\beta}(E) + \frac{e}{h}\int dE (\partial_E f) \sum_{\beta} A_{\alpha\beta}(E)(-eV_\beta)\\
&\quad + \frac{e}{h}\int dE f(E) \sum_{\beta\gamma} \partial_{V_\gamma} A_{\alpha\beta}(E) V_\gamma + \frac{e}{h}\int dE f(E) \frac{1}{2}\sum_{\beta\gamma\mu} \partial_{V_\gamma}\partial_{V_\mu} A_{\alpha\beta}(E) V_\mu V_\gamma\\
&\quad + \frac{e}{h}\int dE (\partial_E f) \sum_{\beta\gamma} \partial_{V_\gamma} A_{\alpha\beta}(E) V_\gamma (-eV_\beta) + \frac{e}{h}\int dE \sum_{\beta} \frac{1}{2}(\partial_{EE} f)(eV_\beta)^2 A_{\alpha\beta}(E) \ .
\end{aligned}$$

To simplify the above expression notice the sum rule,

$$\sum_{\beta} A_{\alpha\beta}(E) = \sum_{\beta nm} \left[\delta_{\alpha\beta}\delta_{nm} - s^{\dagger}_{\alpha n,\beta m}(E) s_{\alpha n,\beta m}(E)\right] = 0 \ , \tag{2.20}$$

which follows from the unitarity condition on the scattering matrix,

$$\sum_{\beta m} s^{\dagger}_{\alpha n,\beta m}(E) s_{\alpha n,\beta m}(E) = 1 \ . \tag{2.21}$$

Applying this sum rule to Eq. (2.19) we find that the first, third and fourth terms in the expansion vanish, which leaves us with,

$$\begin{aligned} < I_\alpha > = & \frac{e}{h}\int dE(-\partial_E f)\sum_\beta A_{\alpha\beta}(E) eV_\beta \\ & + \frac{e}{h}\int dE(-\partial_E f)\sum_{\beta\gamma}\partial_{V_\gamma} A_{\alpha\beta}(E) V_\gamma eV_\beta \\ & + \frac{e}{h}\int dE \sum_\beta \frac{1}{2}(\partial_{EE} f)(eV_\beta)^2 A_{\alpha\beta}(E) \ . \end{aligned} \tag{2.22}$$

We can further simplify the above expression by integrating by parts the last term on the right hand side, we find,

$$\begin{aligned} < I_\alpha > = & \frac{e^2}{h}\int dE(-\partial_E f)\sum_\beta A_{\alpha\beta}(E) V_\beta \\ & + \frac{e^2}{2h}\int dE(-\partial_E f)\sum_{\beta\gamma}\left(e\partial_E A_{\alpha\beta}(E)\delta_{\beta\gamma} + 2\partial_{V_\gamma} A_{\alpha\beta}(E)\right) V_\beta V_\gamma \ . \end{aligned} \tag{2.23}$$

Let us impose gauge invariance by finding the constraints on Eq. (2.23). Physical quantities, like the current, are invariant under a global shift of all the bias potentials, $V_\alpha \rightarrow V_\alpha + \Delta V$. This implies that $A_{\alpha\beta}(E, \{V_\gamma + \Delta V\}) = A_{\alpha\beta}(E, \{V_\gamma\})$. In turn, this leads us to the following constraint,

$$e\partial_E A_{\alpha\beta}(E) + \sum_\gamma \partial_{V_\gamma} A_{\alpha\beta}(E) = 0 \ . \tag{2.24}$$

The above equation simply states that the first order term of the Taylor expansion of $A_{\alpha\beta}(E, \{V_\gamma + \Delta V\})$ in ΔV must vanish since a global gauge invariance leaves the system invariant. Imposing this constraint, Eq. (2.23) becomes,

$$\begin{aligned} < I_\alpha > = & \frac{e^2}{h}\int dE(-\partial_E f)\sum_\beta A_{\alpha\beta}(E) V_\beta \\ & + \frac{e^2}{2h}\sum_{\beta\gamma}\int dE(-\partial_E f)\left(2\partial_{V_\gamma} A_{\alpha\beta}(E) - \partial_{V_\beta} A_{\alpha\beta}(E)\delta_{\beta\gamma}\right) V_\beta V_\gamma \ . \end{aligned} \tag{2.25}$$

We replace the partial derivatives with respect to the bias potentials $\{V_\gamma\}$ with functional derivatives and the characteristic potentials $\{u_\gamma\}$. This way the transport coefficients can be written in terms of quantities which are defined inside the scattering region. This is accomplished by using the following relation,

$$\partial_{V_\gamma} A_{\alpha\beta} = \int d\mathbf{r} \frac{\delta A_{\alpha\beta}}{\delta U(\mathbf{r})} \frac{\partial U(\mathbf{r})}{\partial V_\gamma} = \int d\mathbf{r} \frac{\delta A_{\alpha\beta}}{\delta U(\mathbf{r})} u_\gamma(\mathbf{r}) \ , \tag{2.26}$$

where the characteristic potential is defined by,

$$u_\gamma(\mathbf{r}) = \frac{\partial U(\mathbf{r})}{\partial V_\gamma} \ . \tag{2.27}$$

The electrostatic potential build-up inside the conductor, due to a change in the external bias, is denoted by $U(\mathbf{r})$. Eq. (2.25) becomes,

$$\begin{aligned} < I_\alpha > = & \frac{e^2}{h} \int dE(-\partial_E f) \sum_\beta A_{\alpha\beta}(E) V_\beta \\ & + \frac{e^2}{2h} \sum_{\beta\gamma} \int dE(-\partial_E f) \int d\mathbf{r} \frac{\delta A_{\alpha\beta}}{\delta U(\mathbf{r})} \left(2u_\gamma(\mathbf{r}) - \delta_{\beta\gamma}\right) V_\beta V_\gamma \ . \end{aligned} \tag{2.28}$$

Since we are only interested in zero temperature limit in this work, we take this limit ($T \to 0$) in the above expression:

$$< I_\alpha > = \frac{e^2}{h} \sum_\beta A_{\alpha\beta} V_\beta + \frac{e^2}{2h} \sum_{\beta\gamma} \int d\mathbf{r} \frac{\delta A_{\alpha\beta}}{\delta U(\mathbf{r})} \left(2u_\gamma(\mathbf{r}) - \delta_{\beta\gamma}\right) V_\beta V_\gamma \ , \tag{2.29}$$

where we have used the identity: $\partial_E f_\alpha(E) \to \delta(E - E_F)$ when $T \to 0$, where E_F is the Fermi energy of the electron reservoirs at equilibrium. The above expression is evaluated at the Fermi energy. We can now read off the transport coefficients by comparing Eq. (2.29) with Eq. (2.16), which leads to,

$$G_{\alpha\beta} = \frac{e^2}{h} A_{\alpha\beta} \ , \tag{2.30}$$

and

$$G_{\alpha\beta\gamma} = \frac{e^2}{2h} \int d\mathbf{r} \frac{\delta A_{\alpha\beta}}{\delta U(\mathbf{r})} \left(2u_\gamma(\mathbf{r}) - \delta_{\beta\gamma}\right) \ . \tag{2.31}$$

These expressions will be used in Chapter 4 to study quantum transport in the diffusive regime. In particular, linear and nonlinear conductance fluctuations in the UCF regime will be calculated using these equations.

Next, we derive an expression for the linear AC conductance. We only give a brief account of the derivation since it follows the same lines as the one just performed. The second order term of the expansion of the annihilation operator $\tilde{a}_{\alpha n}(E)$ is (see Eq. (2.10)) is given by,

$$\frac{e}{2\hbar\omega}\hat{O}^{(1)}_{\alpha}\left[\hat{a}_{\alpha m}(E+\hbar\omega)-\hat{a}_{\alpha m}(E-\hbar\omega)\right] \ . \tag{2.32}$$

Putting this expression into the equation for the current operator (see Eq. (2.2)), taking the ensemble average, and expanding all the terms to first order in V_γ, we find after some algebra [83],

$$\begin{aligned} < I_\alpha > &= -ie^2\omega\sum_\beta\int dE(-\partial_E f)\frac{dN_{\alpha\beta}}{dE}V_\beta \\ &+ ie^2\omega\sum_\beta\int dE(-\partial_E f)\int d\mathbf{r}\sum_\gamma\frac{dn_{\alpha\gamma}(\mathbf{r})}{dE}u_\beta(\mathbf{r})V_\beta \ . \end{aligned} \tag{2.33}$$

Taking the limit $T \to 0$ the expression becomes:

$$\begin{aligned} < I_\alpha > &= -ie^2\omega\sum_\beta\frac{dN_{\alpha\beta}}{dE}V_\beta + ie^2\omega\sum_\beta\int d\mathbf{r}\left(\sum_\gamma\frac{dn_{\alpha\gamma}(\mathbf{r})}{dE}\right)u_\beta(\mathbf{r})V_\beta \\ &= -ie^2\omega\sum_\beta E_{\beta\alpha}V_\beta \ . \end{aligned} \tag{2.34}$$

Note that the DC component is omitted from the above expression, i.e. when ω goes to zero, the current is given by the linear DC formula discussed above. The above equation uses the following notation. The local partial density of states (LPDOS) is defined by [29],

$$\frac{dn_{\alpha\beta}(\mathbf{r})}{dE} \equiv -\frac{1}{4\pi i}\sum_{nm}\left[s^{\dagger}_{\alpha n,\beta m}\frac{\delta s_{\alpha n,\beta m}}{\delta eU(\mathbf{r})} - \frac{\delta s^{\dagger}_{\alpha n,\beta m}}{\delta eU(\mathbf{r})}s_{\alpha n,\beta m}\right] \ . \tag{2.35}$$

This then defines the global partial density of states (GPDOS),

$$\frac{dN_{\alpha\beta}}{dE} \equiv \int d\mathbf{r}\frac{dn_{\alpha\beta}(\mathbf{r})}{dE} \ . \tag{2.36}$$

The emittance $E_{\alpha\beta}$ from Eq. (2.34), which is the first order transport coefficient in ω and V_γ, is given by,

$$E_{\alpha\beta} = \frac{dN_{\alpha\beta}}{dE} - D_{\alpha\beta} \ , \tag{2.37}$$

where

$$D_{\alpha\beta} \equiv \int d\mathbf{r} \frac{dn(\mathbf{r},\alpha)}{dE} u_\beta(\mathbf{r}) \ , \tag{2.38}$$

where $dn(\mathbf{r},\alpha)/dE$ is known as the emissivity and is defined below. Clearly, $D_{\alpha\beta}$ represents the internal response of the system to the oscillating AC potential since it depends on the first order characteristic potential, $u_\gamma(\mathbf{r}) = \partial U(\mathbf{r})/\partial V_\gamma$.

The physical meaning of the various scattering DOS has been discussed in [29] and here we include them for completeness of presentation. The quantity $dn_{\alpha\beta}(\mathbf{r})/dE$ of Eq. (2.35) is the LPDOS which describes the local density of states of carriers which enter the device (see Fig. 2.1) at lead α and exits at lead β. This is the most fundamental quantity of all the scattering DOS. We note that partitioning a scattering process using the partial DOS greatly enhances the physical intuition and helps to understand the complicated quantum scattering problem. Clearly, the GPDOS $dN_{\alpha\beta}/dE$, given by Eq. (2.36), is the total partial DOS describing the scattering event of a carrier entering at lead α and leaving at lead β.

The partial local DOS,

$$\frac{dn(\mathbf{r},\alpha)}{dE} = \sum_\beta \frac{dn_{\alpha\beta}(\mathbf{r})}{dE} , \tag{2.39}$$

describes the local density of states of charge carrier which exit the device from lead α regardless of what lead they came in from. We call this quantity the emissivity. The partial DOS

$$\frac{dn(\beta,\mathbf{r})}{dE} = \sum_\alpha \frac{dn_{\alpha\beta}(\mathbf{r})}{dE} \tag{2.40}$$

describes the local probability that an incoming charge carrier enters from lead β regardless which lead it exits. This partial local DOS is called the injectivity. It is obvious that for systems with time reversal symmetry (*e.g.* no magnetic field), injectivity is identical to emissivity. These partial DOS can be calculated from their definition Eq. (2.39) and Eq. (2.40) once the LPDOS is obtained. They can also be directly computed using the scattering wave functions or the Green's functions. In particular, [29, 84] has proven the following expression,

$$\frac{dn(\beta,\mathbf{r})}{dE} = \sum_n \frac{|\psi_{\beta n}(\mathbf{r})|^2}{h v_{\beta n}} , \tag{2.41}$$

where $v_{\alpha n}$ is the electron's incoming velocity in lead β in mode n. Eq. (2.41) provides a practical means for evaluating the partial DOS once the scattering wave functions are known. The consistency between the different approaches for evaluating the injectivity and the emmisivity provide strong constraints on any theoretical prediction made about these quantities.

Finally, we define the total local DOS,

$$\frac{dn(\mathbf{r})}{dE} = \sum_{\alpha\beta} \frac{dn_{\alpha\beta}(\mathbf{r})}{dE} = \sum_{\alpha} \frac{dn(\alpha, \mathbf{r})}{dE} = \sum_{\beta} \frac{dn(\mathbf{r}, \beta)}{dE} . \tag{2.42}$$

The last ingredient that we are missing is the characteristic potential, $u_\alpha(\mathbf{r})$. Once we know how to compute them, we will have all the required quantities needed to investigate the transport coefficients.

2.3 Characteristic Potential

In this section we derive an equation for the first order characteristic potential $u_\alpha(\mathbf{r})$, following [82]. The characteristic potential contains all the information about the response of the internal potential, which we denote by $\delta U(\mathbf{r})$, to first order in the bias potentials $\{V_\gamma\}$. We derive an expression for $u_\alpha(\mathbf{r})$ within the Thomas-Fermi and quasi-neutrality approximation which leads to an analytical expression in term of the LPDOS.

Consider the multi-probe conductor of Fig. 2.1. In the equilibrium situation where all the electro-chemical potentials of the reservoirs are equal to a common value $\mu_\alpha = \mu_\beta = \cdots = \mu$, we denote the potential landscape of this conductor by $U([\mu_\alpha], \mathbf{r})$. U contains all the contributions due to material properties of the conductor, the external confining potential of the split gate as discussed in Chap.1, the effective interaction potential between electrons (*e.g.* Hartree potential), the electron-ion interactions, and any other effects. Next, consider the situation when we apply a bias potential V_α to lead α so that the electro-chemical potential of this lead deviates from μ by an amount $\delta\mu_\alpha = eV_\alpha$, therefore its electro-chemical potential becomes $\mu'_\alpha = \mu + eV_\alpha$. Since $\mu'_\alpha \neq \mu$, an electric current starts to flow through our conductor. In addition, because of the transport of charges and electron-electron interactions, the potential landscape U will be perturbed by an amount $\delta U(\mathbf{r}) = U([\mu_\alpha + \delta\mu_\alpha], \mathbf{r}) - U([\mu_\alpha], \mathbf{r})$. The presence of δU reflects the physical phenomenon of electrostatic induction which is very important for AC and nonlinear DC transport situations. In fact, without δU, an AC theory violates current conservation while a nonlinear DC theory violates gauge invariance. For specific devices, δU can be numerically computed by solving a Poisson equation coupled to the quantum transport equations in a self-consistent fashion [85]. In this work, we are interested in the small bias regime. We therefore calculate δU order by order in terms of the perturbation $\delta\mu_\alpha$,

$$e\delta U([\mu_\alpha], \mathbf{r}) = \sum_\alpha u_\alpha(\mathbf{r})\delta\mu_\alpha + \frac{1}{2}\sum_{\alpha\beta} u_{\alpha\beta}\delta\mu_\alpha\delta\mu_\beta + \cdots , \tag{2.43}$$

where the functions $u_\alpha, u_{\alpha\beta}, \cdots$ are the characteristic potentials which characterize the change in the potential landscape with an external perturbation. Hence, the functions $u_\alpha(\mathbf{r})$ determines the response of the electrostatic potential inside the device to first order in $\delta\mu_\alpha$.

Let's determine the constraints on the characteristic potentials that gauge invariance and current conservation impose. Consider an increase in all the electro-chemical potentials by the same constant amount, $\delta\mu_\alpha = \delta\mu$. Then according to Eq. (2.43) we have, to first order in $\delta\mu$:

$$\delta\mu = e\delta U(\mathbf{r}) = \sum_\alpha u_\alpha(\mathbf{r})\delta\mu \ . \tag{2.44}$$

Therefore the characteristic potentials must satisfy the sum rule,

$$\sum_\alpha u_\alpha(\mathbf{r}) = 1 \ . \tag{2.45}$$

The constraints imposed on $u_\alpha(\mathbf{r})$ by current conservation appear as boundary conditions on the electrostatic potential $\delta U(\mathbf{r})$. Deep inside the α-th reservoir, the interactions are completely screened, therefore an increase of the electro-chemical potential by $\delta\mu_\alpha$ raises the electrostatic potential by the same amount, i.e. $\delta U(\mathbf{r}) = \delta\mu_\alpha/e$ deep in the α-th reservoir. This implies, to first order in $\delta\mu_\alpha$:

$$\delta\mu_\alpha = e\delta U(\mathbf{r}) = u_\alpha(\mathbf{r})\delta\mu_\alpha \ . \tag{2.46}$$

This implies that,

$$u_\alpha(\mathbf{r}) = 1 \quad \text{for } r \text{ deep in the } \alpha\text{-th lead}, \tag{2.47}$$

and

$$u_\alpha(\mathbf{r}) = 0 \quad \text{for } r \text{ deep in the } \beta\text{-th lead where } \alpha \neq \beta\,. \tag{2.48}$$

Eq. (2.47) and Eq. (2.48) serve as the boundary conditions for $u_\alpha(\mathbf{r})$.

What is the equation for the characteristic potentials? Obviously, since δU satisfies a Poisson equation,

$$\nabla^2 \delta U(\mathbf{r}) = -4\pi\delta\rho(\mathbf{r}) \quad , \tag{2.49}$$

the characteristic potentials should also satisfy Poisson's equation. To derive such an equation explicitly, we need the charge density $\delta\rho(\mathbf{r})$ which is established during transport and generates the change of the potential landscape δU for the conductor. Clearly, $\delta\rho$ has two contributions: the injected charge, which comes from external reservoirs and is due to the external bias, and the induced charge, which is established throughout the conductor due to the injection of charges via electrodynamics. To make the discussion simpler, we will further partition these charges by their contributions from each lead,

$$\delta\rho_\alpha(\mathbf{r}) = \delta\rho_{injected,\alpha}(\mathbf{r}) + \delta\rho_{induced,\alpha}(\mathbf{r}) \tag{2.50}$$

where $\delta\rho_{injected,\alpha}(\mathbf{r})$ is the injected charge from the α-th lead and $\delta\rho_{induced,\alpha}(\mathbf{r})$ is the induced charge because of the injection of charges through lead α. The total charge density, which enters the right hand side of Eq. (2.49), is

$$\delta\rho(\mathbf{r}) = \sum_\alpha \delta\rho_\alpha(\mathbf{r}) \quad . \tag{2.51}$$

In the linear response regime, the external injection is proportional to the electrochemical potential change $\delta\mu_\alpha$ discussed above, and is given by [82],

$$\delta\rho_{injected,\alpha}(\mathbf{r}) = \frac{dn(\alpha,\mathbf{r})}{dE}\delta\mu_\alpha \quad . \tag{2.52}$$

This quantity can be easily calculated once the injectivity is known. The physical meaning of Eq. (2.52) is also very clear: the amount of injected charge depends on the driving force $\delta\mu_\alpha$ as well as the partial density of states of injected charges from the α-th lead.

The induced charge density is much more difficult to obtain because it is a direct consequence of electron-electron interactions. Within mean field theory, the induced charge can be formally written as a nonlocal response of the conductor to the local change of the potential landscape δU:

$$\delta\rho_{induced,\alpha}(\mathbf{r}) \;=\; -\int d\mathbf{r}'\; \Pi_\alpha(\mathbf{r},\mathbf{r}') e\delta U(\mathbf{r}') \;. \qquad (2.53)$$

The minus sign simply indicates that the induced charge is opposite in sign compared with the injected charge, and integration is over all space where the potential landscape is varied. The quantity $\Pi_\alpha(\mathbf{r},\mathbf{r}')$ is the response kernel, commonly called the Lindhard function, and it is now solely due to the charge injection through the α-th lead. Therefore the total response function is

$$\Pi(\mathbf{r},\mathbf{r}') \;=\; \sum_\alpha \Pi_\alpha(\mathbf{r},\mathbf{r}') \;. \qquad (2.54)$$

Replacing δU of Eq. (2.53) by Eq. (2.43), to first order in external perturbation, we have,

$$\delta\rho_{induced,\alpha}(\mathbf{r}) \;=\; -\int d\mathbf{r}'\; \Pi_\alpha(\mathbf{r},\mathbf{r}') \sum_\beta u_\beta(\mathbf{r})\delta\mu_\beta \;. \qquad (2.55)$$

From this equation, for a given model of the response Π_α, the induced charge can be computed once the characteristic potential is known.

Substituting Eq. (2.43), Eq. (2.51), Eq. (2.52), and Eq. (2.55) into the Poisson equation Eq. (2.49), we obtain an equation for the first order characteristic potential,

$$-\nabla^2 u_\alpha(\mathbf{r}) + 4\pi e \int d\mathbf{r}'\; \Pi(\mathbf{r},\mathbf{r}') u_\alpha(\mathbf{r}') = 4\pi e \frac{dn(\alpha,\mathbf{r})}{dE} \;. \qquad (2.56)$$

The boundary conditions for this equation are provided by Eq. (2.47) and Eq. (2.48). This equation is readily solvable, at least numerically, if we have a model for the Lindhard function Π. Unfortunately, $\Pi(\mathbf{r},\mathbf{r}')$ is extremely difficult to obtain and therefore has never been calculated from first principles for a multi-probe conductor in the mesoscopic regime. However, the physical meaning of the Lindhard function has been well understood in the development of Fermi liquid theory [86] as the nonlocal charge response, and our kernel Π is the "scattering analog" of the same concept.

In order to put the problem into a solvable form, so that we can compute the AC and nonlinear DC conductances in the diffusive mesoscopic regime, we will, in this work, use the Thomas-Fermi approximation for Π which drastically simplifies the calculation. In this approximation, the non-locality of $\Pi(\mathbf{r},\mathbf{r}')$ is neglected so that $\Pi(\mathbf{r},\mathbf{r}') \approx \delta(\mathbf{r}-\mathbf{r}')\Pi(\mathbf{r})$, indicating that the charge response in our conductor is rather localized. This is reasonable for metallic or highly doped semi-conducting samples where interactions are effectively screened. For our purposes, the Thomas-Fermi approximation provides results which give at least a good qualitative physical picture. By summing over α in Eq. (2.56) and recalling that $\sum_\alpha u_\alpha(\mathbf{r}) = 1$, we obtain,

$$\int d\mathbf{r}\ \Pi(\mathbf{r},\mathbf{r}') = \sum_\alpha \frac{dn(\alpha,\mathbf{r})}{dE} = \frac{dn(\mathbf{r})}{dE} \quad . \tag{2.57}$$

Then within the Thomas-Fermi approximation we conclude that,

$$\Pi(\mathbf{r}) \approx \frac{dn(\mathbf{r})}{dE} \quad . \tag{2.58}$$

Using this approximation, Eq. (2.56) takes on a simpler form which is numerically solvable,

$$-\nabla^2 u_\alpha(\mathbf{r}) + 4\pi e\frac{dn(\mathbf{r})}{dE}u_\alpha(\mathbf{r}) = 4\pi e\frac{dn(\alpha,\mathbf{r})}{dE} \quad . \tag{2.59}$$

Clearly, for a general multi-probe conductor there is little hope to solve this analytically in any precise fashion, and therefore it is usually solved numerically. An example of this is found in [87] where the non-equilibrium charge distribution and the electro-chemical capacitance of atomic clusters were analyzed. For theoretical and qualitative analysis, which is what we are interested in, a further approximation is usually made [88], which is the condition of local charge neutrality. This requires that the total charge be neutral at every point in space, namely $\delta\rho(\mathbf{r}) = 0$, which means that the injected charge is exactly balanced by the induced charge. Therefore, local charge neutrality implies $\nabla^2 u_\alpha = 0$, and from Eq. (2.59), we obtain

$$u_\alpha(\mathbf{r}) \ = \ \frac{dn(\alpha,\mathbf{r})}{dE} \times \left[\frac{dn(\mathbf{r})}{dE}\right]^{-1} \quad . \tag{2.60}$$

We emphasize that $u_\alpha(\mathbf{r})$ can always be directly solved from Eq. (2.59) as in [85]. For physical situations where charge polarization is not very important (such as conductors with good transmission property), local neutrality can be applied. In the rest of this work we compute the characteristic potential within the Thomas-Fermi approximation and the local neutrality condition, since these are applicable to our systems of study.

Finally, let us note that the above procedure can be generalized to higher order characteristic potentials: $u_{\alpha\beta}$, $u_{\alpha\beta\gamma}$, ... Within the Thomas-Fermi approximation the partial charge density from the α-th lead is given by [82]:

$$\delta\rho_\alpha = \frac{dn_\alpha}{dE}(\delta\mu_\alpha - e\delta U) + \frac{1}{2!}\frac{d^2n_\alpha}{dE^2}(\delta\mu_\alpha - e\delta U)^2 + \ldots \; . \tag{2.61}$$

Putting this expansion and Eq. (2.43) into Eq. (2.49) we find, after much work [83]:

$$-\nabla^2 u_{\alpha\beta}(\mathbf{r}) + 4\pi e^2 \frac{dn_\alpha}{dE} u_{\alpha\beta}(\mathbf{r}) = 4\pi e^2 \left(\frac{d^2n_\alpha}{dE^2}\delta_{\alpha\beta} - \frac{d^2n_\beta}{dE^2} u_\alpha(\mathbf{r}) \right. \tag{2.62}$$

$$\left. - \frac{d^2n_\alpha}{dE^2} u_\beta(\mathbf{r}) + \frac{d^2n}{dE^2} u_\alpha(\mathbf{r}) u_\beta(\mathbf{r}) \right) \; . \tag{2.63}$$

This provides an equation for the second order characteristic potential $u_{\alpha\beta}(\mathbf{r})$. Notice that all the quantities involved are known from the linear order calculation, thus $u_{\alpha\beta}(\mathbf{r})$ can be numerically computed. Similarly, the third order characteristic potential $u_{\alpha\beta\gamma}(\mathbf{r})$, requires the knowledge of $u_\alpha(\mathbf{r})$ and $u_{\alpha\beta}(\mathbf{r})$.

2.4 Summary

In this chapter we have elaborated Büttiker's transport theory for linear AC and non linear DC transport coefficients. The major break through in this quantum transport theory is that it respects current conservation and gauge invariance, something that most other transport theories do not satisfy. Moreover, to compute these transport coefficients all that is required is the scattering matrix $s_{\alpha n,\beta m}$, the functional derivative of the scattering matrix $\delta s_{\alpha n,\beta m}/\delta U(\mathbf{r})$, and the first order characteristic potential, $u_\alpha(\mathbf{r})$.

In summary, we have the following results:

- Linear DC conductance:

$$G_{\alpha\beta} = \frac{e^2}{h} A_{\alpha\beta}(E) \ . \tag{2.64}$$

- Second order Nonlinear DC conductance:

$$G_{\alpha\beta\gamma} = \frac{e^3}{2h} \int d\mathbf{r} \frac{\delta A_{\alpha\beta}}{\delta e U(\mathbf{r})} \left(2u_\gamma(\mathbf{r}) - \delta_{\beta\gamma}\right) \ . \tag{2.65}$$

- Linear AC conductance (emittance):

$$E_{\alpha\beta} = \int d\mathbf{r} \frac{dn_{\alpha\beta}(\mathbf{r})}{dE} - \int d\mathbf{r} \frac{dn(\mathbf{r},\alpha)}{dE} u_\beta(\mathbf{r}) \ . \tag{2.66}$$

These expressions are at the heart of our study of linear AC and nonlinear DC quantum transport phenomena.

3

Scattering matrices, Green's functions, and functional derivatives

In the previous chapter we reviewed the scattering matrix approach for computing quantum transport coefficients. The key quantities that are required to compute these quantum transport coefficients are the scattering matrix $s_{\beta m,\alpha n}$, it's functional derivative $\delta s_{\beta m,\alpha n}/\delta U(\mathbf{r})$ and the characteristic potentials $u_\alpha(\mathbf{r})$. While $s_{\beta m,\alpha n}$ can be readily calculated, in contrast we have that $\delta s_{\beta m,\alpha n}/\delta U(\mathbf{r})$ is extremely difficult to compute.

A direct way to compute $\delta s_{\alpha n,\beta m}/\delta U(\mathbf{r})$ for a multi-probe conductor is to follows the procedure in [77]. First, we calculate the scattering matrix $s_{\alpha n,\beta m}$ for the conductor. Next, we add an extra localized scattering potential $\delta U(\mathbf{r}) = \delta U \delta(\mathbf{r} - \mathbf{r}')$ inside the conductor at position $\mathbf{r}'$, where δU is infinitesimal. We then evaluate the new scattering matrix, $s'_{\alpha n,\beta m}$ under the perturbation of $\delta U(\mathbf{r})$. The functional derivative is then given by the limit $\delta U \rightarrow 0$: $\delta s_{\alpha n,\beta m}/\delta U(\mathbf{r}) = (s'_{\alpha n,\beta m} - s_{\alpha n,\beta m})/\delta U$. This procedure is then carried out for each spatial point $\mathbf{r}$ of the multi-probe conductor. Clearly, this method of computing functional derivative is extremely time consuming, and thus quickly becomes impractical when dealing with 2D systems.

In our work, we derive from first principles an expression for the functional derivative of the scattering matrix for a multi-probe conductor. The analytical expression for the functional derivative is expressed in terms of the Green's function and the wave function, which are quantities that are directly computable. Combining this result with a new relation between the wave function and the Green's function leads us to a simple expression for the $\delta s_{\alpha n,\beta m}/\delta U(\mathbf{r})$ in terms of $\psi_{\alpha n}(\mathbf{r})$.

In this chapter we derive an expression for the emittance, $E_{\alpha\beta}$, and the nonlinear conductance, $G_{\alpha\beta\gamma}$, which only requires the scattering matrix and the scattering wave function. These results are used later when we study emittance and nonlinear conductance fluctuations in the diffusive regime. In Section 3.1 we derive expressions for the functional derivatives of the Green's function, the wave function, and the scattering matrix. In Section 3.2 we review the Fisher-Lee relation [89]. This sets up the work in Section 3.3, where we derive the generalized Fisher-Lee relation, which relates the Green's function to the wave function in a way which is similar to the usual Fisher-Lee relation. In Section 3.4 a generalized proof is used to extend the result to Bloch states and multi-probe systems. In the final section we combine the results from the previous sections with those from Chapter 2. This leads us to new expressions for $E_{\alpha\beta}$ and $G_{\alpha\beta\gamma}$, which are easy to evaluate.

3.1 Functional Derivatives

In the previous chapter we derived expressions for the quantum transport coefficients for AC and DC transport. To compute these expressions we must first calculate the functional derivative of the scattering matrix $\delta s_{\beta m,\alpha n}/\delta U(\mathbf{r})$. This quantity arises from the derivative of the scattering matrix with respect to the bias potential via the chain rule,

$$\frac{\partial s_{\beta m,\alpha n}}{\partial V_\gamma} = \int d\mathbf{r} \frac{\delta s_{\beta m,\alpha n}}{\delta U(\mathbf{r})} \frac{\partial U(\mathbf{r})}{\partial V_\gamma} \ . \tag{3.1}$$

One can understand this equation in the following way. The scattering matrix $s_{\beta m,\alpha n}$ corresponds to a solution $\psi_{\alpha n}$ to Schrödinger's equation. The electrostatic potential $U(\mathbf{r})$ in Schrödinger's equation is a solution to Poisson's equation with boundary conditions given by the bias potentials $\{V_\gamma\}$. This implies that a small change in the bias potentials δV_γ leads to a change in the electrostatic potential $\delta U(\mathbf{r})$, which in turn induces a change in the scattering wave functions $\psi_{\alpha n}$, which leads to a change in the scattering matrix $\delta s_{\beta m,\alpha n}$.

Note that the integration in the above equation is nothing more than the continuous version of the chain rule. In the discretised version of this system we replace the function $U(\mathbf{r})$ with a collection of variables $\{U_i\}$, which represent the value of the electrostatic potential in the discretised scattering region. This leads to the following substitution: $s_{\beta m,\alpha n}[U(\mathbf{r})] \to s_{\beta m,\alpha n}(\{U_i\})$. Applying the usual chain rule we find,

$$\frac{\delta s_{\beta m,\alpha n}(\{U_k\})}{\delta V_\gamma} = \sum_i \frac{\delta s_{\beta m,\alpha n}(\{U_k\})}{\delta U_i}\frac{\partial U_i}{\partial V_\gamma} \to \int d\mathbf{r}\frac{\delta s_{\beta m,\alpha n}[U(\mathbf{r})]}{\delta U(\mathbf{r})}\frac{\partial U(\mathbf{r})}{\partial V_\gamma} \ , \tag{3.2}$$

where we have taken the continuous limit in the last step.

In the following section we derive a general formula for the functional derivatives of the scattering matrix. This is accomplished by first computing the functional derivatives of the Green's function using Dyson's equation. The Lippmann-Schwinger equation is then used to obtain an expression for the functional derivatives of the scattering wave functions. Finally, the previous results are used to obtain an expression for the functional derivatives of the scattering matrix. To summarize, we compute in the following order: $\delta G/\delta U \to \delta\psi_{\alpha n}/\delta U \to \delta s_{\beta m,\alpha n}/\delta U$.

3.1.1 Functional Derivatives of the Green's function

By definition the functional derivative of any physical quantity is its response to an infinitesimal delta-function perturbation, $\delta U(\mathbf{r}) = \delta U\delta(\mathbf{r}-\bar{\mathbf{r}})$, where $\bar{\mathbf{r}}$ is located inside the scattering region. Formally, the functional derivative of the Green's function is given by

$$\frac{\delta G(\mathbf{r},\mathbf{r}')}{\delta U(\bar{\mathbf{r}})} = \lim_{\delta U\to 0}\frac{G[U(\mathbf{r})+\delta U\delta(\mathbf{r}-\bar{\mathbf{r}})](\mathbf{r},\mathbf{r}') - G[U(\mathbf{r})](\mathbf{r},\mathbf{r}')}{\delta U} \ , \tag{3.3}$$

where we explicitly show the Green's function dependence on the potential, $U(\mathbf{r})$. The Taylor expansion of the Green's function provides a way to obtain the functional derivative,

$$G[U(\mathbf{r})+\delta U(\mathbf{r})](\mathbf{r},\mathbf{r}') = G[U(\mathbf{r})](\mathbf{r},\mathbf{r}') + \frac{\delta G(\mathbf{r},\mathbf{r}')}{\delta U(\bar{\mathbf{r}})}\delta U + \dots \ . \tag{3.4}$$

To obtain such an expansion Dyson's equation is used.

Let the Hamiltonian $\hat{H}$ represent a free system and $G(\mathbf{r},\mathbf{r}')$ be its corresponding Green's function. We add a perturbation potential $V(\mathbf{r})$ to this system which leads to a new Hamiltonian $\hat{H}_V = \hat{H} + V(\mathbf{r})$ and a new Green's function $G_V(\mathbf{r},\mathbf{r}')$. Dyson's equation relates $G_V(\mathbf{r},\mathbf{r}')$ to $G(\mathbf{r},\mathbf{r}')$ and $V(\mathbf{r})$ via,

$$G_V(\mathbf{r},\mathbf{r}') = G(\mathbf{r},\mathbf{r}') + \int d\mathbf{r}''G(\mathbf{r},\mathbf{r}'')V(\mathbf{r}'')G_V(\mathbf{r}'',\mathbf{r}') \ . \tag{3.5}$$

It is straight forward to show that

$$\hat{H}_V G_V(\mathbf{r}, \mathbf{r}') = -\delta(\mathbf{r} - \mathbf{r}') \ . \tag{3.6}$$

Applying Dyson's equation Eq. (3.5) to the situation where $V(\mathbf{r}) = \delta U(\mathbf{r}) = \delta U \delta(\mathbf{r} - \bar{\mathbf{r}})$, we find

$$\begin{aligned} G_{\delta U}(\mathbf{r}, \mathbf{r}') &= G(\mathbf{r}, \mathbf{r}') + \int d\mathbf{r}'' G(\mathbf{r}, \mathbf{r}') \delta U(\mathbf{r}'') G_{\delta U}(\mathbf{r}'', \mathbf{r}') \\ &= G(\mathbf{r}, \mathbf{r}') + \int d\mathbf{r}'' G(\mathbf{r}, \mathbf{r}'') \delta U \delta(\mathbf{r}'' - \bar{\mathbf{r}}) G_{\delta U}(\mathbf{r}'', \mathbf{r}') \\ &= G(\mathbf{r}, \mathbf{r}') + \delta U G(\mathbf{r}, \bar{\mathbf{r}}) G_{\delta U}(\bar{\mathbf{r}}, \mathbf{r}') \ . \end{aligned} \tag{3.7}$$

Setting $\mathbf{r} = \bar{\mathbf{r}}$ we obtain an equation for $G_{\delta U}(\bar{\mathbf{r}}, \mathbf{r}')$,

$$G_{\delta U}(\bar{\mathbf{r}}, \mathbf{r}') = G(\bar{\mathbf{r}}, \mathbf{r}') + \delta U G(\bar{\mathbf{r}}, \bar{\mathbf{r}}) G_{\delta U}(\bar{\mathbf{r}}, \mathbf{r}') \ . \tag{3.8}$$

Solving for $G_{\delta U}(\bar{\mathbf{r}}, \mathbf{r}')$,

$$\begin{aligned} G_{\delta U}(\bar{\mathbf{r}}, \mathbf{r}') &= [1 - \delta U \eta]^{-1} G(\bar{\mathbf{r}}, \mathbf{r}') \qquad (3.9) \\ &= G(\bar{\mathbf{r}}, \mathbf{r}') + \delta U \eta G(\bar{\mathbf{r}}, \mathbf{r}') - \ldots \ , \end{aligned}$$

where we have set $\eta = G(\bar{\mathbf{r}}, \bar{\mathbf{r}})$ and we have expanded $[1 - \delta U \eta]^{-1}$. Putting this expansion into Eq. (3.7),

$$\begin{aligned} G_{\delta U}(\mathbf{r}, \mathbf{r}') &= G(\mathbf{r}, \mathbf{r}') + \delta U G(\mathbf{r}, \bar{\mathbf{r}}) G_{\delta U}(\bar{\mathbf{r}}, \mathbf{r}') \\ &= G(\mathbf{r}, \mathbf{r}') + \delta U G(\mathbf{r}, \bar{\mathbf{r}}) \left(G(\bar{\mathbf{r}}, \mathbf{r}') + \delta U \eta G(\bar{\mathbf{r}}, \mathbf{r}') - \ldots \right) \\ &= G(\mathbf{r}, \mathbf{r}') + \delta U G(\mathbf{r}, \bar{\mathbf{r}}) G(\bar{\mathbf{r}}, \mathbf{r}') - \ldots \ . \end{aligned} \tag{3.10}$$

Comparing this equation with Eq. (3.4), we find,

$$\frac{\delta G(\mathbf{r}, \mathbf{r}')}{\delta U(\bar{\mathbf{r}})} = G(\mathbf{r}, \bar{\mathbf{r}}) G(\bar{\mathbf{r}}, \mathbf{r}') \ . \tag{3.11}$$

This expression has been derived for 1D cases [90].

We now obtain an expression for the second order functional derivative of the Green's function. This is obtained by the following:

$$\frac{\delta^2 G(\mathbf{r}, \mathbf{r}')}{\delta U(\mathbf{r}_2) \delta U(\mathbf{r}_1)} = \frac{\delta}{\delta U(\mathbf{r}_2)} \left(\frac{\delta G(\mathbf{r}, \mathbf{r}')}{\delta U(\mathbf{r}_1)} \right)$$

$$
\begin{aligned}
&= \frac{\delta}{\delta U(\mathbf{r}_2)}\left(G(\mathbf{r},\mathbf{r}_1)G(\mathbf{r}_1,\mathbf{r}')\right) \\
&= \left(\frac{\delta}{\delta U(\mathbf{r}_2)}G(\mathbf{r},\mathbf{r}_1)\right)G(\mathbf{r}_1,\mathbf{r}') + G(\mathbf{r},\mathbf{r}_1)\left(\frac{\delta}{\delta U(\mathbf{r}_2)}G(\mathbf{r}_1,\mathbf{r}')\right) \\
&= G(\mathbf{r},\mathbf{r}_2)G(\mathbf{r}_2,\mathbf{r}_1)G(\mathbf{r}_1,\mathbf{r}') + G(\mathbf{r},\mathbf{r}_1)G(\mathbf{r}_1,\mathbf{r}_2)G(\mathbf{r}_2,\mathbf{r}')\ .
\end{aligned}
$$

This last equation can be cast into the following form:

$$
\frac{\delta^2 G(\mathbf{r},\mathbf{r}')}{\delta U(\mathbf{r}_2)\delta U(\mathbf{r}_1)} = \sum_{P\in S_2} G(\mathbf{r},\mathbf{r}_{P(1)})G(\mathbf{r}_{P(1)},\mathbf{r}_{P(2)})G(\mathbf{r}_{P(2)},\mathbf{r}')\ , \tag{3.12}
$$

where S_2 is the group of all permutations of two elements and $P(i)$ is the i-th element of the group. In this notation it is straight forward to show, by induction, that the N-th order functional derivative of the Green's function is given by:

$$
\frac{\delta^N G(\mathbf{r},\mathbf{r}')}{\delta U(\mathbf{r}_N)...\delta U(\mathbf{r}_2)\delta U(\mathbf{r}_1)} = \sum_{P\in S_N} G(\mathbf{r},\mathbf{r}_{P(1)})G(\mathbf{r}_{P(1)},\mathbf{r}_{P(2)})\ ...\ G(\mathbf{r}_{P(N-1)},\mathbf{r}_{P(N)})G(\mathbf{r}_{P(N)},\mathbf{r}')\ ,
$$

where S_N is the group of all permutations of N elements. We now have an explicit expression for all the functional derivatives of the Green's function. Let us now compute the functional derivatives of the scattering wave functions.

3.1.2 *Functional Derivatives of the Scattering Wave function*

To compute the functional derivative of the wave function we use, once again, the Taylor expansion,

$$
\psi_{\delta U}(\mathbf{r}) = \psi(\mathbf{r}) + \frac{\delta\psi(\mathbf{r})}{\delta U(\bar{\mathbf{r}})}\delta U + ...\ . \tag{3.13}
$$

In the previous section we obtained an explicit expression for the Taylor expansion by using Dyson's equation, which related $G(\mathbf{r},\mathbf{r}')$ to $G_{\delta U}(\mathbf{r},\mathbf{r}')$. The analogous equation for wave function is the Lippmann-Schwinger equation. Let $\psi(\mathbf{r})$ be the wave function for a free system, $\psi_V(\mathbf{r})$ be the wave function for the perturbed system, and $V(\mathbf{r})$ be the perturbation potential. Then the Lippmann-Schwinger equation is given by,

$$
\psi_V(\mathbf{r}) = \psi(\mathbf{r}) + \int d\mathbf{r}' G_V(\mathbf{r},\mathbf{r}')V(\mathbf{r}')\psi(\mathbf{r}')\ , \tag{3.14}
$$

where $G_V(\mathbf{r},\mathbf{r}')$ is the Green's function of the perturbed system. It is not difficult to show that $\psi_V(\mathbf{r})$ satisfies Schrödinger's equation for the Hamiltonian $H_V = H_0 + V$.

Setting $V(\mathbf{r}) = \delta U(\mathbf{r}) = \delta U \delta(\mathbf{r} - \bar{\mathbf{r}})$, we obtain

$$\begin{aligned} \psi_{\delta U}(\mathbf{r}) &= \psi(\mathbf{r}) + \int d\mathbf{r}' G_{\delta U}(\mathbf{r}, \mathbf{r}') \delta U \delta(\mathbf{r}' - \bar{\mathbf{r}}) \psi(\mathbf{r}') \\ &= \psi(\mathbf{r}) + \delta U G_{\delta U}(r, \bar{\mathbf{r}}) \psi(\bar{\mathbf{r}}) \ . \end{aligned} \tag{3.15}$$

Substituting Eq. (3.10) into Eq. (3.15),

$$\begin{aligned} \psi_{\delta U}(\mathbf{r}) &= \psi(\mathbf{r}) + \delta U G_{\delta U}(\mathbf{r}, \bar{\mathbf{r}}) \psi(\bar{\mathbf{r}}) \\ &= \psi(\mathbf{r}) + \delta U \left(G(\mathbf{r}, \bar{\mathbf{r}}) + \delta U G(\mathbf{r}, \bar{\mathbf{r}}) G(\bar{\mathbf{r}}, \bar{\mathbf{r}}) + \ldots \right) \psi(\bar{\mathbf{r}}) \\ &= \psi(\mathbf{r}) + \delta U G(\mathbf{r}, \bar{\mathbf{r}}) \psi(\bar{\mathbf{r}}) + \ldots \ . \end{aligned} \tag{3.16}$$

Comparing Eq. (3.13) and Eq. (3.16), we conclude,

$$\frac{\delta \psi(\mathbf{r})}{\delta U(\bar{\mathbf{r}})} = G(\mathbf{r}, \bar{\mathbf{r}}) \psi(\bar{\mathbf{r}}) \ . \tag{3.17}$$

We can now compute higher order functional derivatives. The second order functional derivative of the wavefunction is given by,

$$\begin{aligned} \frac{\delta^2 \psi(\mathbf{r})}{\delta U(\mathbf{r}_2) \delta U(\mathbf{r}_1)} &= \frac{\delta}{\delta U(\mathbf{r}_2)} \left(\frac{\delta \psi(\mathbf{r})}{\delta U(\mathbf{r}_1)} \right) \\ &= \frac{\delta}{\delta U(\mathbf{r}_2)} \left(G(\mathbf{r}, \mathbf{r}_1) \psi(\mathbf{r}_1) \right) \\ &= \left(\frac{\delta}{\delta U(\mathbf{r}_2)} G(\mathbf{r}, \mathbf{r}_1) \right) \psi(\mathbf{r}_1) + G(\mathbf{r}, \mathbf{r}_1) \left(\frac{\delta}{\delta U(\mathbf{r}_2)} \psi(\mathbf{r}_1) \right) \\ &= G(\mathbf{r}, \mathbf{r}_2) G(\mathbf{r}_2, \mathbf{r}_1) \psi(\mathbf{r}_1) + G(\mathbf{r}, \mathbf{r}_1) G(\mathbf{r}_1, \mathbf{r}_2) \psi(\mathbf{r}_2) \ . \end{aligned} \tag{3.18}$$

This last expression can be written in the following form:

$$\frac{\delta^2 \psi(\mathbf{r})}{\delta U(\mathbf{r}_2) \delta U(\mathbf{r}_1)} = \sum_{P \in S_2} G(\mathbf{r}, \mathbf{r}_{P(1)}) G(\mathbf{r}_{P(1)}, \mathbf{r}_{P(2)}) \psi(\mathbf{r}_{P(2)}) \ , \tag{3.19}$$

where, once again, S_2 is the group of permutations of two elements and $P(i)$ is the i-th element of the group. Finally, by induction we find the N-th order functional derivative:

$$\frac{\delta^N \psi(\mathbf{r})}{\delta U(\mathbf{r}_N) \ldots \delta U(\mathbf{r}_2) \delta U(\mathbf{r}_1)} = \sum_{P \in S_N} G(\mathbf{r}, \mathbf{r}_{P(1)}) G(\mathbf{r}_{P(1)}, \mathbf{r}_{P(2)}) \ldots G(\mathbf{r}_{P(N-1)}, \mathbf{r}_{P(N)}) \psi(\mathbf{r}_{P(N)}) \ .$$

We will now obtain a general expression for the functional derivatives of the scattering matrix.

3.1.3 Functional Derivatives of the Scattering Matrix

Up to now we have not worried about the type of leads for our quantum conductor. Theoretically, the leads of a conductor are mostly modeled by jellium leads where there is no atomic structure: a lead is a perfect quasi-1D quantum wire where the confining potential of the wire is assumed to be either hard or soft. A hard wall potential means the confining potential has a step function profile which is infinitely high at the wall. A soft wall, on the other hand, is modeled by a potential of finite height which spatially extends to infinity away from the wall. Jellium leads are easy to model because the electrons wavefunction along the leads are plane waves, as we have assumed so far. More recently, quantum transport measurements on atomic and molecular scale nano-electronic systems have received great attention [91, 92, 93, 94, 95, 24, 96, 97] because they represent the ultimate size limit of functional devices. The current-voltage (*I*-*V*) characteristics of these atomic and molecular systems have promising characteristics for device applications, including high nonlinearity, negative differential resistance, electro-mechanic and electrostatic current switching [92, 93, 94, 95, 97]. Demonstrations of molecular based logic gates [92] and non-volatile random access memory device [93, 95] have already been made, and clearly point to the exciting possibility of molecular computing machinery [92]. For these molecular devices, the leads are atomic: they have their own discrete translational symmetry, represented by a collection of atoms at positions $\{\mathbf{R}_I\}$. Therefore, it is useful to consider atomic leads as well as the simpler jellium leads.

All the equations derived so far are valid for jellium as well as atomic leads. In contrast to the Green's function and the wavefunction, the functional derivatives of the scattering matrix depends on the details of the leads that we are modeling. In this section we first derive an expression for the N-th order functional derivative of the scattering matrix for jellium leads. We will then derive the analogous result for a system with atomic leads.

The scattering matrix for a quantum conductor with jellium leads is defined by

[73],

$$\psi_{\alpha n}(\mathbf{r}_\beta) = \sum_{\beta,m}\left[\delta_{\beta\alpha}\delta_{mn}\phi_{\alpha n}(y_\alpha)e^{ik_{\alpha n}\cdot x_\alpha} + \sqrt{\frac{v_{\alpha n}}{v_{\beta m}}}s_{\beta m,\alpha n}\phi_{\beta m}(y_\beta)e^{-ik_{\beta m}\cdot x_\beta}\right] \;, \tag{3.20}$$

where $\mathbf{r}_\beta = (x_\beta, y_\beta)$ are local coordinate systems such that $x_\beta = 0$ is the position of the boundary between the scattering region and β-th lead, $v_{\beta m}$ is the Fermi velocity for the m-th subband in the β-th lead, and $\phi_{\beta m}(y_\beta)$ is the m-th transverse eigenfunction in the β-th lead. This relation between $\psi_{\alpha n}$ and $s_{\beta m,\alpha n}$ can be inverted to obtain an expression for the scattering matrix in terms of the wavefunction,

$$s_{\beta m,\alpha n} = -\delta_{\beta\alpha}\delta_{nm} + \sqrt{\frac{v_{\beta m}}{v_{\alpha n}}}\int_{C_\beta} dy_\beta\phi_{\beta m}(y_\beta)\psi_{\alpha n}(y_\beta, x_\beta = 0) \;, \tag{3.21}$$

where C_β is the boundary surface between the β-th lead and the scattering region, in order to simplify the notation. From now on, x_β represents the position of the boundary between the the β-th lead and the scattering region.

The strategy for computing the $\delta s_{\beta m,\alpha n}/\delta U(\mathbf{r})$ is to apply the results of the two previous sections in combination with Eq. (3.21). Note that the transverse eigenfunction in the leads, $\{\phi_{\beta m}\}$, are unaffected by the presence of a delta function perturbation, $\delta U(\mathbf{r}) = \delta U\delta(\mathbf{r} - \bar{\mathbf{r}})$, in the scattering region. Thus, it is a constant from the point of view of the functional derivative. This leads to the following result,

$$\begin{aligned}
\frac{\delta s_{\beta m,\alpha n}}{\delta U(\mathbf{r})} &= \frac{\delta}{\delta U(\mathbf{r})}\left(\sqrt{\frac{v_{\beta m}}{v_{\alpha n}}}\int_{C_\beta} dy'\phi_{\beta m}(y')\psi_{\alpha n}(x_\beta, y')\right) \\
&= \sqrt{\frac{v_{\beta m}}{v_{\alpha n}}}\int_{C_\beta} dy'\phi_{\beta m}(y')\left(\frac{\delta\psi_{\alpha n}(x_\beta, y')}{\delta U(\mathbf{r})}\right) \\
&= \sqrt{\frac{v_{\beta m}}{v_{\alpha n}}}\int_{C_\beta} dy'\phi_{\beta m}(y')\left(G(x_\beta, y'; \mathbf{r})\psi_{\alpha n}(\mathbf{r})\right) \\
&= \sqrt{\frac{v_{\beta m}}{v_{\alpha n}}}\left(i\hbar v_{\beta m}\int_{C_\beta} dy'\phi_{\beta m}(y')G(x_\beta, y'; \mathbf{r})\right)\psi(\mathbf{r}) \\
&= \frac{-i}{\hbar\sqrt{v_{\beta m}v_{\alpha n}}}\bar{\psi}_{\beta m}(\mathbf{r})\psi_{\alpha n}(\mathbf{r}) \,,
\end{aligned} \tag{3.22}$$

where we have introduced the function $\bar{\psi}_{\beta m}(x, y)$:

$$\bar{\psi}_{\beta m}(\mathbf{r}) \equiv i\hbar v_{\beta m}\int_{C_\beta} dy'\phi_{\beta m}(y')G(x_\beta, y'; \mathbf{r}) \,. \tag{3.23}$$

To compute the higher order derivatives first notice that,

$$\begin{aligned}
\frac{\delta\bar{\psi}_{\beta m}(\mathbf{r})}{\delta U(\bar{\mathbf{r}})} &= \frac{\delta}{\delta U(\bar{\mathbf{r}})}\left(i\hbar v_{\beta m}\int_{C_\beta} d\mathbf{r}'\phi_{\beta m}(x_\beta,y')G(x_\beta,y';\mathbf{r})\right) \\
&= i\hbar v_{\beta m}\int_{C_\beta} d\mathbf{r}'\phi_{\beta m}(x_\beta,y')\left(\frac{\delta}{\delta U(\bar{\mathbf{r}})}G(x_\beta,y';\mathbf{r})\right) \\
&= i\hbar v_{\beta m}\int_{C_\beta} d\mathbf{r}'\phi_{\beta m}(x_\beta,y')\left(G(x_\beta,y';\bar{\mathbf{r}})G(\bar{\mathbf{r}},\mathbf{r})\right) \\
&= \left(i\hbar v_{\beta m}\int_{C_\beta} d\mathbf{r}'\phi_{\beta m}(x_\beta,y')G(x_\beta,y';\bar{\mathbf{r}})\right)G(\bar{\mathbf{r}},\mathbf{r}) \\
&= \bar{\psi}_{\beta m}(\bar{\mathbf{r}})G(\bar{\mathbf{r}},\mathbf{r}) \ .
\end{aligned} \tag{3.24}$$

Let us now compute the second order functional derivative of the scattering matrix,

$$\begin{aligned}
\frac{\delta^2 s_{\beta m,\alpha n}}{\delta U(\mathbf{r}_2)\delta U(\mathbf{r}_1)} &= \frac{\delta}{\delta U(\mathbf{r}_2)}\left(\frac{\delta s_{\beta m,\alpha n}}{\delta U(\mathbf{r}_1)}\right) \\
&= \frac{\delta}{\delta U(\mathbf{r}_2)}\left(\frac{-i}{\hbar\sqrt{v_{\beta m}v_{\alpha n}}}\bar{\psi}_{\beta m}(\mathbf{r}_1)\psi_{\alpha n}(\mathbf{r}_1)\right) \\
&= \frac{-i}{\hbar\sqrt{v_{\beta m}v_{\alpha n}}}\left[\frac{\delta\bar{\psi}_{\beta m}(\mathbf{r}_1)}{\delta U(\mathbf{r}_2)}\psi_{\alpha n}(\mathbf{r}_1) + \bar{\psi}_{\beta m}(\mathbf{r}_1)\frac{\delta\psi_{\alpha n}(\mathbf{r}_1)}{\delta U(\mathbf{r}_2)}\right] \\
&= \frac{-i}{\hbar\sqrt{v_{\beta m}v_{\alpha n}}}\left[\bar{\psi}_{\beta m}(\mathbf{r}_2)G(\mathbf{r}_2,\mathbf{r}_1)\psi_{\alpha n}(\mathbf{r}_1) + \bar{\psi}_{\beta m}(\mathbf{r}_1)G(\mathbf{r}_1,\mathbf{r}_2)\psi_{\beta m}(\mathbf{r}_2)\right] \ .
\end{aligned}$$

This last equation can be rewritten in the following form:

$$\frac{\delta^2 s_{\alpha n,\beta m}}{\delta U(\mathbf{r}_2)\delta U(\mathbf{r}_1)} = \frac{-i}{\hbar\sqrt{v_{\beta m}v_{\alpha n}}}\sum_{P\in S_2}\bar{\psi}_{\alpha n}(\mathbf{r}_{P(1)})G(\mathbf{r}_{P(1)},\mathbf{r}_{P(2)})\psi_{\beta m}(\mathbf{r}_{P(2)}) \ . \tag{3.25}$$

Finally, by induction we find that the N-th order functional derivative of the scattering matrix is given by,

$$\begin{aligned}
\frac{\delta^N s_{\alpha n,\beta m}}{\delta U(\mathbf{r}_N)...\delta U(\mathbf{r}_2)\delta U(\mathbf{r}_1)} &= \frac{-i}{\hbar\sqrt{v_{\beta m}v_{\alpha n}}} \\
&\quad \sum_{P\in S_N}\bar{\psi}_{\alpha n}(\mathbf{r}_{P(1)})G(\mathbf{r}_{P(1)},\mathbf{r}_{P(2)})...G(\mathbf{r}_{P(N-1)},\mathbf{r}_{P(N)})\psi_{\beta m}(\mathbf{r}_{P(N)}) \ .
\end{aligned} \tag{3.26}$$

Let us derive the analogous result for a quantum device attached to atomic leads. The scattering matrix for a system with asymptotic states given by Bloch states is defined by,

$$\psi_{\alpha n}(\mathbf{r}_\beta) = \sum_{\beta,m}\left[\delta_{\beta\alpha}\delta_{mn}\phi^{(in)}_{\alpha n}(\mathbf{r}_\alpha) + \sqrt{\frac{v_{\alpha n}}{v_{\beta m}}}s_{\beta m,\alpha n}\phi^{(out)}_{\beta m}(\mathbf{r}_\beta)\right] \ , \tag{3.27}$$

where $\{\phi^{(in)}_{\alpha n}\}$ are the incoming Bloch states in the n-th subband in the α-th lead and $\{\phi^{(out)}_{\alpha n}\}$ are the outgoing Bloch states in the m-th subband in the β-th lead. This relation can be inverted to obtain an expression for the scattering matrix in terms of the scattering wavefunction,

$$s_{\beta m,\alpha n} = -\delta_{\beta\alpha} I_{nm} + \sqrt{\frac{v_{\beta m}}{v_{\alpha n}}} \int_{C_\beta} d\mathbf{r}' \phi^{(out)\dagger}_{\beta m}(\mathbf{r}')\psi_{\alpha n}(\mathbf{r}') \ , \tag{3.28}$$

where

$$I_{nm} \equiv \int_{C_\beta} d\mathbf{r}\phi^{(in)}_{\alpha m}(\mathbf{r}')\phi^{(out)\dagger}_{\alpha n}(\mathbf{r}') \ , \tag{3.29}$$

where C_β is the first unit cell outside the scattering region at the boundary with the β-th lead region and $\phi^{(out)\dagger}_{\alpha n}$ is the dual of the n-th subband Bloch state in the β-th lead. With this expression it follows from our previous derivation that first order functional derivative of the scattering matrix is given by,

$$\frac{\delta s_{\beta m,\alpha n}}{\delta U(\mathbf{r})} = \frac{-i}{\hbar\sqrt{v_{\beta m}v_{\alpha n}}}\bar{\psi}_{\beta m}(\mathbf{r})\psi_{\alpha n}(\mathbf{r}) \ , \tag{3.30}$$

where

$$\bar{\psi}_{\beta m}(\mathbf{r}) \equiv i\hbar v_{\beta m} \int_{C_\beta} d\mathbf{r}' \phi^{(out)\dagger}_{\beta m}(\mathbf{r}')G(\mathbf{r}',\mathbf{r}) \ . \tag{3.31}$$

To obtain the higher order functional derivatives it suffices to notice that Eq. (3.24) is valid for Bloch states. It then follows that the N-th order functional derivative of the scattering matrix for such a Bloch system has the same form as Eq. (3.26) except that $\bar{\psi}_{\beta m}(\mathbf{r})$ is replaced by Eq. (3.31).

To summarize, we have derived a general expression for the functional derivatives of the scattering matrix from first principles. These results provide a systematic way to compute the functional derivatives of scattering matrix. Next, we find an expression for the scattering wavefunction in terms of the Green's function. This will allow us to express the first order functional derivative of the scattering matrix, $\delta s_{\alpha n,\beta m}/\delta U(\mathbf{r})$, in terms of the wavefunction, $\psi_{\beta m}(\mathbf{r})$.

3.2 The Fisher-Lee Relation for Jellium leads

The scattering matrix tells us the response at one lead given an excitation by an incoming carrier at another. The Green's function, on the other hand, has much more information. It knows the response of the system at an arbitrary point x in space given an excitation originating at x'. Since the Green's function has full knowledge of how a conductor reacts to an arbitrary excitation, it must also contain the scattering matrix. Then we should be able to extract the scattering matrix from the Green's function. The equation that relates the scattering matrix to the Green's function is known as the Fisher-Lee relation [89]. We now give an informal derivation of this relationship following [5].

Consider a device connected to a set of leads. We use a local coordinate system where the boundary of the scattering region with the β-th lead is located at $x_\beta = 0$. We express the Green's function evaluated at the boundaries in the following notation,

$$G_{\beta\alpha}(y_\beta; y_\alpha) \equiv G(x_\beta = 0, y_\beta; x_\alpha = 0, y_\alpha) \ . \tag{3.32}$$

We now express the above Green's function in terms of the scattering matrix. To simplify the situation, for the moment, we ignore the transverse degrees of freedom and treat the system as if it was one dimensional. We know that a unit excitation at $x_\alpha = 0$ gives rise to an wave amplitude A_α^- moving away from the conductor and a wave amplitude A_β^+ moving towards to conductor. The wave going towards the conductor will be scattered into different leads, which leads us to,

$$G_{\beta\alpha} = \delta_{\beta\alpha} A_\alpha^- + S_{\beta\alpha} A_\beta^+ \ . \tag{3.33}$$

It can be shown [5], using the Green's function continuity equations, that

$$A_\beta^+ = A_\beta^- = -\frac{i}{\hbar v_\beta} \ . \tag{3.34}$$

The conventional normalization for the scattering matrix is

$$S_{\beta\alpha} = \sqrt{\frac{v_\beta}{v_\alpha}} s_{\beta\alpha} \ . \tag{3.35}$$

Combining the above equations we find the following result,

$$s_{\beta\alpha} = -\delta_{\beta\alpha} + i\hbar\sqrt{v_\alpha v_\beta} G_{\beta\alpha} \ . \tag{3.36}$$

This is the Fisher-Lee relation in one dimension.

To obtain the multi-mode version of this equation first notice that Eq. (3.33) becomes,

$$G_{\beta\alpha}(y_\beta; y_\alpha) = \sum_{n\in\alpha}\sum_{m\in\beta} \phi_{\alpha n}(y_\alpha)\left[\delta_{\beta\alpha}\delta_{nm}A^-_{\alpha n} + S_{\beta m,\alpha n}A^+_{\beta m}\right]\phi_{\beta m}(y_\beta) \ , \tag{3.37}$$

when the transverse degrees of freedom are taken into account. From the Green's function continuity equations it can be shown [5],

$$A^+_{\beta m} = A^-_{\beta m} = -\frac{i}{\hbar v_{\beta m}} \ . \tag{3.38}$$

The conventional normalization for the multi-mode scattering matrix is,

$$S_{\beta m,\alpha n} = \sqrt{\frac{v_{\beta m}}{v_{\alpha n}}}\, s_{\beta m,\alpha n} \ . \tag{3.39}$$

Therefore,

$$G_{\beta\alpha}(y_\beta; y_\alpha) = \sum_{n\in\alpha}\sum_{m\in\beta} \frac{-i}{\hbar\sqrt{v_{\alpha n}v_{\beta m}}}\phi_{\alpha n}(y_\alpha)\left[\delta_{nm}\delta_{\alpha\beta} + s_{\beta m,\alpha n}\right]\phi_{\beta m}(y_\beta) \, . \tag{3.40}$$

To obtain an equation for the scattering matrix in terms of the Green's function, we invert Eq. (3.40),

$$s_{\beta m,\alpha n} = -\delta_{\alpha\beta}\delta_{nm} + i\hbar\sqrt{v_{\beta m}v_{\alpha n}}\int\!\!\int dy'dy''\phi_{\beta m}(y')G(x_\beta, y'; x_\alpha, y'')\phi_{\alpha n}(y'') \tag{3.41}$$

This is the higher dimensional version of the Fisher-Lee relation.

3.3 The Generalized Fisher-Lee Relation for Jellium leads

In general, we may consider $G(\mathbf{r}, \mathbf{r}')$ to be the electron probability amplitude at position $\mathbf{r}$ given a delta-function excitation at another position $\mathbf{r}'$. The wavefunction, on the other hand, is the probability amplitude for an electron to be at a position $\mathbf{r}$ given some initial probability amplitude. Therefore, the information contained in the wavefunction is also contained in the Green's function.

Let us now prove the following relation between the wavefunction and the Green's function:

$$\psi_{\alpha n}(\mathbf{r}) = i\hbar v_{\alpha n}\int_{C_\alpha} dy'\phi_{\alpha n}(y')G(x_\alpha, y'; \mathbf{r}) \ , \tag{3.42}$$

where $\mathbf{r}$ is located inside the scattering region. We call this equation the Generalized Fisher-Lee relation.

To prove Eq. (3.42) we will first show by direct computation that the relation is true for a perfect 2D quantum wire. Having shown this we will next construct systems which consist of a perfect 2D wire with an arbitrary potential in the scattering region, which can contain both a local and a non-local term. Dyson's equation is then used to obtain an expression for the Green's function for the new system in terms of $G^{(0)}(\mathbf{r},\mathbf{r}')$, the Greens function for a perfect 2D wire, and the potential. Similarly, we use the Lippmann-Schwinger equation to get an expression for the wave functions for the new system in terms of $\psi^{(0)}(\mathbf{r})$ and the potential. With these expressions in hand we use our previous results to show that the Generalized Fisher-Lee relation is true.

First, let us consider a perfect 2D wire with an empty scattering region located in the region $x \in [0, L]$. The lead to the left of the scattering region is denoted as lead-1 and to the right as lead-2. The scattering wavefunction for an incoming mode from lead-1 in the n-th subband

$$\psi_{1n}^{(0)}(\mathbf{r}) = \phi_n(y)e^{ik_n x} \quad , \tag{3.43}$$

where $\phi_n(y)$ is the transverse eigenfunction which depends on the choice of confining potential of the wire. Similarly, the scattering wavefunction for an incoming wave from lead-2 in the m-th mode is given by

$$\psi_{2m}^{(0)}(\mathbf{r}) = \phi_m(y)e^{-ik_n x} \quad . \tag{3.44}$$

Next, the Green's function for a perfect 2D quantum wire is given by [5],

$$G^{(0)}(\mathbf{r},\mathbf{r}') = \sum_n \phi_n(y)\phi_n(y')\frac{e^{ik_n|x-x'|}}{i\hbar v_n} \quad , \tag{3.45}$$

where k_n is the n-th eigen-momentum and v_n is the Fermi velocity of the carrier in the n-th subband.

Using Eq. (3.43), Eq. (3.44), and Eq. (3.45) we now show that the Generalized Fisher-Lee relation is true for a perfect 2D wire. For x inside the scattering region we have that

$$i\hbar v_m \int dy'\phi_m(y')G^{(0)}(0,y';x,y) = i\hbar v_m \int dy'\phi_m(y')\left(\sum_n \phi_n(y)\phi_n(y')\frac{e^{ik_n|x|}}{i\hbar v_n}\right)$$

$$
\begin{aligned}
&= i\hbar v_m \phi_m(y) \frac{e^{ik_m x}}{i\hbar v_m} \\
&= \phi_m(y) e^{ik_m x} \\
&= \psi^{(0)}_{1m}(x,y) \ .
\end{aligned}
$$

Similarly,

$$
\begin{aligned}
i\hbar v_m \int dy' \phi_m(y') G^{(0)}(L, y'; x, y) &= i\hbar v_m \int dy' \phi_m(y') \left(\sum_n \phi_n(y)\phi_n(y') \frac{e^{ik_n|L-x|}}{i\hbar v_n} \right) \\
&= i\hbar v_m \phi_m(y) \frac{e^{ik_m(L-x)}}{i\hbar v_m} \\
&= \phi_m(y) e^{-ik_m(x-L)} \\
&= \psi^{(0)}_{2m}(x,y) \ .
\end{aligned}
$$

We absorbed the phase factor $e^{ik_m L}$ into the definition of the scattering wavefunction since it has no physical effect. Notice that if we use a local coordinate system such that $x_2 = 0$ corresponds to the position of the boundary of the scattering region with lead-2, then the phase factor would be absorbed by the local coordinate system.

Let us now consider a general situation described by the Hamiltonian,

$$
\hat{H} = \hat{H}^0 + \hat{V} \tag{3.46}
$$

where $\hat{H}^0$ is the Hamiltonian for a perfect 2D quantum wire, and $\hat{V}$ is some scattering potential that describes our quantum device. The potential has two pieces, one local and one non-local [1],

$$
\hat{V}(\mathbf{r}) = \hat{V}_{local}(\mathbf{r}) + \hat{V}_{NL}(\mathbf{r}) \tag{3.47}
$$

where

$$
\hat{V}_{NL}(\mathbf{r})\psi(\mathbf{r}) = \sum_{\mu,\nu} Z_{\mu\nu}\chi_\mu(\mathbf{r}) \int d\mathbf{r}' \chi_\nu(\mathbf{r}')\psi(\mathbf{r}') \ . \tag{3.48}
$$

The functions $\chi_\nu(\mathbf{r})$ form a basis for the non-local potential. The matrix $Z_{\mu\nu}$ for the non-local part of the potential is symmetric, $Z_{\mu\nu} = Z_{\nu\mu}$. Because of the general form of the potential, the system can represent a wide variety of quantum device connected

---

[1] A non-local potential is often necessary in defining atomic cores in a typical density functional analysis of molecular devices.

to two jellium leads, like an atomic cluster, a quantum dot, or an atomic wire. The only assumption we make about the potential is that it is Time Reversal Symmetric (TRS), which implies that $G(\mathbf{r},\mathbf{r}') = G(\mathbf{r}',\mathbf{r})$.

Before moving on with our derivation let us notice the following,

$$\begin{aligned}
\int d\mathbf{r}\psi(\mathbf{r})\hat{V}_{NL}(\mathbf{r})G(\mathbf{r},\mathbf{r}'') &= \int d\mathbf{r}\psi(\mathbf{r})\left(\sum_{\mu,\nu} Z_{\mu\nu}\chi_\mu(\mathbf{r})\int d\mathbf{r}'\chi_\nu(\mathbf{r}')G(\mathbf{r}',\mathbf{r}'')\right)\\
&= \int d\mathbf{r}'\int d\mathbf{r}\sum_{\mu,\nu} Z_{\mu\nu}\psi(\mathbf{r})\chi_\mu(\mathbf{r})\chi_\nu(\mathbf{r}')G(\mathbf{r}',\mathbf{r}'')\\
&= \int\int d\mathbf{r}d\mathbf{r}'\sum_{\mu,\nu} Z_{\mu\nu}G(\mathbf{r}'',\mathbf{r}')\chi_\nu(\mathbf{r}')\chi_\mu(\mathbf{r})\psi(\mathbf{r})\\
&= \int d\mathbf{r}'G(\mathbf{r}'',\mathbf{r}')\left(\sum_{\nu,\mu} Z_{\nu\mu}\chi_\nu(\mathbf{r}')\int d\mathbf{r}\chi_\mu(\mathbf{r})\psi(\mathbf{r})\right)\\
&= \int d\mathbf{r}'G(\mathbf{r}'',\mathbf{r}')\left(\sum_{\nu,\mu} Z_{\nu\mu}\chi_\nu(\mathbf{r}')\int d\mathbf{r}\chi_\mu(\mathbf{r})\psi(\mathbf{r})\right)\\
&= \int d\mathbf{r}'G(\mathbf{r}'',\mathbf{r}')\hat{V}_{NL}(\mathbf{r}')\psi(\mathbf{r}') \ , \qquad (3.49)
\end{aligned}$$

where we have used $G(\mathbf{r},\mathbf{r}') = G(\mathbf{r}',\mathbf{r})$ and $Z_{\mu\nu} = Z_{\nu\mu}$. This result will be used in our derivation of the Generalized Fisher-Lee relation.

Using Dyson's equation we obtain an expression for the Green's function in terms of the potential $\hat{V}$ and $G^{(0)}(\mathbf{r},\mathbf{r}')$,

$$G(\mathbf{r},\mathbf{r}') = G^{(0)}(\mathbf{r},\mathbf{r}') + \int d\mathbf{r}''G^{(0)}(\mathbf{r},\mathbf{r}')\hat{V}(\mathbf{r}'')G(\mathbf{r}'',\mathbf{r}') \ . \qquad (3.50)$$

Similarly, the Lippmann-Schwinger equation gives us,

$$\psi_{\alpha n}(\mathbf{r}) = \psi^{(0)}_{\alpha n}(\mathbf{r}) + \int d\mathbf{r}'G(\mathbf{r},\mathbf{r}')\hat{V}(\mathbf{r}')\psi^{(0)}_{\alpha n}(\mathbf{r}') \ . \qquad (3.51)$$

Next, we evaluate the right hand side Eq. (3.42) using Eq. (3.50), we find,

$$\begin{aligned}
& i\hbar v_{\alpha n}\int_{C_\alpha} dy'\phi_{\alpha n}(y')G(x_\alpha,y';\mathbf{r})\\
&= i\hbar v_{\alpha n}\int_{C_\alpha} dy'\phi_{\alpha n}(y')\left(G^{(0)}(x_\alpha,y';\mathbf{r}) + \int d\mathbf{r}''G^{(0)}(x_\alpha,y';\mathbf{r}'')\hat{V}(\mathbf{r}'')G(\mathbf{r}'',\mathbf{r})\right)\\
&= i\hbar v_{\alpha n}\int_{C_\alpha} dy'\phi_{\alpha n}(y')G^{(0)}(x_\alpha,y';\mathbf{r})\\
&+ \int_{C_\alpha} d\mathbf{r}''\left(i\hbar v_{\alpha n}\int dy'\phi_{\alpha n}(y')G^{(0)}(x_\alpha,y';\mathbf{r}'')\right)\hat{V}(\mathbf{r}'')G(\mathbf{r}'',\mathbf{r})\\
&= \psi^{(0)}_{\alpha n}(\mathbf{r}) + \int d\mathbf{r}''\psi^{(0)}_{\alpha n}(\mathbf{r}'')\hat{V}(\mathbf{r}'')G(\mathbf{r}'',\mathbf{r})\\
&= \psi^{(0)}_{\alpha n}(\mathbf{r}) + \int d\mathbf{r}''G(\mathbf{r},\mathbf{r}'')\hat{V}(\mathbf{r}'')\psi^{(0)}_{\alpha n}(\mathbf{r}'') \ , \qquad (3.52)
\end{aligned}$$

where we have used Eq. (3.49) to get the final result. Comparing Eq. (3.52) with Eq. (3.51) we conclude that

$$\psi_{\alpha n}(\mathbf{r}) = i\hbar v_{\alpha n} \int_{C_\alpha} dy' \phi_{\alpha n}(y') G(x_\alpha, y'; \mathbf{r}) \ , \tag{3.53}$$

which is precisely the Generalized Fisher-Lee relation.

3.4 GFL Relation for Multi-Probe and Atomic systems

One limitation of the above result is that it does not apply to multi-probe quantum conductors and/or conductors that are connected to atomic leads. Let us extend the proof of the Generalized Fisher-Lee (GFL) relation to include such systems. We first we prove the GFL for a multi-probe with jellium leads. This is accomplished by using the usual Fisher-Lee relation. We assume, as before, that the systems are time reversal symmetric.

Using the Fisher-Lee relation we compute the functional derivative of the scattering matrix. From Eq. (3.41) and Eq. (3.11) we find,

$$\begin{aligned}
\frac{\delta s_{\beta m,\alpha n}}{\delta U(\mathbf{r})} &= i\hbar\sqrt{v_{\beta m} v_{\alpha n}} \int\int dy' dy'' \phi_{\beta m}(y') \frac{G(x_\beta, y'; x_\alpha, y'')}{\delta U(\mathbf{r})} \phi_{\alpha n}(y'') \\
&= i\hbar\sqrt{v_{\beta m} v_{\alpha n}} \int\int dy' dy'' \phi_{\beta m}(y') G(x_\beta, y'; \mathbf{r}) G(\mathbf{r}; x_\alpha, y'') \phi_{\alpha n}(y'') \\
&= \frac{-i}{\hbar\sqrt{v_{\beta m} v_{\alpha n}}} \left(i\hbar v_{m\beta} \int \phi_{\beta m}(y') dy' G(x_\beta, y'; \mathbf{r}) \right) \left(i\hbar v_{n\alpha} \int dy'' G(x_\alpha, y''; \mathbf{r}) \phi_{\alpha n}(y'') \right) \\
&= \frac{-i}{\hbar\sqrt{v_{\beta m} v_{\alpha n}}} \bar{\psi}_{\beta m}(\mathbf{r}) \bar{\psi}_{\alpha n}(\mathbf{r}) \ ,
\end{aligned} \tag{3.54}$$

where we have assumed TRS and used Eq. (3.23) to obtain the final result. Comparing Eq. (3.54) with Eq. (3.22) we conclude:

$$\psi_{\alpha n}(\mathbf{r}) = \bar{\psi}_{\alpha n}(\mathbf{r}) = i\hbar v_{\beta m} \int_{C_\beta} dy' \phi_{\beta m}(y') G(x_\beta, y'; \mathbf{r}) \ , \tag{3.55}$$

which is the Generalized Fisher-Lee (GFL) relation. To extend this result to Bloch states we simply use the Fisher-Lee relationship for atomic leads and repeat the above procedure. The final result is:

$$\psi_{\alpha n}(\mathbf{r}) = \bar{\psi}_{\alpha n}(\mathbf{r}) = i\hbar v_{\beta m} \int_{C_\beta} d\mathbf{r}' \phi^{(out)\dagger}_{\beta m}(\mathbf{r}') G(\mathbf{r}'; \mathbf{r}) \ , \tag{3.56}$$

where C_β is the first unit cell outside the scattering region in the β-th lead and $\phi^{(out)\dagger}_{\beta m}(\mathbf{r})$ is the dual of an outgoing Bloch states. With these results we only require the wavefunction to compute $\delta s_{\beta m,\alpha n}/\delta U(\mathbf{r})$. This greatly reduces the complexity and computation time required to obtain the functional derivative of the scattering matrix, since there is no need to compute the Green's function.

In this section we proved that the Generalized Fisher-Lee relation is true for all TRS systems. We then rigorously derived the Fisher-Lee relation for systems with atomic leads. Finally, we argued that to compute the first order functional derivative of the scattering matrix we only require the wavefunction.

3.5 Transport Coefficients and LPDOS

We now apply the results from the previous sections to the quantum transport coefficients discussed in Chapter 2. In particular, we obtain equations for the first order nonlinear DC conductance, $G_{\alpha\beta\gamma}$, and linear AC conductance, $E_{\alpha\beta}$. We assume, once again, time reversal symmetry.

We first find an equation for $G_{\alpha\beta\gamma}$ in terms of the scattering wave functions, $\psi_{\alpha n}(\mathbf{r})$ and the characteristic potentials, $u_\alpha(\mathbf{r})$. From Eq. (2.65) we have,

$$G_{\alpha\beta\gamma} = \frac{e^2}{h}\int d\mathbf{r}\frac{\delta A_{\alpha\beta}}{\delta U(\mathbf{r})}\left(2u_\gamma(\mathbf{r}) - \delta_{\beta\gamma}\right) \ , \tag{3.57}$$

where

$$A_{\alpha\beta}(E,\{V_\gamma\}) = \sum_{n,m}\left[\delta_{\alpha\beta}\delta_{nm} - s^\dagger_{\beta m,\alpha n}(E,\{V_\gamma\})s_{\beta m,\alpha n}(E,\{V_\gamma\})\right] \ . \tag{3.58}$$

Let us express $\delta A_{\alpha\beta}/\delta U(\mathbf{r})$ in terms of $\psi_{\alpha n}(\mathbf{r})$,

$$\begin{aligned}
\frac{\delta A_{\alpha\beta}}{\delta U(\mathbf{r})} &= \frac{\delta}{\delta U(\mathbf{r})}\sum_{n,m}\left[\delta_{\alpha\beta}\delta_{nm} - s^\dagger_{\beta m,\alpha n}(E,\{V_\gamma\})s_{\beta m,\alpha n}(E,\{V_\gamma\})\right] \\
&= -\frac{\delta}{\delta U(\mathbf{r})}\sum_{n,m}\left[s^\dagger_{\beta m,\alpha n}s_{\beta m,\alpha n}\right] \\
&= -\sum_{n,m}\left[s^\dagger_{\beta m,\alpha n}\frac{\delta s_{\beta m,\alpha n}}{\delta U(\mathbf{r})} + c.c.\right] \\
&= -2\sum_{n,m} Re\left[s^\dagger_{\beta m,\alpha n}\frac{\delta s_{\beta m,\alpha n}}{\delta U(\mathbf{r})}\right]
\end{aligned}$$

$$
\begin{aligned}
&= -2\sum_{n,m} Re\left[s^{\dagger}_{\beta m,\alpha n}\frac{-i}{\hbar\sqrt{v_{\beta m}v_{\alpha n}}}\psi_{\beta m}(\mathbf{r})\psi_{\alpha n}(\mathbf{r})\right] \\
&= -2\sum_{n,m} Im\left[\frac{\psi_{\beta m}(\mathbf{r})s^{\dagger}_{\beta m,\alpha n}\psi_{\alpha n}(\mathbf{r})}{\hbar\sqrt{v_{\beta m}v_{\alpha n}}}\right] \quad , \qquad (3.59)
\end{aligned}
$$

where we have used Eq. (3.22). Using this expression for $\delta A_{\alpha\beta}/\delta U(\mathbf{r})$ we now have an equation for $G_{\alpha\beta\gamma}$, which is expressed in terms of $\psi_{\alpha n}(\mathbf{r})$ and $u_{\alpha}(\mathbf{r})$. This result is used in Chapter 4 when we study nonlinear DC conductance fluctuations in the diffusive regime.

To obtain the emittance, $E_{\alpha\beta}$, we must first derive expressions for the local partial DOS. From Eq. (2.35), the LPDOS is given by,

$$
\begin{aligned}
\frac{dn_{\alpha\beta}(\mathbf{r})}{dE} &= -\frac{1}{4i\pi}\sum_{n,m}\left[s^{\dagger}_{\beta m,\alpha n}\frac{\delta s_{\beta m,\alpha n}}{\delta eU(\mathbf{r})} - c.c.\right] \\
&= -\frac{1}{2\pi}\sum_{n,m}\left(Im\left[s^{\dagger}_{\alpha n,\beta m}\frac{\delta s_{\alpha n,\beta m}}{\delta eU(\mathbf{r})}\right]\right) \\
&= -\frac{1}{2\pi}\sum_{n,m}\left(Im\left[s^{\dagger}_{\beta m,\alpha n}\frac{-i}{e\hbar\sqrt{v_{\beta m}v_{\alpha n}}}\psi_{\beta m}(\mathbf{r})\psi_{\alpha n}(\mathbf{r})\right]\right) \\
&= -\frac{1}{2\pi}\sum_{n,m}\left(Re\left[\frac{\psi_{\beta m}(\mathbf{r})s^{\dagger}_{\beta m,\alpha n}\psi_{\alpha n}(\mathbf{r})}{e\hbar\sqrt{v_{\beta m}v_{\alpha n}}}\right]\right) \quad . \qquad (3.60)
\end{aligned}
$$

With this result the emittance can be expressed in terms of the scattering matrix, scattering wavefunction, and the characteristic potentials. In Chapter 4 we use this result to study emittance fluctuations in a diffusive conductor in the mesoscopic regime.

To summarize, in this chapter we have developed theoretical tools which we will use to study nonlinear DC and linear AC quantum transport coefficients. In particular, we have found from first principles an expression for the functional derivative of the scattering matrix, $\delta s_{\beta m,\alpha n}/\delta U(\mathbf{r})$, in terms of the wavefunction, $\psi_{\alpha n}(\mathbf{r})$. This greatly reduces the computational effort required to calculate $G_{\alpha\beta\gamma}$ and $E_{\alpha\beta}$.

4

Exact N-impurity Solution: Admittance Fluctuations

In Chapter 2 we reviewed a quantum theory for linear AC and nonlinear DC quantum transport, which conserves current and is gauge invariant. In particular, we derived expressions for the emittance, $E_{\alpha\beta}$, and the nonlinear conductance, $G_{\alpha\beta\gamma}$. In Chapter 3 we derived a new expression for the functional derivative of the scattering matrix, $\delta s_{\alpha n,\beta m}/\delta U(\mathbf{r})$, expressed in terms of the scattering wave functions, $\psi_{\alpha n}(\mathbf{r})$. This leads to equations for $E_{\alpha\beta}$ and $G_{\alpha\beta\gamma}$ in terms of the $s_{\alpha n,\beta m}$, $\psi_{\alpha n}(\mathbf{r})$, and $u_{\alpha}(\mathbf{r})$. Within the Thomas-Fermi and local neutrality approximations, we can express $u_{\alpha}(\mathbf{r})$ in terms of $\psi_{\alpha n}(\mathbf{r})$. This leaves us with expressions for the emittance, $E_{\alpha\beta}$, and the nonlinear conductance, $G_{\alpha\beta\gamma}$, in terms of the scattering matrix and the wave function. We now apply these results to investigate conductance fluctuations. In particular, we are interested in emittance and nonlinear conductance fluctuations in the diffusive regime, where universal conductance fluctuations are found for linear DC conductance.

Our approach is to generate a disordered conductor in the diffusive regime using an impurity potential which consists of localized elastic scattering centers given by, $V(\mathbf{r}) = \sum_i \gamma\delta(\mathbf{r}-\mathbf{r}_i)$, as used by Al'tshuler, Lee, Stone, and Fuckuyama [43]. With this choice of impurities we can exactly solve Dyson's equation. This leads us to an exact expression for the N-delta impurity Green's function, which we denote by $G^{(N)}(\mathbf{r},\mathbf{r}')$. The Lippmann-Schwinger equation is then used to obtain an exact expression for $\psi^{(N)}_{\alpha n}(\mathbf{r})$, the N-delta impurity scattering wave function. Combining these results with the results from Chapter 3 we obtain exact expressions for the scattering matrix, $s^{(N)}_{\beta m,\alpha n}$, and it's functional derivative, $\delta s^{(N)}_{\beta m,\alpha n}/\delta U(\mathbf{r})$. Once all these results are derived we use them to compute the transport coefficients $E_{\alpha\beta}$ and $G_{\alpha\beta\gamma}$. We then study the sample-to-sample emittance fluctuations, $\Delta E_{\alpha\beta}$, and the nonlinear conductance fluctuations, $\Delta G_{\alpha\beta\gamma}$. These quantities are computed by evaluating numerically our exact expressions for $E_{\alpha\beta}$ and $G_{\alpha\beta\gamma}$ and then performing statistical analysis. But first, we compute the fluctuations of the usual linear DC conductance, $G_{\alpha\beta}$, in order to locate the UCF transport regime. Moreover, since we have an exact solution for the N-delta impurity problem, we can probe the full parameter space, N and γ, where N is the number of impurities and γ the strength of the impurities. This allows us to study the crossover from one regime to another, for instance, from the ballistic regime to the UCF regime.

In Section 4.1, we derive expressions for $G^{(N)}(\mathbf{r},\mathbf{r}')$, $\psi^{(N)}_{\alpha n}(\mathbf{r})$, $\delta s^{(N)}_{\beta m,\alpha n}/\delta U(\mathbf{r})$, and $s^{(N)}_{\beta m,\alpha n}$. In Section 4.2 these general results are applied to the specific case of 1-delta impurity in a perfect quasi-1D quantum wire, for which the scattering matrix and it's functional derivative has been found using a mode matching method [76, 77]. Our results are compared to these, and are found to be consistent. In Section 4.3 we apply our technique to the N-delta impurity situation for a perfect 2D quantum wire. We then study $\Delta G_{\alpha\beta}$, $\Delta E_{\alpha\beta}$, and $\Delta G_{\alpha\beta\gamma}$ for different values of N and γ. In particular, we find values for N and γ which leads to $\Delta G_{\alpha\beta}$ in the UCF regime.

4.1 Exact Solution to the N-impurity problem

In the next section we derive exact expressions for the N-delta impurity Green's function, wave function, scattering matrix and it's functional derivative. These theoretical results are crucial for our later work on emittance and nonlinear conductance fluctuations. Similar results can be obtained for the N-delta magnetic impurity Green's function and wave function (see appendices). The essential ingredient in these derivations is that the delta-function impurities can always be integrated out of our equations. This simplifies the integral equations, which provide exact expressions for $G^{(N)}(\mathbf{r},\mathbf{r}')$ and $\psi^{(N)}(\mathbf{r})$, to algebraic equations which are easily solved. Once expressions for $G^{(N)}(\mathbf{r},\mathbf{r}')$ and $\psi^{(N)}(\mathbf{r})$ are found the results from Chapter 3 are used to compute

$s^{(N)}_{\alpha n,\beta m}$ and $\delta s^{(N)}_{\alpha n,\beta m}/\delta U(\mathbf{r})$.

4.1.1 The N-delta impurity Green's function

Let us consider a system described by an "unperturbed" Hamiltonian $H^{(0)}$. For example, the system can be a quantum wire, a 4-probe Hall bar, or a molecular device. The Green's function corresponding to this system is denoted by $G^{(0)}(\mathbf{r},\mathbf{r}')$. We add to this system N-delta impurities, which leads to the new Hamiltonian,

$$\hat{H}^{(N)} = \hat{H}^{(0)} + V^{(N)}(\mathbf{r}) \ , \tag{4.1}$$

where the impurity potential is given by,

$$V^{(N)}(\mathbf{r}) = \sum_{i=1}^{N} \gamma_i \delta(\mathbf{r} - \mathbf{r}_i) \ . \tag{4.2}$$

The strength of the impurities are represented by $\{\gamma_i\}$ and their positions by $\{\mathbf{r}_i\}$.

To obtain the Green's function for this new system, $G^{(N)}(\mathbf{r},\mathbf{r}')$, we use the following approach. First, we view the system described by $H^{(0)}$ as a free system and the one represented by $H^{(N)}$ as the perturbed one. The potential $V^{(N)}(\mathbf{r})$ is treated as the perturbation potential. Using Dyson's equation we express the perturbed Green's function, $G^{(N)}(\mathbf{r},\mathbf{r}')$, in terms of the free Green's function, $G^{(0)}(\mathbf{r},\mathbf{r}')$, and the perturbation potential $V^{(N)}(\mathbf{r})$. Finally, we solve Dyson's equation exactly.

Dyson's equation is given by,

$$G^{(N)}(\mathbf{r},\mathbf{r}') = G^{(0)}(\mathbf{r},\mathbf{r}') + \int d\mathbf{r}'' G^{(0)}(\mathbf{r},\mathbf{r}'') V^{(N)}(\mathbf{r}'') G^{(N)}(\mathbf{r}'',\mathbf{r}') \ . \tag{4.3}$$

Integrating out the delta function impurities we find,

$$G^{(N)}(\mathbf{r},\mathbf{r}') = G^{(0)}(\mathbf{r},\mathbf{r}') + \sum_{i=1}^{N} G^{(0)}(\mathbf{r},\mathbf{r}_i)\gamma_i G^{(N)}(\mathbf{r}_i,\mathbf{r}') \ . \tag{4.4}$$

Setting $\mathbf{r} = \mathbf{r}_j$, for $j = 1, ..., N$ in Eq. (4.4), we generate a system of N equations for the N unknowns $\{G^{(N)}(\mathbf{r}_i,\mathbf{r}')\}$, given by,

$$\begin{aligned} G^{(N)}(\mathbf{r}_j,\mathbf{r}') &= G^{(0)}(\mathbf{r}_j,\mathbf{r}') + \sum_{i=1}^{N} G^{(0)}(\mathbf{r}_j,\mathbf{r}_i)\gamma_i G^{(N)}(\mathbf{r}_i,\mathbf{r}') \\ &= G^{(0)}(\mathbf{r}_j,\mathbf{r}') + \sum_{i=1}^{N} \eta_{ji}\gamma_i G^{(N)}(\mathbf{r}_i,\mathbf{r}') \ , \end{aligned}$$

where we have set $\eta_{ji} = G^{(0)}(\mathbf{r}_j, \mathbf{r}_i)$. Solving this set of equations we find:

$$G^{(N)}(\mathbf{r}_i, \mathbf{r}') = \sum_{j=1}^{N} [\delta_{ij} - \eta_{ij}\gamma_j]^{-1} G^{(0)}(\mathbf{r}_j, \mathbf{r}') \ . \tag{4.5}$$

Finally, substituting Eq. (4.5) into Eq. (4.4) we find,

$$\begin{aligned} G^{(N)}(\mathbf{r}, \mathbf{r}') &= G^{(0)}(\mathbf{r}, \mathbf{r}') + \sum_{i=1}^{N} G^{(0)}(\mathbf{r}, \mathbf{r}_i)\gamma_i \left(\sum_{j=1}^{N} [\delta_{ij} - \eta_{ij}\gamma_j]^{-1} G^{(0)}(\mathbf{r}_j, \mathbf{r}') \right) \\ &= G^{(0)}(\mathbf{r}, \mathbf{r}') + \sum_{i,j=1}^{N} G^{(0)}(\mathbf{r}, \mathbf{r}_i)\gamma_i M_{ij} G^{(0)}(\mathbf{r}_j, \mathbf{r}') \ , \end{aligned} \tag{4.6}$$

where

$$M_{ij} = [\delta_{ij} - \eta_{ij}\gamma_j]^{-1} \ . \tag{4.7}$$

Thus, we have found how to add N delta impurities to any system. Note that the only ingredient required in this derivation was Dyson's equation.

4.1.2 The N-delta impurity scattering wave function

We are now ready to obtain an expression for the N-delta impurity wave function, $\psi^{(N)}_{\alpha n}(\mathbf{r})$. This is accomplished by expressing the wave function, $\psi^{(N)}_{\alpha n}(\mathbf{r})$, in terms of the free wave function, $\psi^{(0)}_{\alpha n}(\mathbf{r})$, the N-impurity Green's function, $G^{(N)}(\mathbf{r}, \mathbf{r}')$, and the potential $V^{(N)}(\mathbf{r})$, via the Lippmann-Schwinger equation. Using the results from the previous section we find an exact expression for the wave function.

Let $\psi^{(N)}(\mathbf{r})$ be the perturbed wave function, $\psi^{(0)}(\mathbf{r})$ the free wave function, $G^{(N)}(\mathbf{r}, \mathbf{r}')$ the perturbed Green's function, and $V^{(N)}(\mathbf{r})$ is the perturbation potential. The Lippmann-Schwinger equation is given by,

$$\psi^{(N)}(\mathbf{r}) = \psi^{(0)}(\mathbf{r}) + \int d\mathbf{r}' G^{(N)}(\mathbf{r}, \mathbf{r}') V^{(N)}(\mathbf{r}') \psi^{(0)}(\mathbf{r}') \ . \tag{4.8}$$

Integrating out all the delta-functions impurities we obtain,

$$\psi^{(N)}(\mathbf{r}) = \psi^{(0)}(\mathbf{r}) + \sum_{k=1}^{N} G^{(N)}(\mathbf{r}, \mathbf{r}_k)\gamma_k \psi^{(0)}(\mathbf{r}_k) \ . \tag{4.9}$$

Substituting Eq. (4.6) into Eq. (4.9), we find,

$$\begin{aligned} \psi^{(N)}(\mathbf{r}) &= \psi^{(0)}(\mathbf{r}) + \sum_{k=1}^{N} \left(G^{(0)}(\mathbf{r}, \mathbf{r}_k) + \sum_{i,j=1}^{N} G^{(0)}(\mathbf{r}, \mathbf{r}_i)\gamma_i M_{ij} G^{(0)}(\mathbf{r}_j, \mathbf{r}_k) \right) \gamma_k \psi^{(0)}(\mathbf{r}_k) \\ &= \psi^{(0)}(\mathbf{r}) + \sum_{k=1}^{N} G^{(0)}(\mathbf{r}, \mathbf{r}_k)\gamma_k \psi^{(0)}(\mathbf{r}_k) + \sum_{i,j,k=1}^{N} G^{(0)}(\mathbf{r}, \mathbf{r}_i)\gamma_i M_{ij}\eta_{jk}\gamma_k \psi^{(0)}(\mathbf{r}_k) \ . \end{aligned}$$

This is an exact expression for the N-impurity wave function in term of $\psi^{(0)}(\mathbf{r})$, $G^{(0)}(\mathbf{r},\mathbf{r})$, and M_{ij} (see Eq. (4.7)).

It would appear that the N-impurity wave function, $\psi^{(N)}(\mathbf{r})$, depends on three center interactions, i.e. terms that depends on 3 different impurity positions. But since the N-impurity Green's function depends only on two center interactions it is reasonable to suspect that the 3 center term in $\psi^{(N)}(\mathbf{r})$ is artificial.

Let us now turn the 3 center term into a 2 center term:

$$\begin{aligned}
\psi^{(N)}(\mathbf{r}) &= \psi^{(0)}(\mathbf{r}) + \sum_{k=1}^{N} G^{(0)}(\mathbf{r},\mathbf{r}_k)\gamma_k\psi^{(0)}(\mathbf{r}_k) + \sum_{i,j,k=1}^{N} G^{(0)}(\mathbf{r},\mathbf{r}_i)\gamma_i M_{ij}\eta_{jk}\gamma_k\psi^{(0)}(\mathbf{r}_k) \\
&= \psi^{(0)}(\mathbf{r}) + \sum_{i,k=1}^{N} G^{(0)}(\mathbf{r},\mathbf{r}_i)\gamma_i\left(\delta_{ik}\right)\psi^{(0)}(\mathbf{r}_k) + \sum_{i,j,k=1}^{N} G^{(0)}(\mathbf{r},\mathbf{r}_i)\gamma_i\left(M_{ij}\eta_{jk}\gamma_k\right)\psi^{(0)}(\mathbf{r}_k) \\
&= \psi^{(0)}(\mathbf{r}) + \sum_{i,j,k=1}^{N} G^{(0)}(\mathbf{r},\mathbf{r}_i)\gamma_i\left(\delta_{ij}\delta_{jk} + M_{ij}\eta_{jk}\gamma_k\right)\psi^{(0)}(\mathbf{r}_k) \\
&= \psi^{(0)}(\mathbf{r}) + \sum_{i,j,k=1}^{N} G^{(0)}(\mathbf{r},\mathbf{r}_i)\gamma_i M_{ij}\left(M_{jk}^{-1} + \eta_{jk}\gamma_k\right)\psi^{(0)}(\mathbf{r}_k) \\
&= \psi^{(0)}(\mathbf{r}) + \sum_{i,j,k=1}^{N} G^{(0)}(\mathbf{r},\mathbf{r}_i)\gamma_i M_{ij}\left(\delta_{jk} - \eta_{jk}\gamma_k + \eta_{jk}\gamma_k\right)\psi^{(0)}(\mathbf{r}_k) \\
&= \psi^{(0)}(\mathbf{r}) + \sum_{i,j,k=1}^{N} G^{(0)}(\mathbf{r},\mathbf{r}_i)\gamma_i M_{ij}\left(\delta_{jk}\right)\psi^{(0)}(\mathbf{r}_k) \\
&= \psi^{(0)}(\mathbf{r}) + \sum_{i,j=1}^{N} G^{(0)}(\mathbf{r},\mathbf{r}_i)\gamma_i M_{ij}\psi^{(0)}(\mathbf{r}_j) \ .
\end{aligned}$$

Thus, the N-delta impurity wave function is simply given by,

$$\psi^{(N)}(\mathbf{r}) = \psi^{(0)}(\mathbf{r}) + \sum_{i,j=1}^{N} G^{(0)}(\mathbf{r},\mathbf{r}_i)\gamma_i M_{ij}\psi^{(0)}(\mathbf{r}_j) \ . \tag{4.10}$$

Before moving on let us check the above result by re-deriving it using a different approach. This new derivation simply reuses the method that was employed to obtain $G^{(N)}(\mathbf{r},\mathbf{r}')$ from Dyson's equation. An alternate form of the Lippmann-Schwinger equation is given by,

$$\psi^{(N)}(\mathbf{r}) = \psi^{(0)}(\mathbf{r}) + \int d\mathbf{r}' G^{(0)}(\mathbf{r},\mathbf{r}')V^{(N)}(\mathbf{r}')\psi^{(N)}(\mathbf{r}') \ . \tag{4.11}$$

Integrating out the delta-functions we find,

$$\psi^{(N)}(\mathbf{r}) = \psi^{(0)}(\mathbf{r}) + \sum_{i=1}^{N} G^{(0)}(\mathbf{r},\mathbf{r}_i)\gamma_i\psi^{(N)}(\mathbf{r}_i) \ . \tag{4.12}$$

Setting, $\mathbf{r} = \mathbf{r}_j$ for $j = 1, ..., N$, we generate a system of N equations for the N unknowns $\{\psi^{(N)}(\mathbf{r}_j)\}$:

$$\psi^{(N)}(\mathbf{r}_j) = \psi^{(0)}(\mathbf{r}) + \sum_{i=1}^{N} G^{(0)}(\mathbf{r}_j, \mathbf{r}_i)\gamma_i \psi^{(N)}(\mathbf{r}_i) \ . \tag{4.13}$$

Solving this system we find,

$$\psi^{(N)}(\mathbf{r}_i) = \sum_{j=1} M_{ij}\psi^{(0)}(\mathbf{r}_j) \ . \tag{4.14}$$

where M_{ij} is given by Eq. (4.7). Putting this result into Eq. (4.12) we obtain the final result,

$$\psi^{(N)}(\mathbf{r}) = \psi^{(0)}(\mathbf{r}) + \sum_{i,j=1}^{N} G^{(0)}(\mathbf{r}, \mathbf{r}_i)\gamma_i M_{ij}\psi^{(0)}(\mathbf{r}_j) \ . \tag{4.15}$$

Thus, we have found consistent expressions for the N-delta impurity wave function, from two different approaches.

4.1.3 The functional derivative for the N-impurity problem

Now that we have an equation for the scattering wave function, $\psi^{(N)}_{\alpha n}(\mathbf{r})$, we are in position to find an expression $\delta s^{(N)}_{\beta m,\alpha n}/\delta U(\mathbf{r})$. It was shown in Chapter 3 that the functional derivative of the scattering matrix can be expressed in the following way:

Using Eq. (3.22) we have,

$$\frac{\delta s^{(N)}_{\beta m,\alpha n}}{\delta U(\mathbf{r})} = \frac{-i}{\hbar\sqrt{v_{\beta m}v_{\alpha n}}}\left(\int_{C_\beta} dy'\phi_{\beta m}(y')G^{(N)}(x_\beta, y'; \mathbf{r})\right)\psi^{(N)}_{\alpha n}(\mathbf{r}) \ , \tag{4.16}$$

where $G^{(N)}(\mathbf{r}, \mathbf{r}')$ and $\psi^{(N)}_{\alpha n}(\mathbf{r})$ are given by Eq. (4.6) and Eq. (4.10), respectively. Substituting these equations into the above expression,

$$\begin{aligned}
\frac{\delta s^{(N)}_{\beta m,\alpha n}}{\delta U(\mathbf{r})} &= \frac{-i}{\hbar\sqrt{v_{\beta m}v_{\alpha n}}}\left(i\hbar v_{\beta m}\int_{C_\beta} dy'\phi_{\beta m}(y')\left(G^{(0)}(x_\beta, y'; \mathbf{r}) + \sum_{i,j=1}^{N} G^{(0)}(x_\beta, y'; \mathbf{r}_i)\gamma_i M_{ij}G^{(0)}(\mathbf{r}_j, \mathbf{r})\right)\right. \\
&\quad \left(\psi^{(0)}_{\alpha n}(\mathbf{r}) + \sum_{i,j=1}^{N} G^{(0)}(\mathbf{r}, \mathbf{r}_i)\gamma_i M_{ij}\psi^{(0)}_{\alpha n}(\mathbf{r}_j)\right) \\
&= \frac{-i}{\hbar\sqrt{v_{\beta m}v_{\alpha n}}}\left(i\hbar v_{\beta m}\int_{C_\beta} dy'\phi_{\beta m}(y')G^{(0)}(x_\beta, y'; \mathbf{r})\right)\psi^{(0)}_{\alpha n}(\mathbf{r}) \\
&+ \frac{-i}{\hbar\sqrt{v_{\beta m}v_{\alpha n}}}\left(i\hbar v_{\beta m}\int_{C_\beta} dy'\phi_{\beta m}(y')\sum_{i,j=1}^{N} G^{(0)}(x_\beta, y'; \mathbf{r}_i)\gamma_i M_{ij}G^{(0)}(\mathbf{r}_j, \mathbf{r})\right)\psi^{(0)}_{\alpha n}(\mathbf{r})
\end{aligned}$$

$$+\frac{-i}{\hbar\sqrt{v_{\beta m}v_{\alpha n}}}\left(i\hbar v_{\beta m}\int_{C_\beta}dy'\phi_{\beta m}(y')G^{(0)}(x_\beta,y';\mathbf{r})\right)\left(\sum_{i,j=1}^{N}G^{(0)}(\mathbf{r},\mathbf{r}_i)\gamma_i M_{ij}\psi^{(0)}_{\alpha n}(\mathbf{r}_j)\right)$$
$$+\frac{-i}{\hbar\sqrt{v_{\beta m}v_{\alpha n}}}\left(i\hbar v_{\beta m}\int_{C_\beta}dy'\phi_{\beta m}(y')\sum_{i,j=1}^{N}G^{(0)}(x_\beta,y';\mathbf{r}_i)\gamma_i M_{ij}G^{(0)}(\mathbf{r}_j,\mathbf{r})\right)$$
$$\left(\sum_{i,j=1}^{N}G^{(0)}(\mathbf{r},\mathbf{r}_i)\gamma_i M_{ij}\psi^{(0)}_{\alpha n}(\mathbf{r}_j)\right)\ .$$

This leads us to the final result:

$$\frac{\delta s^{(N)}_{\beta m,\alpha n}}{\delta U(\mathbf{r})}=\frac{\delta s^{(0)}_{\beta m,\alpha n}}{\delta U(\mathbf{r})}$$
$$+\frac{-i}{\hbar\sqrt{v_{\beta m}v_{\alpha n}}}\left(\sum_{i,j=1}^{N}\bar{\psi}^{(0)}_{\beta m}(\mathbf{r}_i)\gamma_i M_{ij}G^{(0)}(\mathbf{r}_j,\mathbf{r})\right)\psi^{(0)}_{\alpha n}(\mathbf{r})$$
$$+\frac{-i}{\hbar\sqrt{v_{\beta m}v_{\alpha n}}}\bar{\psi}^{(0)}_{\beta m}(\mathbf{r})\left(\sum_{i,j=1}^{N}G^{(0)}(\mathbf{r},\mathbf{r}_i)\gamma_i M_{ij}\psi^{(0)}_{\alpha n}(\mathbf{r}_j)\right)$$
$$+\frac{-i}{\hbar\sqrt{v_{\beta m}v_{\alpha n}}}\left(\sum_{i,j=1}^{N}\bar{\psi}^{(0)}_{\beta m}(\mathbf{r}_i)\gamma_i M_{ij}G^{(0)}(\mathbf{r}_j,\mathbf{r})\right)\left(\sum_{i,j=1}^{N}G^{(0)}(\mathbf{r},\mathbf{r}_i)\gamma_i M_{ij}\psi^{(0)}_{\alpha n}(\mathbf{r}_j)\right)\ ,$$

where $\bar{\psi}^{(0)}_{\alpha n}(\mathbf{r})$ is given by Eq. (3.23). The contributions to the functional derivative from the impurities are clearly seen.

4.1.4 *The Scattering Matrix of the N-impurity problem*

Let us find the effect of the N-delta impurities on the scattering matrix. Recall that the scattering matrix is obtained from the wave function. In particular, the scattering matrix for an impurity free system, which we denote by $s^{(0)}_{\beta m,\alpha n}$, has the following form,

$$s^{(0)}_{\beta m,\alpha n}=-\delta_{\beta\alpha}\delta_{nm}+\sqrt{\frac{v_{\beta m}}{v_{\alpha n}}}\int_{C_\beta}dy'\phi_{\beta m}(y')\psi^{(0)}_{\alpha n}(x_\beta,y')\ . \tag{4.17}$$

Similarly, the N-impurity scattering matrix, $s^{(N)}_{\beta m,\alpha n}$, is given by

$$s^{(N)}_{\beta m,\alpha n}=-\delta_{\beta\alpha}\delta_{nm}+\sqrt{\frac{v_{\beta m}}{v_{\alpha n}}}\int_{C_\beta}dy'\phi_{\beta m}(y')\psi^{(N)}_{\alpha n}(x_\beta,y')\ . \tag{4.18}$$

Substituting Eq. (4.10) into the above equation we find,

$$s^{(N)}_{\beta m,\alpha n}=-\delta_{\beta\alpha}\delta_{nm}+\sqrt{\frac{v_{\beta m}}{v_{\alpha n}}}\int_{C_\beta}dy'\phi_{\beta m}(y')\left(\psi^{(0)}_{\alpha n}(x_\beta,y')+\sum_{i,j=1}^{N}G^{(0)}(x_\beta,y',\mathbf{r}_i)\gamma_i M_{ij}\psi^{(0)}_{\alpha n}(\mathbf{r}_j)\right)$$

$$
\begin{aligned}
&= -\delta_{\beta\alpha}\delta_{nm} + \sqrt{\frac{v_{\beta m}}{v_{\alpha n}}}\int_{C_\beta} dy'\phi_{\beta m}(y')\psi^{(0)}_{\alpha n}(x_\beta, y') \\
&+ \sqrt{\frac{v_{\beta m}}{v_{\alpha n}}}\int_{C_\beta} dy'\phi_{\beta m}(y')\sum_{i,j=1}^{N} G^{(0)}(x_\beta, y', \mathbf{r}_i)\gamma_i M_{ij}\psi^{(0)}_{\alpha n}(\mathbf{r}_j) \\
&= s^{(0)}_{\beta m,\alpha n} + \frac{-i}{\hbar\sqrt{v_{\beta m}v_{\alpha n}}}\left(i\hbar v_{\beta m}\int_{C_\beta} dy'\phi_{\beta m}(y')\sum_{i,j=1}^{N} G^{(0)}(x_\beta, y', \mathbf{r}_i)\right)\gamma_i M_{ij}\psi^{(0)}_{\alpha n}(\mathbf{r}_j) \\
&= s^{(0)}_{\beta m,\alpha n} + \frac{-i}{\hbar\sqrt{v_{\beta m}v_{\alpha n}}}\sum_{i,j=1}^{N} \bar{\psi}^{(0)}_{\beta m}(\mathbf{r}_i)\gamma_i M_{ij}\psi^{(0)}_{\alpha n}(\mathbf{r}_j) \ ,
\end{aligned}
$$

where we have used the definition of $\bar{\psi}^{(0)}_{\beta m}(\mathbf{r})$ (see Eq. (3.23)).

If the underlying system is time reversal symmetric (TRS) then the system with N-impurities is also TRS, since elastic scattering does not break TRS. The Generalized Fisher-Lee relation, Eq. (3.53), then implies,

$$
s^{(N)}_{\beta m,\alpha n} = s^{(0)}_{\beta m,\alpha n} + \frac{-i}{\hbar\sqrt{v_{\beta m}v_{\alpha n}}}\sum_{i,j=1}^{N} \psi^{(0)}_{\beta m}(\mathbf{r}_i)\gamma_i M_{ij}\psi^{(0)}_{\alpha n}(\mathbf{r}_j) \ . \tag{4.19}
$$

Notice that we only need the free wave function, $\psi^{(0)}_{\alpha n}$, in order to obtain the N-impurity scattering matrix $s^{(N)}_{\alpha n,\beta m}$.

4.1.5 Summary

In these last four subsections we have shown how to obtain the N-delta impurity Green's function, wave function, scattering matrix, and it's functional derivative, in terms of their impurity free counter parts: $G^{(0)}(\mathbf{r},\mathbf{r}')$, $\psi^{(0)}_{\alpha n}(\mathbf{r})$, $s^{(0)}_{\beta m,\alpha n}$, and $\delta s^{(N)}_{\beta m,\alpha n}/\delta U(\mathbf{r})$.

In summary, we have found:

- The N-impurity Green's function:

$$
G^{(N)}(\mathbf{r},\mathbf{r}') = G^{(0)}(\mathbf{r},\mathbf{r}') + \sum_{i,j=1}^{N} G^{(0)}(\mathbf{r},\mathbf{r}_i)\gamma_i M_{ij}G^{(0)}(\mathbf{r}_j,\mathbf{r}') \ . \tag{4.20}
$$

- The N-impurity wave function:

$$
\psi^{(N)}_{\alpha n}(\mathbf{r}) = \psi^{(0)}_{\alpha n}(\mathbf{r}) + \sum_{i,j=1}^{N} G^{(0)}(\mathbf{r},\mathbf{r}_i)\gamma_i M_{ij}\psi^{(0)}_{\alpha n}(\mathbf{r}_j) \ . \tag{4.21}
$$

- The N-impurity scattering matrix:

$$s^{(N)}_{\beta m,\alpha n} = s^{(0)}_{\beta m,\alpha n} + \frac{-i}{\hbar\sqrt{v_{\beta m}v_{\alpha n}}} \sum_{i,j=1}^{N} \bar{\psi}^{(0)}_{\beta m}(\mathbf{r}_i)\gamma_i M_{ij}\psi^{(0)}_{\alpha n}(\mathbf{r}_j) \ . \tag{4.22}$$

- The N-impurity scattering matrix functional derivative:

$$\frac{\delta s^{(N)}_{\beta m,\alpha n}}{\delta U(\mathbf{r})} = \frac{-i}{\hbar\sqrt{v_{\beta m}v_{\alpha n}}} \left(i\hbar v_{\beta m} \int_{C_\beta} dy' \phi_{\beta m}(y') G^{(N)}(x_\beta, y'; \mathbf{r}) \right) \psi^{(N)}_{\alpha n}(\mathbf{r}) \ . \tag{4.23}$$

Using these results we can study emittance fluctuations, $\Delta E_{\alpha\beta}$, and nonlinear conductance fluctuations, $\Delta G_{\alpha\beta\gamma}$, in the diffusive regime. Note that our results are perfectly general. They are valid in any dimension, for any confinement potential, and in the presence of a magnetic field. Thus, we have a general set of tools to study quantum interference effects in phase coherent conductors. Note that in the presence of a magnetic field one cannot use the generalised Fisher-Lee relation to simplify the expression for the functional derivative of the scattering matrix, and thus one must compute the Green's function.

4.2 *One impurity in a 2D pipe: An Analytical Solution*

In this section we reproduce the results found in [76] and [77]. In [76] an exact expression for the wave function $\psi(\mathbf{r})$ was obtained for a perfect quasi-1D wire with one delta impurity placed in the scattering region. The wave function $\psi(\mathbf{r})$ was computed using a mode matching technique. The scattering matrix was then obtained from $\psi(\mathbf{r})$. The electrons incoming energy was chosen such that only one mode propagates through the wire. In [77] the functional derivative of the scattering matrix was computed, by adding an extra infinitesimal delta-function perturbation, $\delta U(\mathbf{r}) = \delta U \delta(\mathbf{r} - \bar{r})$, where $\delta U \to 0$. Let's use our results from the previous section to obtain expressions for the wave function, the scattering matrix and its functional derivative. This exercise serves as a confirmation of our results.

Let us first compute the scattering matrix elements $s^{(1)}_{1m,1n}$ and $s^{(1)}_{2m,1n}$. To accomplish this we require the free scattering wave functions, $\psi^{(0)}_{1n}(\mathbf{r})$ and $\psi^{(0)}_{2n}(\mathbf{r})$. For a perfect quasi-1D quantum wire, these are given by [5],

$$\psi^{(0)}_{1n}(\mathbf{r}) = \phi_n(y)e^{+ik_nx} \quad \text{and} \quad \psi^{(0)}_{2n}(\mathbf{r}) = \phi_n(y)e^{-ik_nx} \ . \tag{4.24}$$

From Eq. (4.22) we have,

$$\begin{aligned} s^{(1)}_{2m,1n} &= s^{(0)}_{2m,1n} + \frac{-i}{\hbar\sqrt{v_{2m}v_{1n}}}\psi_{2m}(\mathbf{r})\gamma_1 M_{11}\psi_{1n}(\mathbf{r}) \\ &= s^{(0)}_{2m,1n} + \frac{-i}{\hbar\sqrt{v_{2m}v_{1n}}}\left(\phi_m(y_1)e^{-ik_mx_1}\right)\gamma_1 M_{11}\left(\phi_n(y_1)e^{+ik_nx_1}\right) \\ &= \delta_{mn} + \frac{-i}{\hbar\sqrt{v_{2m}v_{1n}}}\frac{\gamma_1\phi_m(y_1)\phi_n(y_1)}{1-\gamma_1\eta_{11}}e^{i(k_n-k_m)x_1} \ , \end{aligned}$$

where we have used $s^{(0)}_{2m,1n} = \delta_{mn}$, for a perfect quasi-1D quantum wire, and $M_{11} = [1-\gamma_1\eta_{11}]^{-1}$. Let us set $x_1 = 0$, $y_1 = y_0$, $\gamma_1 = \gamma$, $\eta_1 = \eta$, and $v_n = 2k_n$ in the above equation so that we have the same notation and units as in [76]. We then find

$$\begin{aligned} s^{(1)}_{2m,1n} &= \delta_{nm} + \frac{-i}{2\sqrt{k_mk_n}}\frac{\gamma\phi_m(y_0)\phi_n(y_0)}{1-\gamma\eta} \\ &= \delta_{nm} + \frac{-i}{2\sqrt{k_mk_n}}\frac{\Gamma_{nm}}{\alpha} \ , \end{aligned}$$

where $\Gamma_{nm} = \gamma\phi_n(y_0)\phi_m(y_0)$ and $\alpha = 1-\gamma\eta$. Following [76], we have that

$$c_1 \equiv s^{(1)}_{21,11} = 1 - \frac{i\Gamma_{11}}{2k_1\alpha} \ , \tag{4.25}$$

which is exactly their result. Following the same procedure we find,

$$b_1 \equiv s^{(1)}_{11,11} = \frac{-i\Gamma_{11}}{2k_1\alpha} \ , \tag{4.26}$$

which is also in agreement.

We now compute the functional derivative of the scattering matrix using Eq. (4.23). To do this we must compute the wavefunction. The first ingredient needed is the impurity free Green's function for a perfect quasi-1D wire is given by [5],

$$G^{(0)}(\mathbf{r},\mathbf{r}') = \sum_n \phi_n(y)\phi_n(y')\frac{e^{ik_n|x-x'|}}{i\hbar v_n} \ . \tag{4.27}$$

From Eq. (4.21) we have

$$\begin{aligned} \psi^{(1)}_{1n}(\mathbf{r}) &= \psi^{(0)}_{1n}(\mathbf{r}) + G^{(0)}(\mathbf{r},\mathbf{r}_1)\gamma_1 M_{11}\psi^{(0)}_{1n}(\mathbf{r}_1) \\ &= \phi_n(y)e^{ik_nx} + \left(\sum_m \phi_m(y)\phi_m(y_1)\frac{e^{ik_m|x-x_1|}}{i\hbar v_m}\right)\left(\frac{\gamma_1}{1-\gamma_1\eta_{11}}\phi_n(y_1)e^{ik_nx_1}\right) \\ &= \phi_n(y)e^{ik_nx} + \sum_m \frac{\gamma_1\phi_n(y_1)\phi_m(y_1)e^{ik_nx_1}}{i\hbar v_m(1-\gamma_1\eta_{11})}\phi_m(y)e^{ik_m|x-x_1|} \ . \end{aligned}$$

Using the same notation and units as in [77], we find,

$$\begin{align}\psi^{(1)}_{11}(x,y) &= \phi_1(y)e^{+ik_1x} + \sum_m \frac{-i\gamma_1\phi_1(y_1)\phi_m(y_1)}{2k_m(1-\gamma_1\eta_{11})}\phi_m(y)e^{ik_m|x|} \nonumber\\ &= \phi_1(y)e^{+ik_1x} + \sum_m \frac{-i\Gamma_{1m}}{2k_m\alpha}\phi_m(y)e^{ik_m|x|} \ . \tag{4.28}\end{align}$$

Similarly,

$$\psi^{(1)}_{21}(x,y) = \phi_1(y)e^{-ik_1x} + \sum_m \frac{-i\Gamma_{1m}}{2k_m\alpha}\phi_m(y)e^{ik_m|x|} \ . \tag{4.29}$$

The functional derivative of the scattering matrix is given by (see Eq. (4.23)),

$$\frac{\delta s^{(1)}_{\beta m,\alpha n}}{\delta U(\mathbf{r})} = \frac{-i}{2\sqrt{k_m k_n}}\psi^{(1)}_{\beta m}(\mathbf{r})\psi^{(1)}_{\alpha n}(\mathbf{r}) \ , \tag{4.30}$$

where we have used the Generalized Fisher-Lee relation. Using Eq. (4.25), Eq. (4.28), Eq. (4.29), and Eq. (4.30), we find, for $x < x_1 = 0$,

$$\begin{align}\frac{\delta c_1}{\delta U(\mathbf{r})} &= \frac{\delta s^{(1)}_{21,11}}{\delta U(\mathbf{r})} \tag{4.31}\\ &= \frac{-i}{2k_1}\psi^{(1)}_{21}(x,y)\psi^{(1)}_{11}(x,y) \tag{4.32}\\ &= \frac{1}{2ik_1}\left(\sum_m c_m\phi_m(y)e^{-ik_mx}\right)\psi(x,y) \ , \nonumber\end{align}$$

where we have set $\psi(x,y) = \psi_{11}(x,y)$ and $c_m = \delta_{1m} - i\Gamma_{1m}/(2k_m\alpha)$. This is the result found in [77]. Similarly, we have that,

$$\begin{align}\frac{\delta b_1}{\delta U(\mathbf{r})} &= \frac{\delta s^{(1)}_{11,11}}{\delta U(\mathbf{r})} \tag{4.33}\\ &= \frac{-i}{2k_1}\psi^{(1)}_{11}(\mathbf{r})\psi^{(1)}_{11}(\mathbf{r}) \tag{4.34}\\ &= \frac{1}{2ik_1}\psi(\mathbf{r})\psi(\mathbf{r}) \ , \nonumber\end{align}$$

which is also consistent with the results in [77]. Now that we have verified our formalism against known results, we move onto the heart of our work, studying emittance and nonlinear conductance in diffusive conductors.

4.3 *Admittance Fluctuation in the UCF regime*

We now study emittance fluctuations, ΔE_{21}, and nonlinear conductance fluctuations, ΔG_{111}, in the Universal Conductance Fluctuations (UCF) regime. For a disordered conductor described by the elastic mean free path l_m and conductor linear size L, the quantity l_m/L has been considered [98] as the fraction of all the M transmission channels in the disordered sample (*e.g.* in 2D) for which the transmission probability is of order unity, *i.e.* these $M_{eff} \sim M(l_m/L)$ channels are the open channels responsible for conduction. Then the conventional UCF phenomenon can be viewed as a reflection of the sample-to-sample fluctuation of M_{eff}, which is related to a single parameter l_m.

In our study, we take advantage of the fact that we have access to the full parameter space, N and $\{\gamma_i\}$. This allows us investigate the crossover from the ballistic regime to the UCF regime, and from the UCF regime to the insulating regime. This will lead us to gain a better understanding of the physics behind the crossover from one regime to another. We start by studying the fluctuations of G_{21} in order to find where the UCF regime is located.

To start, let us compute the N-delta impurity scattering matrix for a quasi-1D quantum wire. The free scattering wavefunction for this system, $\psi_{1n}^{(0)}$ and $\psi_{2m}^{(0)}$, are given by Eq. (4.24). Putting these expression into Eq. (4.22) we find,

$$\begin{aligned} s_{2m,1n}^{(N)} &= s_{2m,1n}^{(0)} + \frac{-i}{\hbar\sqrt{v_{2m}v_{1n}}} \sum_{i,j=1}^{N} \psi_{2m}^{(0)}(\mathbf{r}_i)\gamma_i M_{ij} \psi_{1n}^{(0)}(\mathbf{r}_j) \\ &= \delta_{nm} + \frac{-i}{\hbar\sqrt{v_m v_n}} \sum_{i,j=1}^{N} \phi_m(y_i) e^{-ik_m x_i} \gamma_i M_{ij} \phi_n(y_j) e^{ik_n x_j} \\ &= \delta_{nm} + \frac{-i}{\hbar\sqrt{v_m v_n}} \sum_{i,j=1}^{N} \gamma_i M_{ij} \phi_m(y_i)\phi_n(y_j) e^{i(k_n x_j - k_m x_i)} \ , \end{aligned} \tag{4.35}$$

and

$$\begin{aligned} s_{1m,1n}^{(N)} &= s_{1m,1n}^{(0)} + \frac{-i}{\hbar\sqrt{v_{1m}v_{1n}}} \sum_{i,j=1}^{N} \psi_{1m}^{(0)}(\mathbf{r}_i)\gamma_i M_{ij} \psi_{1n}^{(0)}(\mathbf{r}_j) \\ &= \frac{-i}{\hbar\sqrt{v_m v_n}} \sum_{i,j=1}^{N} \gamma_i M_{ij} \phi_m(y_i)\phi_n(y_j) e^{i(k_n x_j + k_m x_i)} \ . \end{aligned} \tag{4.36}$$

These expressions for the scattering matrix are used to compute the linear DC conductance, with the help of the Landauer-Büttiker formula Eq. (1.21).

Let us now compute the functional derivative of the N-delta impurity scattering matrix. To do this we first obtain expressions for the wave functions $\psi_{1n}^{(N)}$ and $\psi_{2m}^{(N)}$.

Putting Eq. (4.24) and Eq. (4.27) into Eq. (4.21) we find,

$$
\begin{aligned}
\psi_{1n}^{(N)}(\mathbf{r}) &= \psi_{1n}^{(0)}(\mathbf{r}) + \sum_{i,j=1}^{N} G^{(0)}(\mathbf{r},\mathbf{r}_i)\gamma_i M_{ij}\psi_{1n}^{(0)}(\mathbf{r}_j) \\
&= \phi_n(y)e^{ik_n x} + \sum_{i,j=1}^{N}\left(\sum_n \phi_n(y)\phi_n(y_i)\frac{e^{ik_n|x-x_i|}}{i\hbar v_n}\right)\gamma_i M_{ij}\phi_n(y_j)e^{ik_n x_j} \\
&= \phi_n(y)e^{ik_n x} + \sum_n \phi_n(y)\left(\sum_{i,j=1}^{N}\gamma_i M_{ij}\phi_n(y_i)\phi_n(y_j)\frac{e^{ik_n(|x-x_i|+x_j)}}{i\hbar v_n}\right), \quad (4.37)
\end{aligned}
$$

and

$$
\begin{aligned}
\psi_{2n}^{(N)}(\mathbf{r}) &= \psi_{2n}^{(0)}(\mathbf{r}) + \sum_{i,j=1}^{N} G^{(0)}(\mathbf{r},\mathbf{r}_i)\gamma_i M_{ij}\psi_{2n}^{(0)}(\mathbf{r}_j) \\
&= \phi_n(y)e^{-ik_n x} + \sum_n \phi_n(y)\left(\sum_{i,j=1}^{N}\gamma_i M_{ij}\phi_n(y_i)\phi_n(y_j)\frac{e^{ik_n(|x-x_i|-x_j)}}{i\hbar v_n}\right). \quad (4.38)
\end{aligned}
$$

Now that we have expressions for $\psi_{1n}^{(N)}(\mathbf{r})$ and $\psi_{2n}^{(N)}(\mathbf{r})$, we use equation Eq. (4.23) to obtain an explicit expression for $\delta s_{\beta m,\alpha n}^{(N)}/\delta U(\mathbf{r})$. We can now use the results from Chapter 3 to obtain exact expressions for E_{21} and G_{111}.

4.3.1 Linear DC conductance G_{21}

Our first objective is to find the UCF regime. Our parameter space is given by the variables that control the strength of the impurity potential. These are, the number of impurities, N, and the strength of each impurity, $\{\gamma_i\}$. To simplify our analysis, without changing any of the essential features, we set all the impurity strengths equal to one common value γ, i.e. $\gamma_i = \gamma$ for $i = 1,...,N$. With this simplification the impurity potential strength is fixed by only two parameters N and γ.

We are now ready to compute G_{21} for different random impurity configurations. We choose the transverse eigenfunction, $\phi_n(y)$, to be the usual sine functions, $\phi_n(y) = \sqrt{2/W}\sin(n\pi y/W)$, where W is the width of the quantum wire. We fix the incoming energy of the electron such that there are 18 propagating modes in the wire, whose contributions are summed up. Our procedure is the following: first we generate a random impurity configuration, $\{\mathbf{r}_i\}$, where $i = 1,...,N$, which we then use to evaluate the quantity M_{ij}, by direct matrix inversion. The impurity positions are

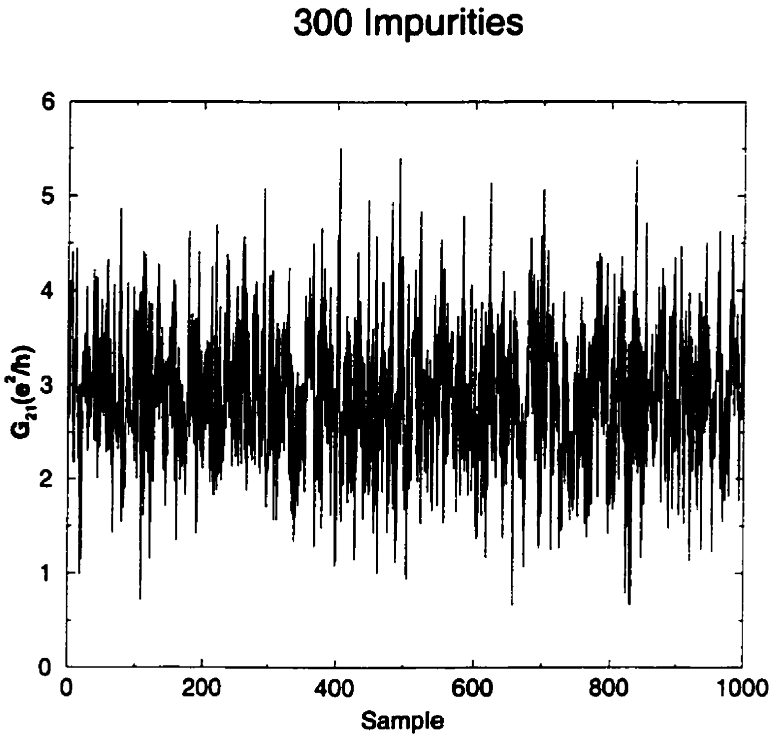

Figure 4.1: Plot of the linear DC conductance G_{21} versus sample number, for $N = 300$ and $\gamma = 100$. Each data point corresponds to the conductance for a fixed random impurity configuration $\{\mathbf{r}_i\}$. The large fluctuations seen in this graph corresponds to quantum interference effects. With this choice of parameters the system is in the UCF regime, where $\Delta G_{21} \approx 0.86e^2/h$. As the figure indicates, 1000 samples were used. The choice of units for the conductance is $G_0 = e^2/h$.

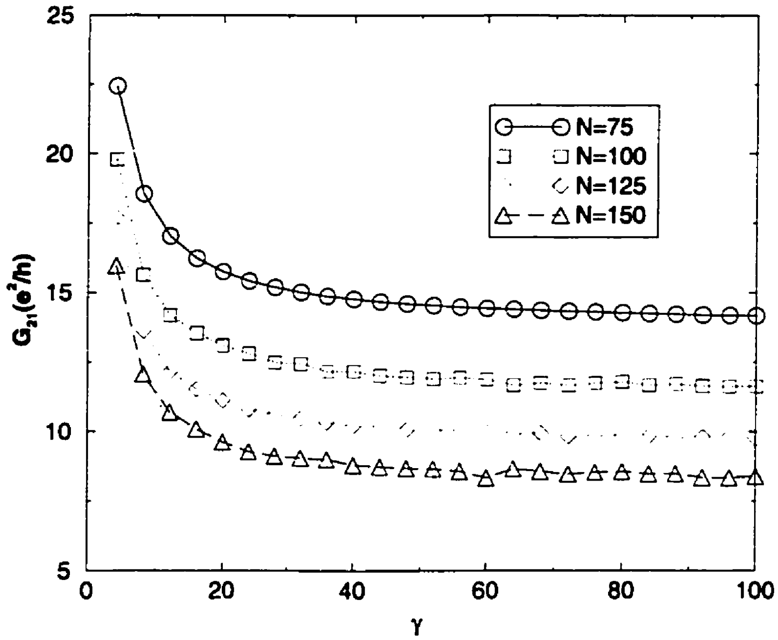

Figure 4.2: Plots of $< G_{21} >$ versus γ for a variety of values of N, from $N = 75$ to $N = 150$. Each data point on each of the curves is obtained by averaging over a 1000 random impurity configurations. As the number of impurities is increased the computation time increases as N^2, which effectively limits the range of values that we can explore in a reasonable time. We clearly see that the conductances dependence on γ is weak for high values of $\gamma > 40$. The choice of units for the conductance is $G_0 = e^2/h$.

chosen to be randomly and uniformly distributed throughout the scattering region. Once we have the matrix M_{ij}, we use Eq. (4.36) to obtain the scattering matrix, which is then used to compute the conductance for this impurity configuration using Eq. (2.64). Finally, sample-to-sample statistical analysis is carried out by averaging over many random impurity configurations for fixed values of N and γ. We have checked numerical convergence for the conductance fluctuations.

In Fig. 4.1 we plot the conductance versus the sample number. We have fixed the number of impurities to be $N = 300$ and set the impurity strength equal to $\gamma = 100$. This graph is very reminiscent of typical data from numerical studies of universal conductance fluctuations [54, 55, 56]. For these values of N and γ we find that the conductance fluctuations is equal to $\Delta G_{21} \approx 0.86e^2/h$, where $\Delta G_{21} = \sqrt{< G_{21}^2 > - < G_{21} >^2}$, which is the expected value of conductance fluctuations for the UCF regime in 2D systems [55].

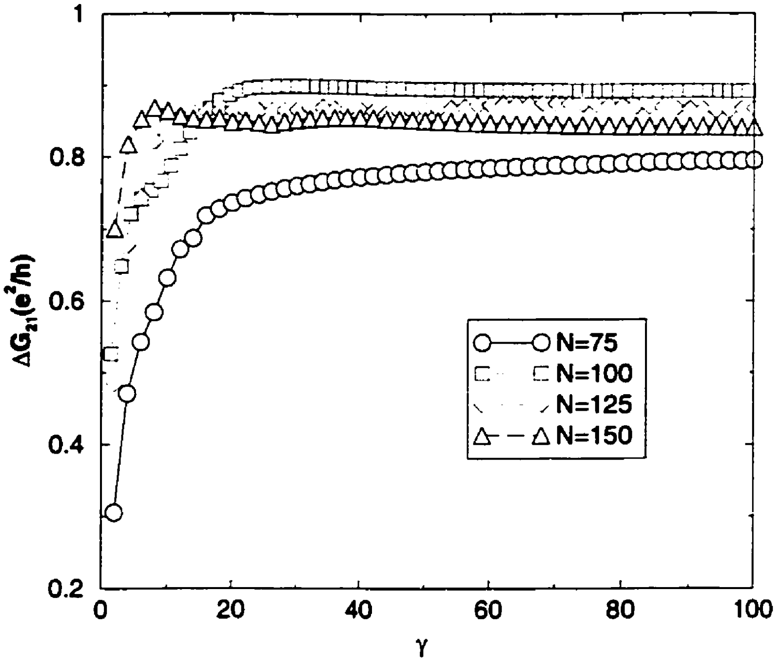

Figure 4.3: Plots of ΔG_{21} versus γ for a variety of values of N, from $N = 75$ to $N = 150$. The data points for each curves are obtained by averaging over a 1000 impurity configurations. We clearly see that the conductances fluctuations become independent of the disorder parameters, N and γ, and have the universal value $\Delta G_{21} \approx 0.86e^2/h$ (within 5% error), when $N \geq 100$ and $\gamma > 10$. The unit of conductance is $G_0 = e^2/h$.

In Fig. 4.2 we plot the average conductance $< G_{21} >$ versus the impurity strength, γ, for a variety of values for N. Over 1000 impurity configurations were used to average. The decrease of $< G_{21} >$ is vary rapid for smaller values of γ but it becomes quite slow when γ is large. The sample is metallic even for the largest γ(=100), as eighteen incoming channels add up to a conductance of the order $10G_0$, where $G_0 = e^2/h$. At large γ, $< G_{21} >$ depends on N very sensitively as Fig. 4.2 shows.

In Fig. 4.3 we plot the conductance fluctuations versus the impurity strength for different values of N. First, note that for $N \geq 100$ and $\gamma > 10$ the conductance fluctuations are independent of the disorder parameters, N and γ, and have the usual universal value for 2D diffusive conductors, $\Delta G_{21} \approx 0.86e^2/h$ (within 5% error). This behavior persists all the way up to $N = 325$ (and $\gamma > 10$), after which point the conductance fluctuations start to decrease as N is further increased. For $N = 75$ the conductance fluctuations are slightly under the universal value, for the full range of values for γ. When the value of N is too low ($N < 75$) the transport is not in the UCF regime, no matter the value for γ, i.e. the disorder is not strong enough to generate maximal interference effects. Therefore, ΔG_{21} is less than the UCF value. Indeed, in the limit $N = 0$, our conductor is a perfect quasi-1D wire for which $\Delta G_{21} = 0$ identically. On the other hand when N is high ($N > 350$) the conductor approaches the insulating state. In this situation the wavefunction starts to be localized so that the conductance fluctuations are again reduced from the UCF value. Therefore, between $N = 100$ and $N = 325$ (and $\gamma > 10$) we have the UCF regime, for our choice of incoming energy E. Note that UCF also exists for larger values of N but with smaller values of $\gamma < 10$.

Now that we have identified a region of the parameter space where the UCF regime is, let us move our attention to the actual distribution functions of G_{21}, which we denote by $P(G_{21})$. In Fig. 4.4 and Fig. 4.5 we show the histogram of the conductance for different values of N, from $N = 50$ to $N = 500$ with $\gamma > 80$. These are, essentially, the distribution functions of G_{21}. When N is small, e.g. $N = 50$, the distribution resembles a narrow Gaussian like function, whose *rms* is smaller than the universal value. As the number of impurities is increased, the Gaussian like distribution becomes wider until the UCF regime is reached around $N = 100$. As N is increased from 100 to 300 the distribution remains unchanged except that it's average value, $< G_{21} >$, decreases. This is the UCF regime. As the average value of G_{21} decreases, with increasing value of N, the distribution approaches the insulating regime ($G_{21} = 0$), i.e. when no current flows through the system. As N increase beyond 300 the tail of the Gaussian like distribution starts to accumulate against the $G_{21} = 0$ limit. The distribution becomes narrower, which leads to a reduced value for ΔG_{21}, the *rms* of the distribution. Therefore, the end of the UCF regime starts when the tail of the distribution $P(G_{21})$ starts to accumulate against the hard wall at $G_{21} = 0$.

We now have identified a region in the parameter space where the UCF regime is located. We have also obtained a good understanding of G_{21} and ΔG_{21} dependence on N and γ. In the following sections we investigate the transport coefficients E_{21}

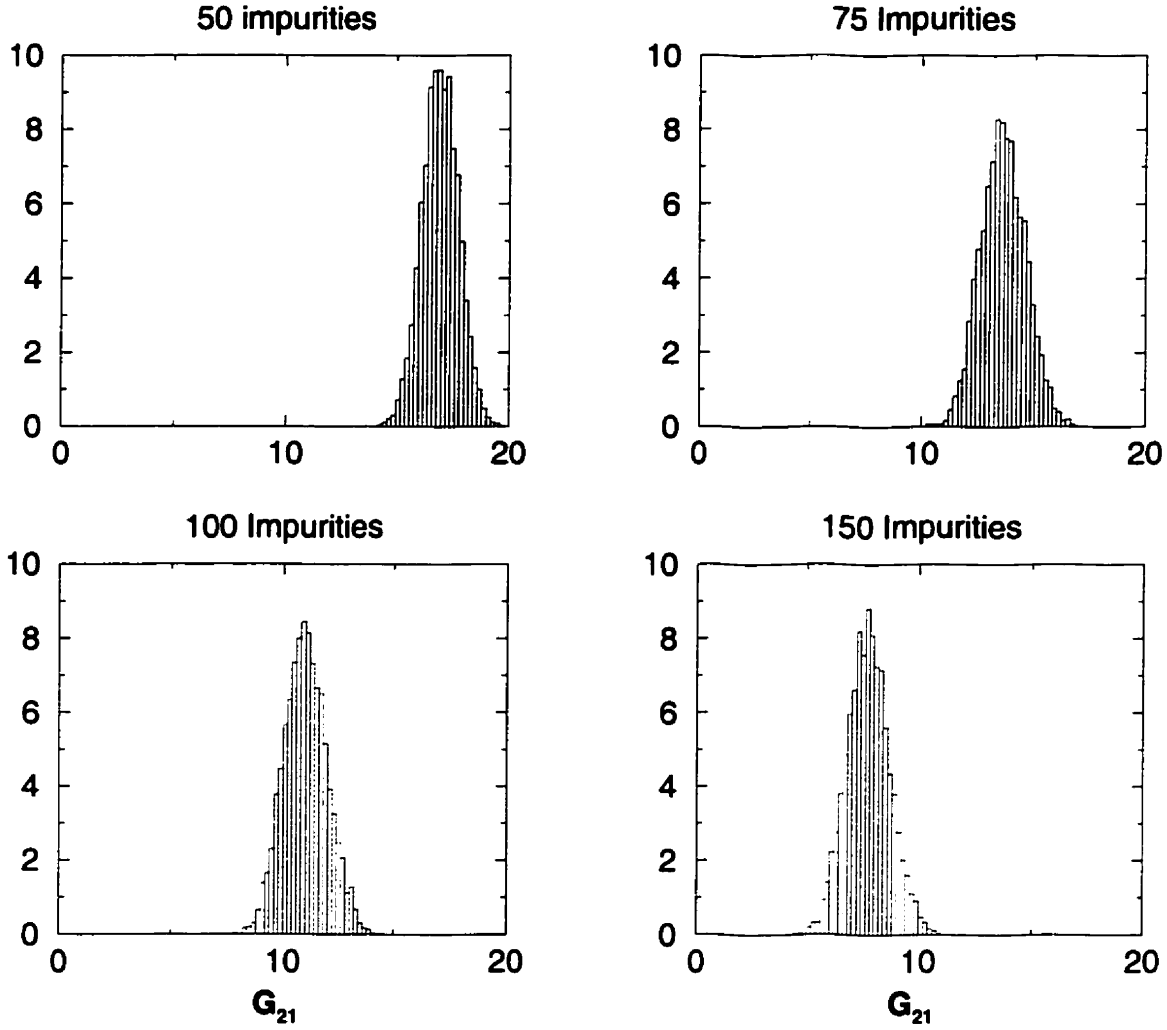

Figure 4.4: Histograms for G_{21} for different values of N, from $N = 50$ to $N = 150$. The value of the impurity strength is $\gamma = 80$. As the value of N increases from $N = 50$ to $N = 100$, the Gaussian like distribution increases in width, i.e. it *rms* increases. Already at $N = 75$ the distribution function $P(G_{21})$ is almost identical to the $N = 150$ distribution. This is expected since $\Delta G_{21} \approx 0.80$ for $N = 75$ and $\Delta G_{21} \approx 0.86$ for $N = 150$. We have used over 10000 different random impurity configurations to obtain each histogram. The units for the conductance is $G_0 = e^2/h$.

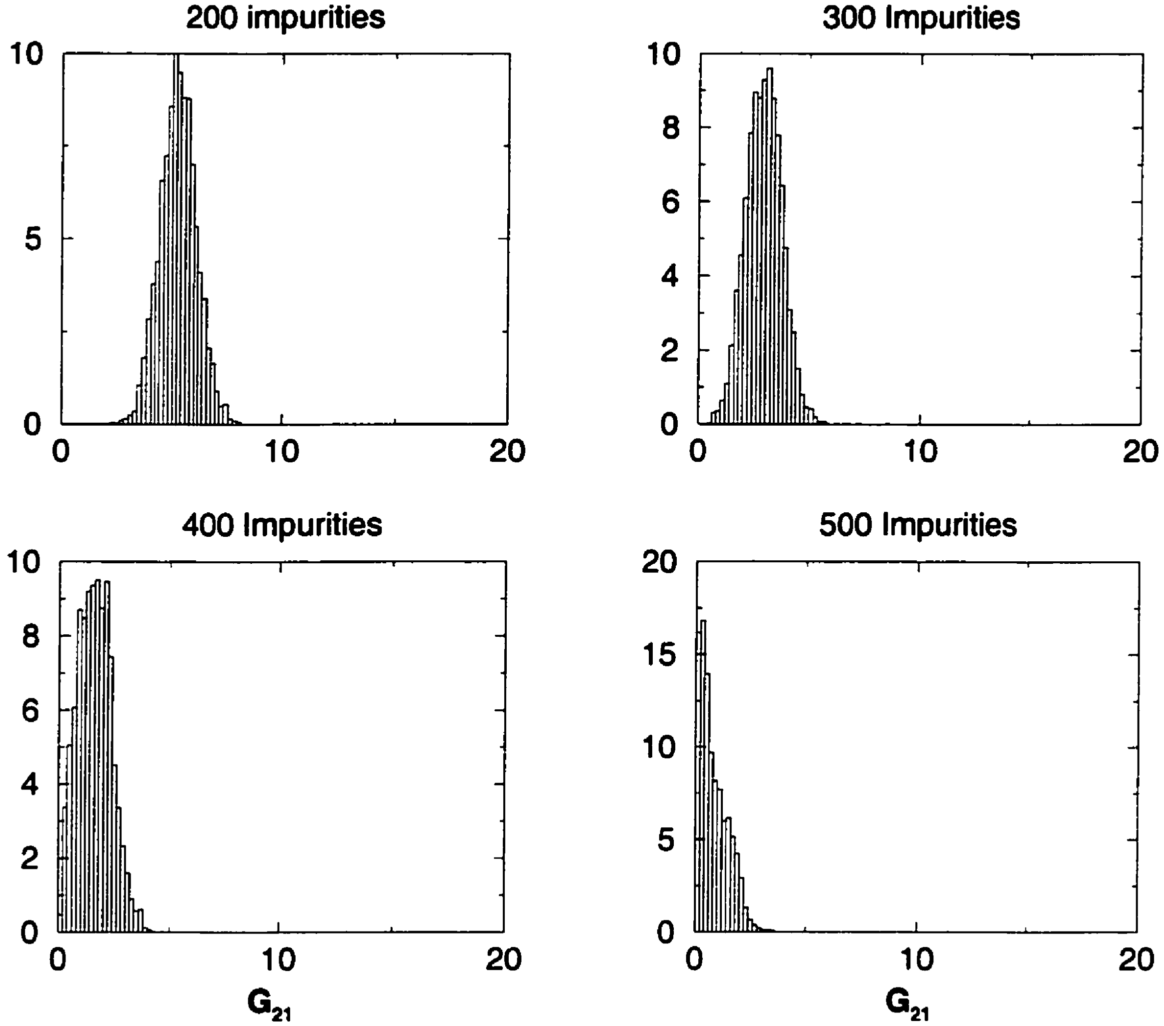

Figure 4.5: Histograms for G_{21} for different values of N, from $N = 200$ to $N = 500$. The value of the impurity strength is again chosen to be $\gamma = 80$. As the value of N increases from $N = 200$ to $N = 300$ the Gaussian like distribution retains it's shape and simply moves towards the $G_{21} = 0$ limit. At $N = 400$ the distribution function $P(G_{21})$ starts to accumulate against the $G_{21} = 0$ limit, which reduces the value of ΔG_{21}. For $N = 500$ the distribution has lost it's original shape and it's *rms* is significantly reduced. The units for the conductance is $G_0 = e^2/h$.

and G_{111}.

4.3.2 Linear AC conductance E_{21}

In this subsection we report the behavior of emittance E_{21}. In particular, we will study the emittance fluctuations in the UCF regime. The procedure for this study follows the same line as the one in the previous section. We use expressions for the scattering matrix Eq. (4.36), the wavefunction Eq. (4.37), and the characteristic potential Eq. (2.60), to evaluate the expression for E_{21} Eq. (2.66) for a given random impurity configuration $\{\mathbf{r}_i\}$. This procedure is repeated for many impurity configurations, typically 1000 to 10000. One major difference between computing G_{21} and E_{21}, is that the emittance requires the scattering wavefunction, $\psi_{\alpha n}(\mathbf{r})$, while the conductance only requires the scattering matrix, $s_{\alpha n,\beta m}$. On a numerical level this make the computation of E_{21} much more intensive than G_{21}, even with an exact expression for the scattering wavefunction.

For highly disordered sample $l_m << L$, we expect a capacitive-like dynamic response because of the large resistance. On the other hand, when the degree of disorder is reduced the response can be inductive-like. Hence, we expect the distribution function for E_{21}, which will be calculated below, to change as the degree of disorder changes, indicating a crossover from a capacitive response to an inductive response.

In Fig. 4.6 we plot typical sample-to-sample fluctuations for the emittance. We have used the same parameter as in Fig. 4.1 from the previous subsection, $N = 300$ and $\gamma = 100$. For this degree of disorder it is apparent that E_{21} fluctuates between negative and positive values, indicating that the dynamic response of the disordered conductor depends on impurity configuration. Recall that a system is said to have an capacitive response when $E_{21} = -E_{11} < 0$ and an inductive response when $E_{21} = -E_{11} > 0$. We see from Fig. 4.6 that depending on the impurity configuration, the AC current can either be leading or lagging the AC voltage. Thus, a simple rearrangement of impurity positions can change the dynamic nature of conduction in the diffusive regime. Therefore, the AC current can be leading or lagging quite randomly from sample to sample.

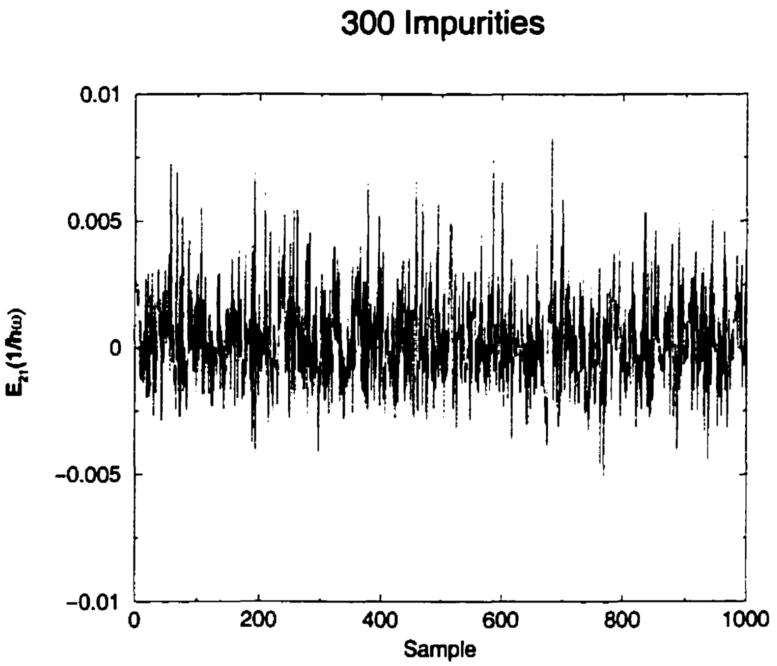

Figure 4.6: Plot of E_{21} versus sample number for $N = 300$ and $\gamma = 100$. With this choice of parameters, the system is in the UCF regime. The graph clearly shows that depending on positions of the impurities, the dynamic response of the conductor can either be inductive ($E_{21} > 0$), or capacitive ($E_{21} < 0$). Thus, the dynamical nature of the response depends on the impurity configuration. The unit for emittance is $E_0 = 1/\hbar\omega$.

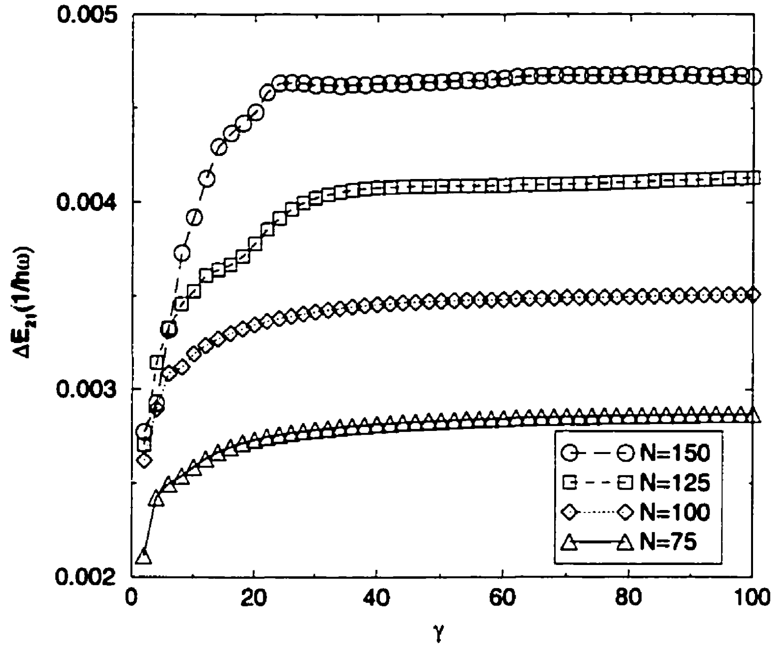

Figure 4.7: Plots of ΔE_{21} versus γ for a several values of N, from $N = 75$ to $N = 150$. Each data point was computed by averaging over 1000 random impurity configurations. We clearly see that the emittance fluctuations depend only weakly on γ for large values of $\gamma > 25$. On the other hand, the emittance fluctuations are very sensitive to the number of impurities, N. The unit for emittance is $E_0 = 1/\hbar\omega$.

In Fig. 4.7 we plot the emittance fluctuations as a function of the impurity strength γ for several different impurity number N. For each data point, 1000 random impurity configurations were averaged. Fig. 4.7 clearly shows that when γ is large enough ($\gamma > 25$), ΔE_{21} seems to be independent of γ, showing some generic behavior with respect to the impurity scattering strength. However, because E_{21} depends on the electrostatic potential build-up inside the conductor [64, 82], as reflected by the functional derivative in LPDOS (see Eq. (2.35)), ΔE_{21} is thus expected to be a sensitive function of the degree of disorder determined by impurity number N. Our results indeed confirms this picture as shown in Fig. 4.7.

Let us now turn our attention to the distribution functions $P(E_{21})$. Of the two contributions to E_{21}, namely the external charge injection due to the time dependent disturbance and the internal response due to Coulomb interactions, the external contribution is given by global partial density of states. This is related to the electron dwell time of the scattering region [84, 29]. The distribution function of dwell time has been analyzed within the random matrix theory [99, 100] for chaotic cavities, and within the invariant embedding formalism for 1D disordered system [101]. Their universal properties have been well studied [102, 103]. However, the statistical properties of the internal response is much more complicated and it has only been included within the very crude constant capacitance charging model for chaotic cavities [99, 104]. Here we numerically investigate $P(E_{21})$ from first principles where the internal response is calculated through the LPDOS. Fig. 4.8 shows $P(E_{21})$ obtained from our numerical analysis for different values of N. Each of the graphs were obtained by generating over 10000 data points, each of which corresponds to a random impurity configuration. When N is small, *e.g.*, $N = 50$, $P(E_{21})$ is centered around a positive value of E_{21}, which indicates a predominantly inductive dynamic response (see Fig. 4.8). This is consistent with the fact that the system is rather conductive for this degree of disorder. Also note that the distribution function is quite symmetric. As N is increased to 300, the larger degree of disorder makes the system less conductive, and the center of the distribution is shifted to center near zero (see Fig. 4.9). While the distribution is still quite symmetric, it is now wider indicating a larger fluctuation amplitude ΔE_{21}, as seen in Fig. 4.7. When N is increased further, $P(E_{21})$ not only shifts its center to a negative value of E_{21}, it becomes asymmetric (see Fig. 4.9). For large N the disordered system is less conductive, therefore we expect a capacitive dynamic response (*e.g.* a parallel plate capacitor has zero DC conductance). This is clearly shown by the shift of the distribution toward negative values of emittance. For $N = 500$ the body of the distribution is located on the capacitive side while the right tail of $P(E_{21})$ extends far into the inductive side. We note that the random matrix theory predicts a capacitance distribution which is also asymmetric, for an one-probe chaotic cavity [99].

This study of emittance demonstrates the fundamental differences between transport coefficients that only depends on the external response versus transport coefficients which also depend on the internal response. The internal response for the

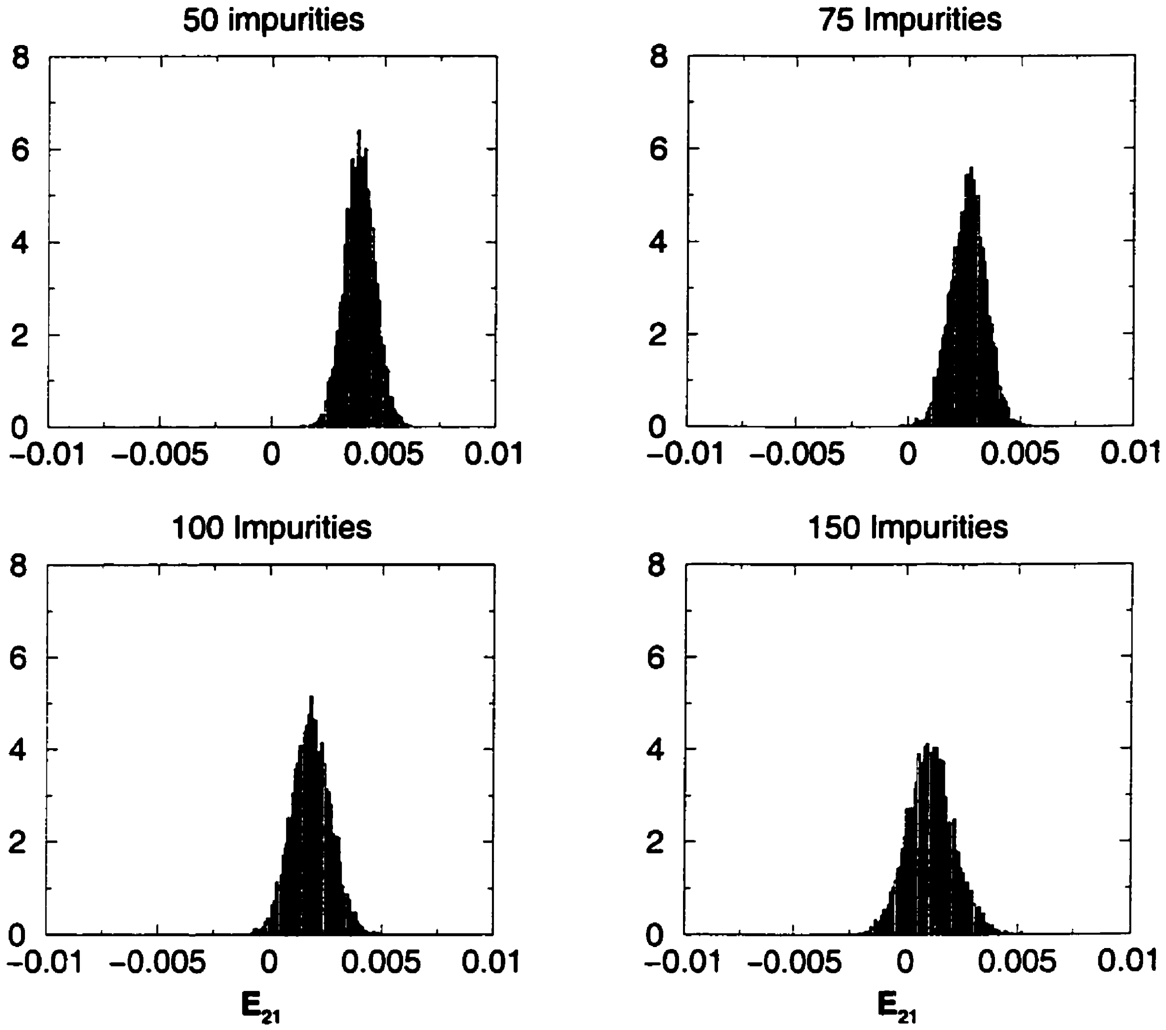

Figure 4.8: Histograms of E_{21} for different values of N, from $N = 50$ to $N = 150$. The value of the impurity strength is chosen to be $\gamma = 80$. As the value of N increases from $N = 50$ to $N = 150$, we have a Gaussian like distribution whose width increases with N. Moreover, the average value of E_{21} approaches zero, as N is increased. The distribution becomes more and more capacitive, which is consistent with the system becoming less and less conductive as N is increased. We have used over 10000 different random impurity configurations to obtain each histogram. The unit for emittance is $E_0 = 1/h\omega$.

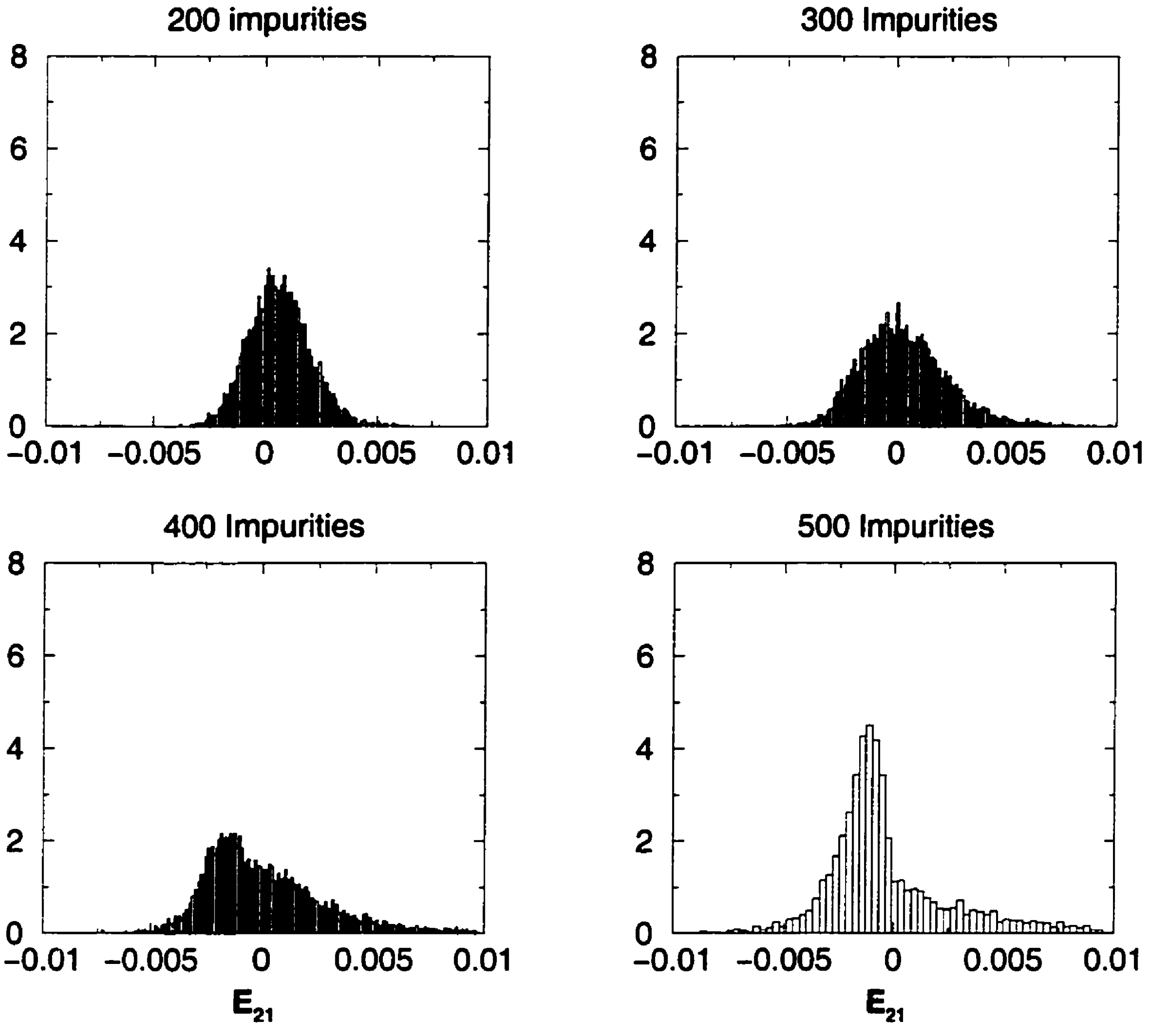

Figure 4.9: Histograms of E_{21} for different values of N, from $N = 200$ to $N = 500$. The value of the impurity strength is set equal to $\gamma = 80$. As the value of N increases from $N = 200$ to $N = 500$, the Gaussian like distribution developed a long tail in the inductive side. At $N = 500$ the body of the distribution is in the capacitive side while its tail extends far into the inductive side. We have used over 10000 different random impurity configurations for each graph. The unit for emittance is $E_0 = 1/\hbar\omega$.

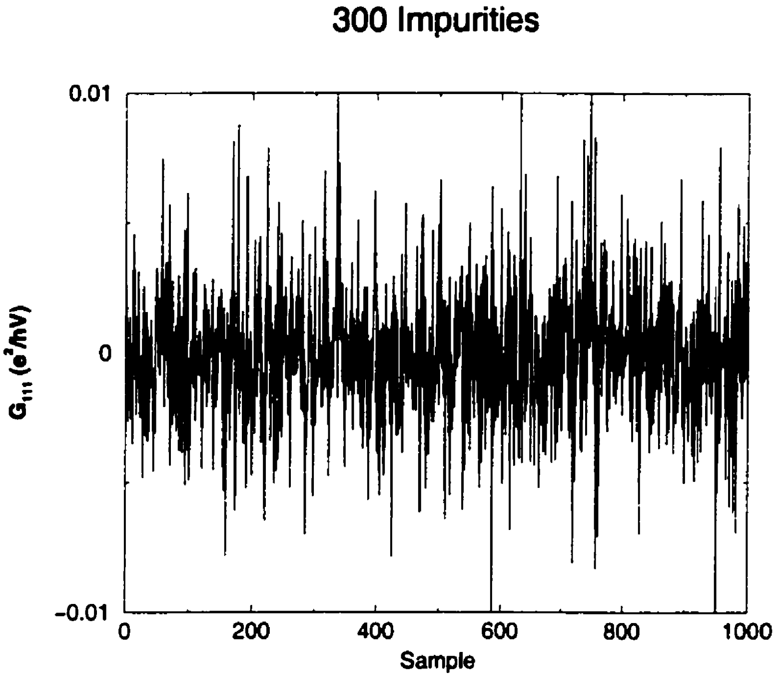

Figure 4.10: Plot of the nonlinear conductance G_{111} versus sample number for $N = 300$ and $\gamma = 100$. The graph shows that depending on the position of the impurities, the current going through the system can either be increased ($G_{111} > 0$) or decreased ($G_{111} < 0$), by the nonlinear current term. The unit for G_{111} is $G'_0 = e^2/hV$.

emittance, for example, leads to an asymmetric distribution function $P(E_{21})$, which is in contrast to the perfectly symmetric distribution for the G_{21} (away from $G_{21} = 0$). We now turn our attention to the nonlinear conductance G_{111}.

4.3.3 Nonlinear DC conductance G_{111}

In this subsection we study the behavior of the nonlinear DC conductance. We choose G_{111} as our nonlinear transport coefficient. This is equivalent to any other of the nonlinear conductances, $G_{\alpha\beta\gamma}$. From gauge invariance we have, $G_{111} + G_{112} = 0$ and $G_{111} + G_{121} = 0$, which implies $G_{111} = -G_{112} = -G_{121}$. As for current conservation it imposes the condition $G_{111} + G_{211} = 0$, which leads to $G_{111} = -G_{211}$. The rest of the coefficients are related to G_{111} using the other gauge invariance conditions.

We now study the nonlinear conductance fluctuations. The procedure for this follows the same lines as what was used to obtain emittance fluctuations. We use expressions for the scattering matrix Eq. (4.36), the wavefunction Eq. (4.37) and the characteristic potential Eq. (2.60), to evaluate the expression for G_{111} (see Eq. (2.65)), for a given random impurity configuration $\{\mathbf{r}_i\}$. We repeat this procedure for many impurity configurations, usually 1000 to 10000. Computing G_{111} is much more computationally intensive than G_{21} since it requires the wavefunction.

In Fig. 4.10 we plot the fluctuations of G_{111} from sample-to-sample. We use, once again, the same values for the disorder parameters that were chosen in the previous subsections, $N = 300$ and $\gamma = 100$. From Fig. 4.10 we see that conductance fluctuations are centered around $G_{111} = 0$. This is understood by the following. Using Eq. (2.16) we can evaluate the current going through the first lead, I_1. Combining this with the identities $G_{111} = -G_{112} = -G_{121} = G_{122}$ and $G_{11} = -G_{12}$, we arrive at the equation,

$$I_1 = G_{11}(V_1 - V_2) + G_{111}(V_1 - V_2)^2 \ . \tag{4.39}$$

Therefore, for a conductor with a symmetric potential landscape, $U(x,y) = U(-x,y)$, the current I_1 must be equal to $-I_1$ when we interchange the bias V_1 with V_2. This implies that the expression for the current cannot have a quadratic term, and hence the nonlinear conductance must vanish, $G_{111} = 0$. For our diffusive conductors, on average the random impurity configurations is symmetric, it then follows that the average conductance feels a symmetric potential landscape, which implies $< G_{111} >= 0$, which is what is seen in Fig. 4.10. For a specific sample, however, depending on the impurity configuration the we can have either $G_{111} > 0$ or $G_{111} < 0$. This implies that the nonlinear current contribution can either increase or decrease the total current depending on the impurity configuration.

In Fig. 4.11 we plot the nonlinear conductance fluctuations ΔG_{111} versus the number of impurities N. This graph clearly shows that ΔG_{111} depends very sensitively on the number of impurities. This behavior for ΔG_{111} originates from its dependence on the internal response of the device, which is characterized by the characteristic potential, $u_\alpha(\mathbf{r})$. To better understand the nonlinear conductance and its fluctuations, we turn to the distribution functions $P(G_{111})$.

In Fig. 4.12 and Fig. 4.13 we show the distribution functions for G_{111} for different

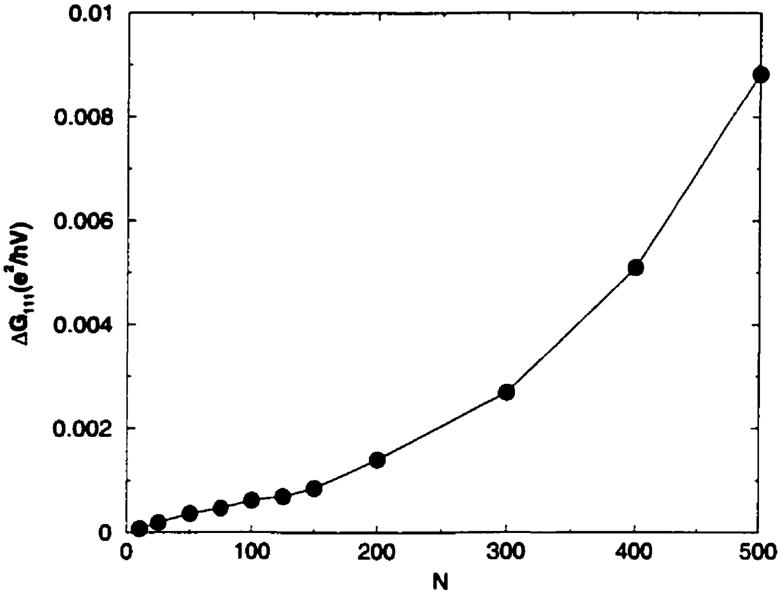

Figure 4.11: Plot of ΔG_{111} versus N, the number of impurities. The nonlinear conductance fluctuations depends very sensitively on N. When the value of N is low ($N < 150$) the increase of ΔG_{111} is approximately linear. As N goes from 150 to 500 the curve is looks like an exponential. The fluctuations grow very quickly with N for large $N > 150$. The unit for G_{111} is $G'_0 = e^2/hV$.

values of N. All the distributions functions are symmetric and centered around zero, since $< G_{111} >= 0$. When the value of N is low, around 50 (see Fig. 4.12), the distribution is a narrow Gaussian like function. As N increases from 50 to 150 the body of the distribution spreads symmetrically so that the $P(G_{111})$ slowly becomes a wider Gaussian like function. This is consistent with the slow increase in ΔG_{111}, as N is increased from 50 to 150, as seen in Fig. 4.11. As N is increased from 200 to 500 the distribution function change from a Gaussian like function to a symmetric exponentially decaying function centered around $< G_{111} >= 0$. The width of the distribution increases dramatically, which indicates that a wide range of values for the nonlinear conductance is reached. This picture is consistent with Fig. 4.11 which shows that the conductance fluctuations, i.e the *rms* of $P(G_{111})$, increases in an exponential like fashion as N increases.

In summary, we have analyzed the sample-to-sample fluctuations for linear DC, linear AC, and nonlinear DC conductance, in two dimensional disordered mesoscopic conductors. We found that the distribution function for G_{21} is a Gaussian like func-

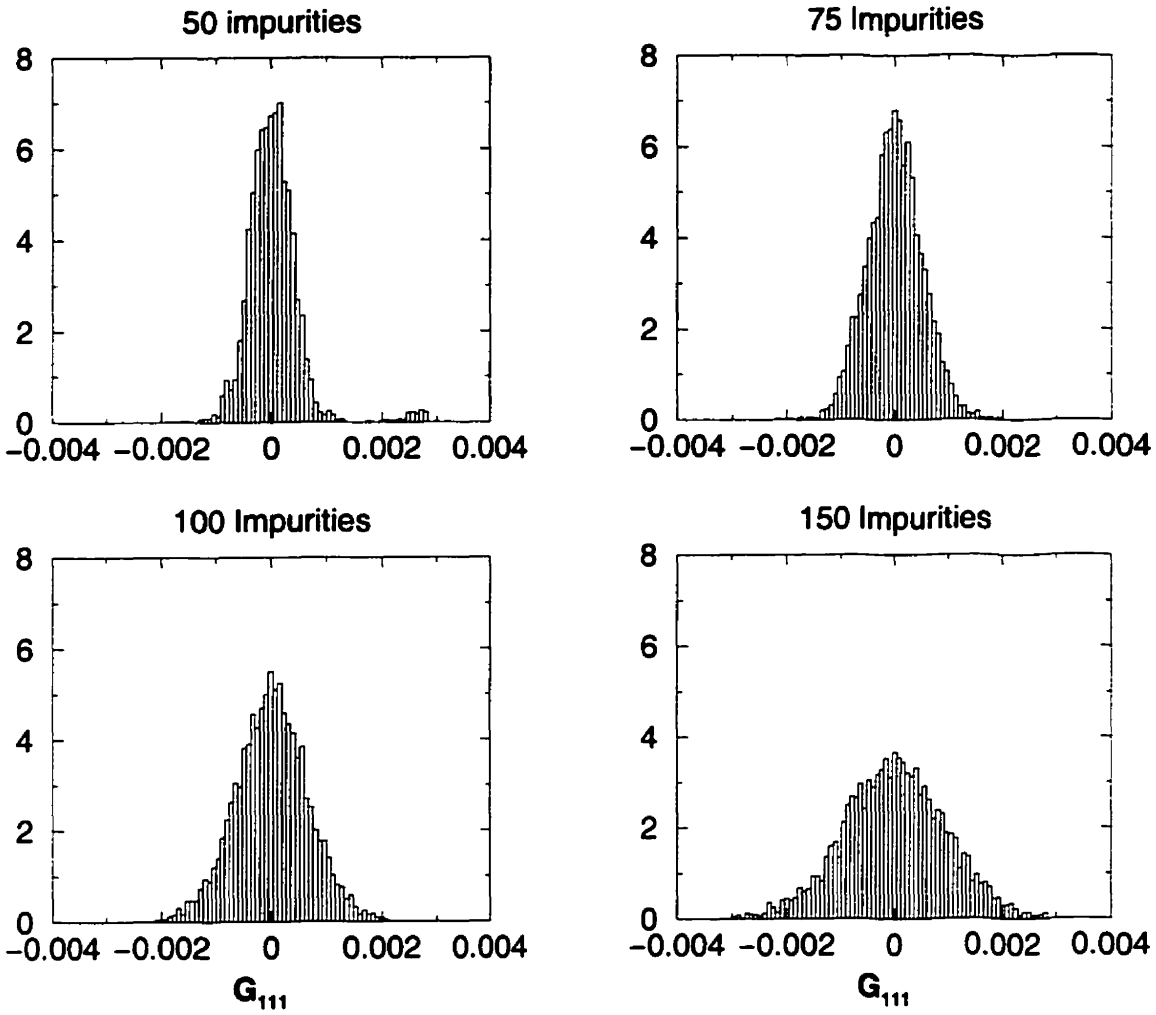

Figure 4.12: Histograms for G_{111} for different values of N, from $N = 50$ to $N = 150$. The value of the impurity strength is chosen to be $\gamma = 80$. As the value of N increases from $N = 50$ to $N = 150$ we have a Gaussian like distribution whose body spreads symmetrically around $G_{111} = 0$. The width of the distribution increases proportionally with N, which is consistent with Fig. 4.11. We have used over 10000 different random impurity configurations to obtain each distribution function. The unit for G_{111} is $G_0' = e^2/hV$.

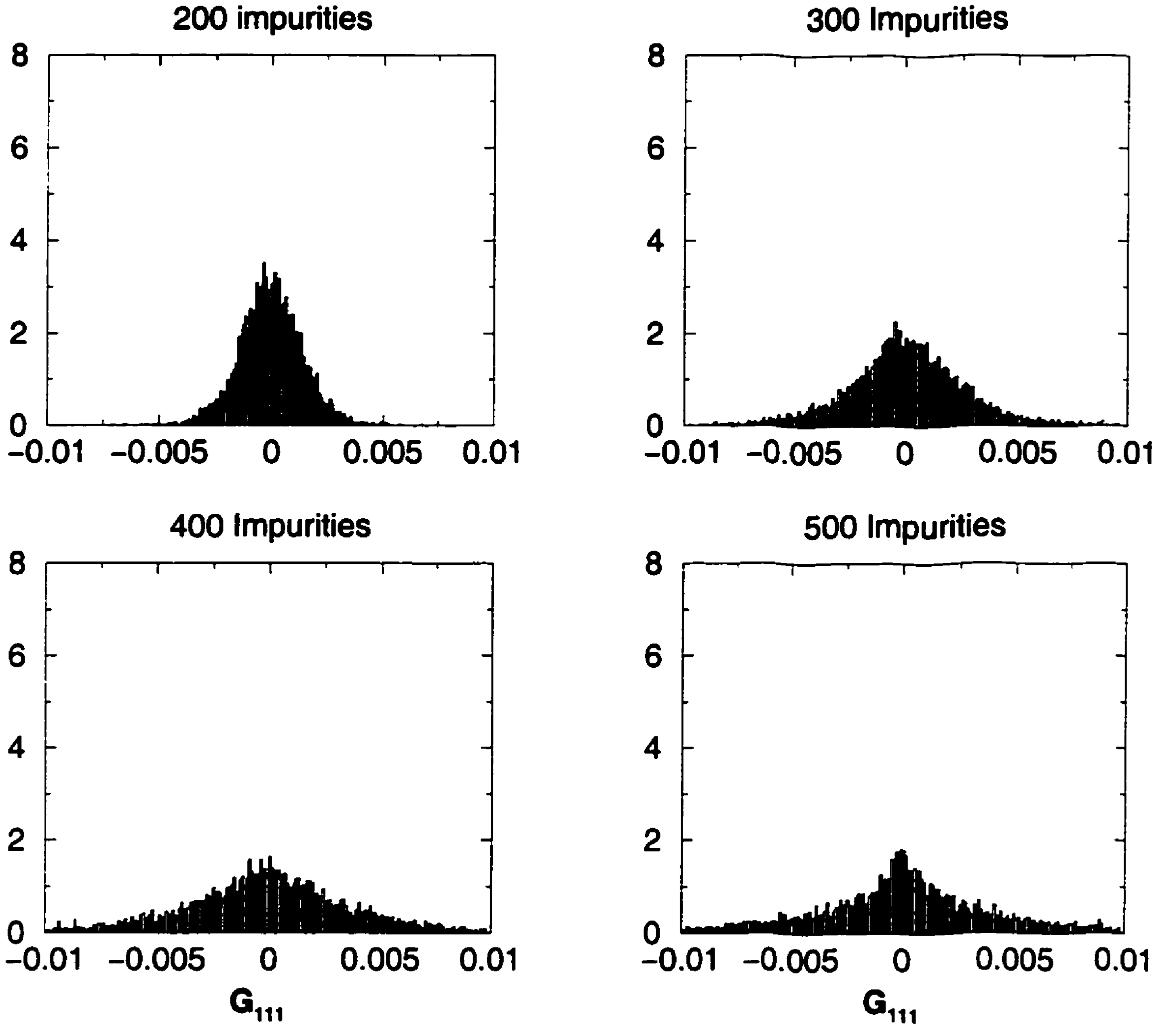

Figure 4.13: Histograms for G_{111} for different values of N, from $N = 200$ to $N = 500$. The value of the impurity strength is chosen to be $\gamma = 80$. As the value of N increases from $N = 200$ to $N = 500$ the distribution changes its shape from a Gaussian like function to a symmetric exponentially decaying function. The width of the distribution grows very rapidly from $N = 200$ to $N = 500$, which is consistent with what is seen in Fig. 4.11. We have used over 10000 different random impurity configurations to obtain each of these functions. The unit for G_{111} is $G'_0 = e^2/hV$.

tion for values of N and γ in the diffusive regime. When the tail of the Gaussian distribution starts to accumulate against the $G_{21} = 0$ limit, the value of ΔG_{21} is reduced from it's universal value $0.86e^2/h$. In contrast to the distribution function for G_{21}, we found that $P(E_{21})$ is symmetric for small disorder and asymmetric for strong disorder. When the value of N is low, the distribution $P(E_{21})$ is symmetric and centered around a positive value of E_{21}, which corresponds to an inductive behavior. But when the value of N is high the distribution $P(E_{21})$ becomes asymmetric: the body of the distribution is in the capacitive side $E_{21} < 0$, while having a long tail which extends deep into the inductive side. This type of asymmetry has been shown for chaotic cavities [99, 103]. Thus, the distribution function of the emittance depends on the dynamic response of the conductor: for an inductive like response the distribution is symmetric while for an capacitive response it is asymmetric.

We found that the distribution function for the nonlinear conductance at low disorder is Gaussian like. The average value of the distribution is $< G_{111} >= 0$. As the degree of disorder increases the width of the Gaussian like distribution increases in a linear fashion. At high values of disorder, $P(G_{111})$ looks like a symmetric exponentially decaying function, the body of the Gaussian distribution has speared symmetrically into two long tails. The fluctuations, at large values for the disorder, increase in an exponential manner. Thus, the distribution function of the nonlinear conductance depends on the internal response of the conductor: for small disorder the distribution is symmetric and Gaussian like, while for strong disorder the distribution is a symmetric exponentially decaying function.

To explore our theoretical predictions experimentally one needs to assume ergodicity. Experimentally, one cannot average over impurity configurations since it would imply performing experiments on thousands of samples, which were all prepared the same way. This of course is not feasable. Instead one should use perform the averaging over the bias potential or magnetic field and invoke the ergodicity principle, which says that is equivalent to averaging over impurity configurations.

5

Extended Transfer Matrix study of an Antidot system

So far we have investigated conductance fluctuation phenomena in diffusive quantum conductors using mainly analytical techniques. In our model, used in the previous chapter, the diffusive scattering is provided by localized impurities, which are represented by delta-functions. Physically, the existence of such impurities can either be intentional or accidental. For example, a semiconductor can be doped intentionally while defects occur randomly during the fabrication process of a conductor. These impurities can effectively limit the number of conducting quantum channels which connect the electrodes for the incoming charge carriers to the electrodes for outgoing carriers. Sample-to-sample conductance fluctuations occur because the impurities are distributed randomly from one sample to another, and UCF occurs because of interference effects due to coherent scattering in diffusive conductors.

In the last decade or so, artificial impurities can be carefully fabricated and placed in a coherent quantum conductor to control the flow of charge [1, 44, 45]. Very interesting quantum interference phenomena can be produced in a controlled fashion using these artificial structures. Perhaps the most interesting artificial impurity is the antidot, which is simply a potential peak in an otherwise flat potential landscape. In a quantum device, such as a multi-probe quantum dot, if one antidot whose size can be controlled by an external voltage is placed inside the dot, the device shows important characteristics of quantum chaotic scattering, as shown in the experimental study of [1, 44, 45]. The presence of antidots inside a conductor may also cause *weak localization*, meaning a decrease of conductance with respect to the classical value [5]. More complicated weak localization phenomenon is also observed for arrays or for random distributions of antidots which "dope" a conductor [59]. Quantum transport properties of a four-probe quantum dot, in which an antidot is confined, has been found [105], in a magnetic field, to cross over from the quantum Hall regime to a regime dominated by quantum interference, as the antidot size is increased. Such a crossover is accompanied by a set of approximate but interesting micro-symmetries between elements of the scattering matrix [106].

There are many ways of fabricating an artificial impurity, but up to now two methods seem to dominate. The first approach, known as etching, consists of drilling a hole in the 2DEG. The region where the hole is becomes a forbidden zone where the charge carriers cannot enter. In this region we effectively have a hard wall potential. The second method is the split gate technique discussed before, which consists of depositing a metallic disk on top of an insulating layer which is resting on the 2DEG and then applying a negative electric potential on the disk. When the negative electric potential is on, it creates a repulsive potential in the 2DEG beneath the disk, which prevents the electrons from entering that region. One major advantage of the latter approach is that the size of the antidot can be tuned by simply changing the applied electric potential. An increase in the (negative) potential will increase the effective size of the restricted area for the charge carriers.

In this chapter we develop and apply an extended transfer matrix technique to investigate the experimental results in [1]. We use this numerical technique to compute the magneto conductance, i.e. the linear DC conductance $G(B)$ as a function of the magnetic field B, for the experimental device reported in [1]. In this experimental study, a 2D device was fabricated using an AlGaAs/GaAs heterostructure, which contained a 2D electron gas with mobility $10^6 cm^2/Vs$ and Fermi wavelength $\lambda_F^* = 330\mathring{A}$. The device consists of six electrostatic gates: four of the gates are used to define the wire's boundaries, and the two other gates are used to define two antidots which are placed symmetrically inside the wires boundaries. The electrostatic potential applied to the antidots can be adjusted so that many configurations can be generated using the same device, as seen in Fig. 5.1. In particular, for small gate voltage on the anti-

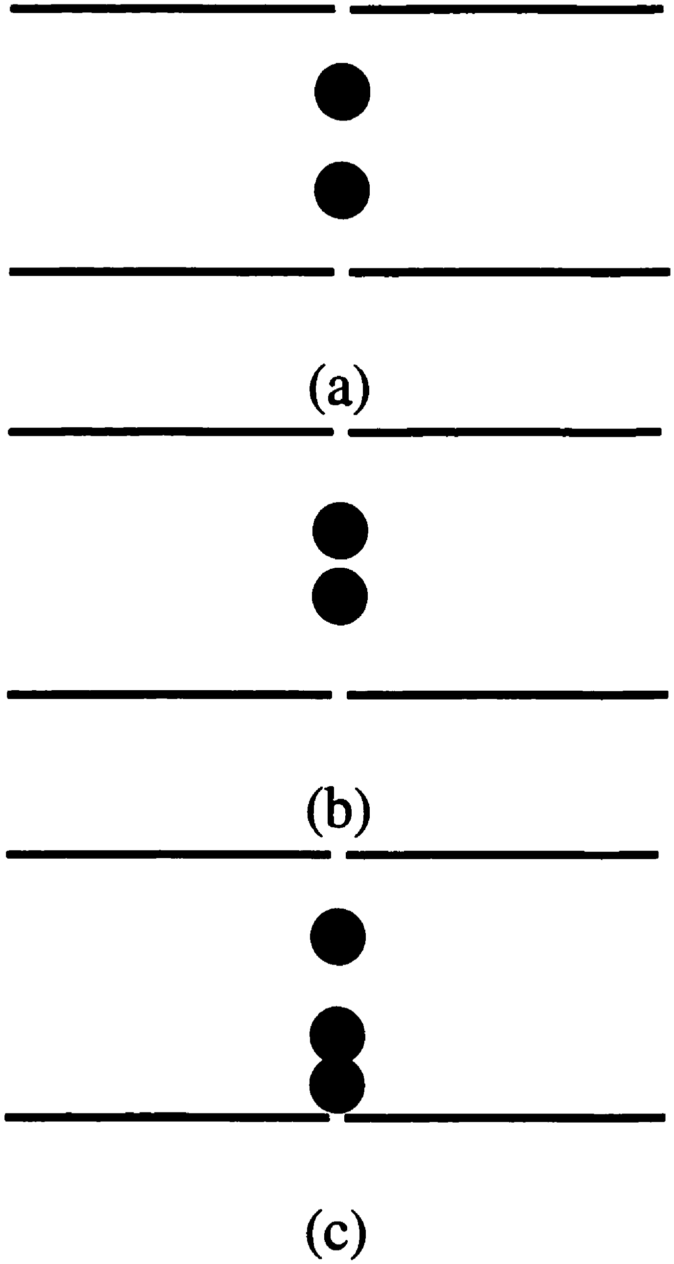

Figure 5.1: Schematic diagrams of the experimental system studied. Each of the configurations are realized by adjusting the (negative) potential bias on the split gates which define the antidots and the boundaries.

dots, the configuration seen in Fig. 5.1(a) is established. In this configuration three quantum point contacts are formed, two of them are between the antidots and the walls, and the third is between the two antidots. Recall that a quantum point contact (QPC) is a constriction which limits the number of subbands that can propagate through the contact region. For larger voltages, the space between the two antidots can be pinched off, this effectively produces a larger antidot and eliminates one of the QPC's (see Fig. 5.1(b)). Finally, a large voltage can be applied to one of the antidots and the nearby wall. In this situation, seen in Fig. 5.1(c), the quantum point contact between the lower antidot and the wall is closed. The experimental system in[1] was cooled down to about $100mK$ and a uniform magnetic field was applied in the direction perpendicular to the device. Using this device, "molecular orbits" around the antidots were created and investigated using a magnetic field.

In contrast to the work from the previous chapter, we will now use a numerical scheme to solve the quantum scattering problem. Because of the finite size of the artificial impurities, we can no longer use Dyson's equation to obtain an exact solution for the Green's function. Moreover, in the presence of a magnetic field, there is no known analytical expression for the Green's functionfunction for a perfect 2D quantum wire. Thus, we need a numerical technique to solve the transport problem. For this purpose, we have developed an extended transfer matrix approach to obtain the wave function and scattering matrix. They provide us with all the required information to compute the linear DC conductance, which we will compare with the experimental results.

In the following we discuss in detail the extended transfer matrix technique. This includes the solution to the generalized eigenvalue equation, which arise when a finite magnetic field B is applied. We then discuss the properties of the wave function in the scattering region and in the lead region. The presence of the magnetic field changes the usual form of the wave function, and thus care must be taken to construct it. The current associated with the scattering wave function is also discussed. Finally, we apply the transfer matrix technique to the experimental device of [1]. These results

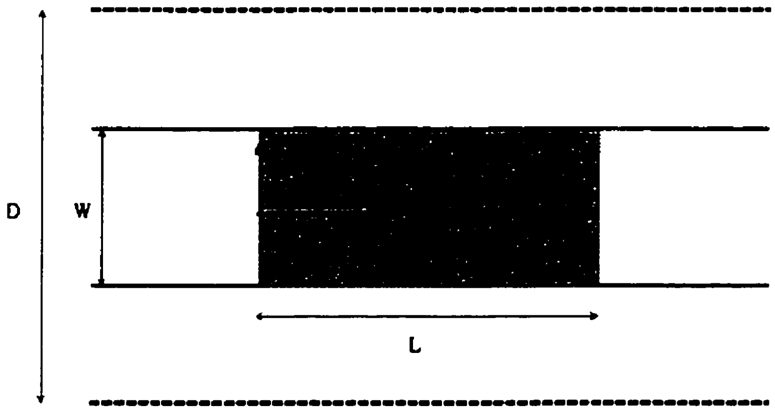

Figure 5.2: Schematic plot of a 2 dimensional quantum wire. The region of width W between the two solid lines is the wire region, the shaded region in the middle is the quantum scattering region, the un-shaded region on both ends are the leads. The two thick dashed lines indicated the two auxiliary hard walls (see text).

are then compared to the experimental data.

5.1 The Generalized Eigen-Momentum Equation

The first step of our calculation is to determine a proper basis set for expanding the scattering wave function. When $B = 0$, the basis set is just sine functions for a hard wall confinement. But when $B \neq 0$, we must compute the basis functions. Consider an infinitely long perfect 2D quantum wire shown in Fig. 5.2. Instead of using the usual hard wall boundary conditions to model the lateral confinement, we use, this time, a soft wall potential. By soft wall potential we mean a step potential whose height is not infinite, but is much greater than the electrons incoming energy.

In the presence of a magnetic field the wave function satisfies the following Schrödinger equation:

$$\left[-\frac{\hbar^2}{2m_*}\frac{\partial^2}{\partial x^2}+\frac{\hbar^2}{2m_*}\left(i\frac{\partial}{\partial y}+\frac{qB}{\hbar c}x\right)^2+V(x,y)\right]\psi(x,y)=E\psi(x,y)\ , \tag{5.1}$$

where the vector potential is $\vec{A}=B(0,x,0)$ and $V(x,y)$ is the confinement potential. We chose V to be a soft wall potential away from the wires boundaries. To simplify our theoretical work we add to V a hard wall potential far away from the boundaries, such that the wave function is essentially zero at the hard wall. Recall that in the region where the soft wall potential is the wave function decays exponentially. Adding a hard wall potential leads us naturally to use sine functions as a basis for decomposing the transverse part of the wave function. $\vec{A}$ represents a uniform magnetic field pointing in the z direction, which is the direction perpendicular to the 2D plane (see Fig. 5.2).

In contrast to the zero B field case, Schrödinger's equation Eq. (5.1) is no longer trivially separable. The anzats $\psi(x,y)=e^{ik_m y}u_m(x)$ does not lead to an equation for $u_m(x)$ which is independent of k_m. We can nevertheless break up the wave function into a longitudinal and a transversal piece: a plane wave along the transport direction, and a transverse part describing the modes. The price for such a decomposition is that we no longer have a simple eigenvalue equation for the transversal eigenfunction. Therefore, a generalized eigenvalue problem must be solved.

In the left lead region we use the following anzats for the wave function: $\psi(x,y)=exp[ik_m^L y]u_m^L(x)$, where L denotes the left lead. Putting this expression into Eq. (5.1) we find,

$$\left[-\frac{\hbar^2}{2m_*}\frac{\partial^2}{\partial x^2}+\frac{\hbar^2}{2m^*}\left(k_m^L-\frac{qB}{\hbar c}x\right)^2+V(x)\right]u_m^L(x)=Eu_m^L(x)\ . \tag{5.2}$$

For later convenience, let us rewrite the above equation in a more compact form:

$$\left[-\frac{\partial^2}{\partial x^2}+\left(k_m^L-\frac{x}{l_B^2}\right)^2+V_*(x)\right]u_m^L(x)=k^2u_m^L(x)\ , \tag{5.3}$$

where $k^2=2m_*/\hbar^2E$, $V_*=2m_*/\hbar^2V$, and $l_B^2=\sqrt{c\hbar/qB}$ is the magnetic length. Notice that a new length scale, the magnetic length l_B, has been introduced. This length scale represents the spatial extension of the wave function in the presence of a finite magnetic field B. Note that for a fixed value of the electrons energy E, Eq. (5.3) is a quadratic eigenvalue equation for k_n. One important consequence of having to deal with a general eigenvalue equation is that the solutions are going to be complex. Thus, the longitudinal eigen momentums, k_n, are general complex numbers.

Let us now cast the generalized eigenvalue equation into a matrix form. First, we need to decompose the eigen functions $u_n^L(y)$ onto a fixed basis. This is accomplished by expressing $u_n^L(y)$ as a sum of sine functions, which naturally from a basis for our hard wall boundary conditions far away from the soft wall confinement potential. Decomposing $u_n^L(x)$ onto the sine basis $\phi_\alpha(x) = \sqrt{2/D}\sin[\frac{\alpha\pi}{D}(x + D/2)]$ we write:

$$u_m(x) = \sum_{\alpha=1}^{N} \chi_{\alpha m}\phi_\alpha(x) = \sum_{\alpha=1}^{N} \chi_{\alpha m}\sqrt{\frac{2}{D}}\sin[\frac{\alpha\pi}{D}(x + D/2)] \ . \tag{5.4}$$

We drop the superscript L for $u_m(x)$ and k_m, to simplify the notation and for later convenience. We choose N large enough such that we obtain numerical convergence. Putting this equation into Eq. (5.3) we find,

$$\sum_{\alpha=1}^{N} \left[(\frac{\alpha\pi}{W})^2 + (k_n + \frac{x}{l_B^2})^2 + V_*(x) \right] \chi_{\alpha n}\phi_\alpha(x) = k^2 \sum_{\alpha=1}^{N} \chi_{\alpha n}\phi_\alpha(x) \ . \tag{5.5}$$

We can simplify this last expression by multiplying it by $\phi_\beta^*(x)$ and integrating over the transverse direction, x. We find,

$$\left[k_n^2 + (\frac{\beta\pi}{W})^2 \right] \chi_{\beta n} + \sum_{\alpha=1}^{N} \left(\int dx \phi_\beta^*(x) \left[\frac{2xk_n}{l_B^2} + \frac{x^2}{l_B^4} + V_*(x) \right] \phi_\alpha(x) \right) \chi_{\alpha n} = k^2 \chi_{\beta n} . \tag{5.6}$$

Next, we rewrite the above equation,

$$\sum_{\alpha} \left[k^2 - (\frac{\alpha\pi}{W})^2 - k_n^2 \right] \delta_{\beta\alpha}\chi_{\alpha n} - \sum_{\alpha} \left(\int dx \phi_\beta^*(x) \left[\frac{2xk_n}{l_B^2} + \frac{x^2}{l_B^4} + V_*(x) \right] \phi_\alpha(x) \right) \chi_{\alpha n} = 0 . \tag{5.7}$$

We are now ready to express the generalized eigenvalue equation in terms of matrices. To this end we introduce the following vectors and matrices:

$$\chi_n = \left(\chi_{1n} \ , \chi_{2n} \ , \cdots \ , \chi_{Nn} \right) \ , \tag{5.8}$$

$$\hat{E} = \begin{pmatrix} k^2 - (\frac{\pi}{W})^2 & 0 & \dots & \dots \\ 0 & k^2 - (\frac{2\pi}{W})^2 & \dots & \dots \\ \dots & \dots & \dots & \dots \\ \dots & \dots & \dots & k^2 - (\frac{N\pi}{W})^2 \end{pmatrix} , \tag{5.9}$$

$$\hat{X}_{\alpha\beta} = \int dx \phi^*_\beta(x) \frac{x}{l_B^2} \phi_\alpha(x) , \tag{5.10}$$

and

$$\hat{V}_{*\alpha\beta} = \int dx \phi^*_\beta(x) V_*(x) \phi_\alpha(x) . \tag{5.11}$$

Using these matrices we obtain a compact expression for the generalized eigenvalue equation Eq. (5.7),

$$\hat{E}\chi_n - k_n^2\chi_n - k_n 2\hat{X}\chi_n - \hat{X}^2\chi_n - \hat{V}_*\chi_n = 0 \ . \tag{5.12}$$

Finally, we introduce the effective Hamiltonian $\hat{H} = \hat{E} - \hat{X}^2 - \hat{V}_*$, to obtain a simple form for the generalized eigenvalue equation,

$$\hat{H}\chi_n = k_n(k_n + 2\hat{X})\chi_n \ , \tag{5.13}$$

which can be solved numerically. Thus, Eq. (5.13) gives us the transverse eigenvectors.

Before moving on let us take a moment to see what happens to the usual orthogonality conditions for our generalized eigenvalue equation. By taking the adjoint of Eq. (5.13) and multiplying it by χ_n from the right we find,

$$\chi_n^*\hat{H}\chi_n = \chi_n^* k_n^*(k_n^* + 2\hat{X})\chi_n \ . \tag{5.14}$$

To obtain the above result we have used the fact that $\hat{H}$ and $\hat{X}$ are both symmetric matrices. Similarly, by multiplying Eq. (5.13) from the left with χ_n^* we obtain,

$$\chi_n^*\hat{H}\chi_n = \chi_n^* k_n(k_n + 2\hat{X})\chi_n \ . \tag{5.15}$$

Therefore,

$$\chi_m^* k_n(k_n + 2\hat{X})\chi_n = \chi_m^* k_m^*(k_m^* + 2\hat{X})\chi_n \ . \tag{5.16}$$

This can be rewritten in the following form,

$$(k_n - k_m^*)\chi_m^*[k_m^* + k_n + 2\hat{X}]\chi_n = 0. \tag{5.17}$$

This last equation says that $\chi_m^*[k_m^* + k_n + 2\hat{X}]\chi_n \neq 0$, only when $k_n = k_m^*$. This orthogonality condition will come in handy when simplifying the expression for the current. Finally, our choice of normalization for the generalized eigen vectors is,

$$\chi_n^*[k_n^* + k_n + 2\hat{X}]\chi_n = 1. \tag{5.18}$$

This choice of normalization will also be useful when computing the particle current associated to the wave function.

As discussed already, in general k_n is a complex number. We will therefore divide the k_n into two groups in order to identify which solutions represent charge carriers moving from left to right and vice versa. The two groups are defined as follows:

- First group: Right moving modes, $Im(k_n) = 0$ and $Re(k_n) > 0$, and local evanescent modes, which are right decaying, $Im(k_n) > 0$.
- Second group: Left moving modes, $Im(k_n) = 0$ and $Re(k_n) < 0$, and local evanescent modes, which are left decaying, $Im(k_n) < 0$.

Note that some of the solutions from the first group are related to the solutions from the second group. To see this, let us first notice that for any given solution χ_n of the generalized eigenvalue equation, the complex conjugate χ_n^* is a solution to,

$$\hat{H}\chi_n^* = k_n^*(k_n^* + 2\hat{X})\chi_n^* \ . \tag{5.19}$$

This means that $(\chi_{k_n})^* = \chi_{k_n^*}$, where we have explicitly written out the dependence of χ_n on the eigen momentum k_n. Notice that for a real eigen momentum, $k_n^* = k_n$, the associated eigen-vector is therefore real, $(\chi_{k_n})^* = \chi_{k_n^*} = \chi_{k_n}$. Thus, real solutions from the first or second group are unrelated. Next, let us consider complex solutions k_n. In this case we have for a given complex k_n that its conjugate k_n^* is the eigen momentum for the eigenvector $\chi_{k_n^*} = (\chi_{k_n})^*$. Thus, for a complex solution k_n from the first group, it's complex conjugate k_n^* is a solution from the second group, and vice versa. For this reason, we say that the complex solutions come in conjugate pairs.

5.1.1 Current in the presence of a magnetic field

The current in the presence of a magnetic field can be measured in either the left or the right lead (see Fig. 5.2) and is given by,

$$I = \frac{\hbar}{2m_*}\int_0^D dx \left[\psi^*(x,y)(-i\frac{\partial}{\partial y} + \frac{x}{l_B^2})\psi(x,y) - \psi(x,y)(-i\frac{\partial}{\partial y} - \frac{x}{l_B^2})\psi^*(x,y)\right] , \tag{5.20}$$

where the wave function $\psi(x,y)$ is evaluated in one of the leads. For example, the wave function in the right lead has the following form,

$$\psi(x,y) = \sum_{k_n}\sum_{\alpha=1}^{N} t_{k_n} e^{ik_n y}\chi_{\alpha n}\phi_\alpha(x), \tag{5.21}$$

where the sum over the generalized eigen momentum, k_n, only includes right moving states, t_{k_n} represents the transmission amplitudes, and $\chi_{\alpha n}$ are solutions to the generalized eigenvalue equation for the right lead. Putting Eq. (5.21) into Eq. (5.20),

$$I = \frac{\hbar}{2m_*}\sum_{k_n,k_m}\left(t_{k_n}t^*_{k_m}e^{i(k_n-k^*_m)y}\chi^*_{k_m}[k^*_m + k_n + 2\hat{X}]\chi_{k_n}\right) . \tag{5.22}$$

In the above equation, the only non-zero terms are those with real k_n's, i.e. those with $k^*_m = k_n$. This follows from the orthogonality condition Eq. (5.17). Therefore,

$$\begin{aligned} I &= \frac{\hbar}{2m_*}\sum_{k_n \in real}\left(t_{k_n}t^*_{k_n}\chi_{k_n}[2k_n + 2\hat{X}]\chi_{k_n}\right) \\ &= \frac{\hbar}{2m_*}\sum_{k_n \in real}|t_{k_n}|^2 . \end{aligned} \tag{5.23}$$

This expression is essentially the Landauer-Büttiker equation for charge carriers in the presence of a magnetic field.

5.2 Extended Transfer Matrix Algorithm

Let us now solve the quantum scattering problem for a two probe device. To compute the wavefunction everywhere inside the system we will use a transfer matrix technique. Let us briefly give an overview of the transfer matrix technique. To be specific, consider the device shown in Fig. 5.2, where we specified the left lead, the scattering region, and the right lead. The first step is to solve Schrödinger's equation in the leads. This is accomplished by solving the transverse eigenvalue problem in each lead using using our basis set obtained in the last section, Eq. (5.4). We next find all the wave functions in the scattering region. To do this we divide the scattering region into small slices such that in each slice the potential is approximately constant along the direction of propagation, $V(x,y) \approx V(x,y_i)$, where y_i is the position of the i-th slice. Schrödinger's equation in each slice is then solved. The wave functions are then related using the continuity equations. The continuity equations simply express the fact that the wavefunction and it's first derivative are both continuous. This way, the total wavefunction in the scattering region is obtained.

5.2.1 The wavefunction in the leads

To be specific, we take the incoming electron to be in the left lead in the n-th mode. The scattering wavefunction in the left lead has the following form:

$$\psi(x,y<0) = I_n e^{ik_n^L y} u_n^L(x) + \sum_{m=1}^{N} r_{nm} e^{iq_m^L y} v_m^L(x) \ , \tag{5.24}$$

where $\{q_m^L\}$ are the left moving eigen momentums and $\{v_m^L\}$ are the corresponding left moving eigen vectors, for the left lead region. Similarly, $\{k_m^L\}$ are the right moving eigen momentums and $\{u_m^L\}$ are the corresponding right moving eigen vectors, in the left lead. These were obtained in the last section. The incoming wave amplitude I_n uses right moving eigen solutions. Recall that in the zero B situation there is no difference between right moving and left moving eigen vectors, and a right moving eigen momentum k_n is related to a left moving eigen momentum by the transformation $k_n \to -k_n$. Finally, r_{nm} is the probability amplitude for an incoming electron in the n-th channel to be reflected into the m-th channel.

Similarly, the scattering wavefunction in the right lead has the following form:

$$\psi(x,y>L) = \sum_{m=1}^{N} t_{nm} e^{ik_m^R y} u_m^R(x) \ , \tag{5.25}$$

where $\{k_m^R\}$ are the right moving eigen momentums and $\{u_m^R\}$ are the corresponding right moving eigen-vectors, in the right lead. The coefficients t_{nm} represent the probability amplitude for an incoming electron in the n-th channel scatters through the systems and leaves in the m-th channel by the right lead.

5.2.2 The wavefunction in the scattering region

Let us now develop the transfer matrix technique to solve Schrödinger's equation every where inside the scattering region. The first step is to divide the scattering region into M small slices such that the potential is essentially constant along the y direction in each slice, $0 = y_1 < y_2 < y_3 < ... < y_M < y_{M+1} = L$, where we have chosen $\{y_i\}$ such that $y_{i+1} - y_i = \Delta = L/M << 1$. When Δ is small enough, $V(x, y_i < y < y_{i+1}) \approx V(x, y_i) \equiv V_i(x)$. Using this approximation we can solve Schrödinger's equation in each slice, the same way it was done for the leads. Therefore, the wavefunction in the i-th slice, $y \in [y_i, y_{i+1}]$, has the following general form,

$$\psi^{(i)}(x,y) = \sum_{m=1}^{N} \left[A_n^{(i)} e^{ik_m^{(i)}(y-y_i)} u_m^{(i)}(x) + B_n^{(i)} e^{iq_m^{(i)}(y-y_i)} v_m^{(i)}(x) \right] \ , \tag{5.26}$$

where $i = 1, ..., M$ and the sum is over the transverse eigen modes. The coefficients $A_m^{(i)}$ and $B_m^{(i)}$ are unknown, which we will find later. As before, $k_m^{(i)}$ is a right moving eigen momentum, $u_m^{(i)}(x)$ is the corresponding right moving eigen vector, $q_m^{(i)}$ is a left moving eigen momentum, and $v_m^{(i)}(x)$ is the corresponding left moving eigen vector, in the i-th slice.

Let us now relate all the wavefunction of Eq. (5.26) together. Recall that the wavefunction and it's first derivative are continuous across the boundary between the i-th slices and the $(i-1)$-th slice. This implies that at $y = y_i$,

$$\psi^{(i-1)}(x, y_i) = \psi^{(i)}(x, y_i) \ , \tag{5.27}$$

and

$$\frac{\partial}{\partial y}\psi^{(i-1)}(x, y_i) = \frac{\partial}{\partial y}\psi^{(i)}(x, y_i) \ . \tag{5.28}$$

Putting Eq. (5.26) into Eq. (5.27) and Eq. (5.28) we find,

$$\sum_{n=1}^{N} \left[A_n^{(i-1)} e^{ik_n^{(i-1)}\Delta} u_n^{(i-1)}(x) + B_n^{(i-1)} e^{iq_n^{(i-1)}\Delta} v_n^{(i-1)}(x) \right] = \sum_{n=1}^{N} \left[A_n^{(i)} u_n^{(i)}(x) + B_n^{(i)} v_n^{(i)}(x) \right] \ , \tag{5.29}$$

and

$$\sum_{n=1}^{N}\left[A_n^{(i-1)}(ik_n^{(i-1)})e^{ik_n^{(i-1)}\Delta}\,u_n^{(i-1)}(x)+B_n^{(i-1)}(iq_n^{(i-1)})e^{iq_n^{(i-1)}\Delta}\,v_n^{(i-1)}(x)\right]=$$

$$\sum_{n=1}^{N}\left[A_n^{(i)}(ik^{(i)})u_n^{(i)}(x)+B_n^{(i)}(iq_n^{(i)})v_n^{(i)}(x)\right]\ . \qquad (5.30)$$

We decompose the above equations onto the sine basis to eliminate their spatial dependence. First, we expand the right moving modes, $u_n^{(i)}$, and left moving modes, $v_n^{(i)}$, on the sine basis functions,

$$u_n^{(i)}(x)=\sum_{\alpha}V_{\alpha n}^{(i)}\phi_\alpha(x)\ , \qquad (5.31)$$

and

$$v_n^{(i)}(x)=\sum_{\alpha}W_{\alpha n}^{(i)}\phi_\alpha(x)\ . \qquad (5.32)$$

All the information of the eigenfunctions $u_n^{(i)}$ and $v_n^{(i)}$ is contained in the matrices $V_{\alpha n}^{(i)}$ and $W_{\alpha n}^{(i)}$. Using these expressions we find,

$$\sum_{n=1}^{N}\left[A_n^{(i-1)}e^{ik_n^{(i-1)}\Delta}V_{\alpha n}^{(i-1)}+B_n^{(i-1)}e^{iq_n^{(i-1)}\Delta}W_{\alpha n}^{(i-1)}\right]=$$

$$\sum_{n=1}^{N}\left[A_n^{(i)}V_{\alpha n}^{(i)}+B_n^{(i)}W_{\alpha n}^{(i)}\right]\ , \qquad (5.33)$$

and

$$\sum_{n=1}^{N}\left[A_n^{(i-1)}(ik_n^{(i-1)})e^{ik_n^{(i-1)}\Delta}V_{\alpha n}^{(i-1)}+B_n^{(i-1)}(iq_n^{(i-1)})e^{iq_n^{(i-1)}\Delta}W_{\alpha n}^{(i-1)}\right]=$$

$$\sum_{n=1}^{N}\left[A_n^{(i)}(ik^{(i)})V_{\alpha n}^{(i)}+B_n^{(i)}(iq_n^{(i)})W_{\alpha n}^{(i)}\right]\ . \qquad (5.34)$$

Next, we define vectors and matrices in order to express Eq. (5.33) and Eq. (5.34) in matrix form. Let:

$$\chi_1^{(i)}=(A_1^{(i)},A_2^{(i)},...,A_N^{(i)})\ , \qquad (5.35)$$

$$\chi_2^{(i)}=(B_1^{(i)},B_2^{(i)},...,B_N^{(i)})\ , \qquad (5.36)$$

$$[D_1^{(i)}]_{nm}=e^{(ik_n^{(i)}\Delta)}\delta_{nm},\quad \text{and}\quad [D_2^{(i)}]_{nm}=e^{(iq_n^{(i)}\Delta)}\delta_{nm},\ , \qquad (5.37)$$

$$[K_1^{(i)}]_{nm}=ik_n^{(i)}\delta_{nm},\quad \text{and}\quad [K_2^{(i)}]_{nm}=iq_n^{(i)}\delta_{nm}\ , \qquad (5.38)$$

$$[V^{(i)}]_{nm} = V^{(i)}_{nm}, \quad \text{and} \quad [W^{(i)}]_{nm} = W^{(i)}_{nm} \; . \tag{5.39}$$

Eq. (5.33) and Eq. (5.34) become,

$$V^{(i-1)} D_1^{(i-1)} \chi_1^{(i-1)} + W^{(i-1)} D_2^{(i-1)} \chi_2^{(i-1)} = V^{(i)} \chi_1^{(i)} + W^{(i)} \chi_2^{(i)} \; , \tag{5.40}$$

and

$$V^{(i-1)} D_1^{(i-1)} K_1^{(i-1)} \chi_1^{(i-1)} + W^{(i-1)} K_2^{(i-1)} D_2^{(i-1)} \chi_2^{(i-1)} = V^{(i)} K_1^{(i)} \chi_1^{(i)} + W^{(i)} K_2^{(i)} \chi_2^{(i)} \; , \tag{5.41}$$

where $i = 1, ..., M+1$. We have added the continuity equations between the last slice and the right lead. We are now faced with the problem of solving a system of $2(M+1)$ equations with $2(M+1)$ unknowns, $\chi_1^{(i)}$ and $\chi_2^{(i)}$. We could solve this system iteratively, by expressing the unknowns in the i-th slice, $\chi_1^{(i)}$ and $\chi_2^{(i)}$, in terms of the unknowns in the $(i-1)$-th slice $\chi_1^{(i-1)}$ and $\chi_2^{(i-1)}$. Once iterated this would lead to an equation relating the variables from the first slice, I_m and r_{nm}, to the one from the last slice, t_{nm}. This final equation could be solved and an expression for r_{nm} and t_{nm}, in terms of I_m, could be obtained. The problem with this procedure is that it is not numerically stable, because of the repeated multiplication of the exponential factors $exp[iq_n^{(i)}] \geq 1$ (when the imaginary part of $q_n^{(i)}$ is negative).

To get around this problem that conventional transfer matrix approaches run into, we must reformulate our equations in such a way that avoids multiplying the divergent factors over and over. To this end we group the vectors $\chi_1^{(i)}$ and $\chi_2^{(i)}$ into a $2N$ vector given by,

$$\chi^{(i)} = \begin{pmatrix} \chi_1^{(i)} \\ \chi_2^{(i-1)} D_2^{(i-1)} \end{pmatrix} \; . \tag{5.42}$$

Using these new vector $\chi^{(i)}$ we can now rewrite the continuity equations in a tridiagonal matrix form. The continuity equation, Eq. (5.40) and Eq. (5.41), are now given by,

$$L_1^{(i)} \chi^{(i-1)} + L_2^{(i)} \chi^{(i)} + L_3^{(i)} \chi^{(i+1)} = 0 \; , \tag{5.43}$$

where

$$L_1^{(i)} = \begin{pmatrix} V^{(i-1)} D_1^{(i-1)} & 0 \\ V^{(i-1)} K_1^{(i-1)} D_1^{(i-1)} & 0 \end{pmatrix} \; , \tag{5.44}$$

$$L_2^{(i)} = \begin{pmatrix} V^{(i)} & -W^{(i-1)} \\ V^{(i-1)}D_1^{(i-1)} & -W^{(i-1)}D_2^{(i-1)} \end{pmatrix} , \tag{5.45}$$

and

$$L_3^{(i)} = \begin{pmatrix} 0 & W^{(i)}(D_2^{(i)})^{-1} \\ 0 & W^{(i)}K_2^{(i)}(D_2^{(i)})^{-1} \end{pmatrix} . \tag{5.46}$$

There are no amplifying factors in Eq. (5.43), thus it can be iterated without danger. At the start of the iteration, we have $\chi^{(1)} = (\chi_1^{(1)}, \hat{r}\hat{D}_2^{(L)})$, where $\hat{r}$ is the reflection amplitudes (see Eq. (5.24)) and $\hat{D}_2^{(L)}$ is the matrix from Eq. (5.37) for the left lead. The corresponding equation is

$$\hat{L}_2^{(1)}\chi^{(1)} + \hat{L}_3^{(1)}\chi^{(2)} = -\hat{L}_1^{(1)}I_m, \tag{5.47}$$

where I_m is the incoming wave amplitude in the n-th mode, $(I_m)_n = \delta_{nm}$. At the end of the iteration, we have $\chi^{(M+1)} = (\hat{t}, \chi_2^{(M)}\hat{D}_2^{(M)})$, where $\hat{t}$ are the transmission amplitudes (see Eq. (5.25)). The last equation is,

$$\hat{L}_1^{(M+1)}\chi^{(M)} + \hat{L}_2^{(M+1)}\chi^{(M+1)} = 0. \tag{5.48}$$

Eq. (5.43), Eq. (5.47) and Eq. (5.48) form a complete set of tri-diagonal matrix equations, which can be iteratively solved by standard routines. In particular, we can solve this tridiagonal system of matrix equations without any divergences, because they are no amplifying factors being repeatedly multiplied.

5.3 Numerical Results

We now apply the extended transfer matrix technique to investigate the quantum wire reported in [1]. Recall that the experimental device is a $1\mu m$ wide by $5\mu m$ long quantum wire, fabricated on an $AlGaAs/GaAs$ heterostructure, with two antidots with a diameter of $0.2\mu m$ placed inside. The Fermi wavelength of the charge carriers is $\lambda_F^* = 330\AA$. In our theoretical study, we use the same parameters as those of the experiment, except for the Fermi energy, we discuss this below. The different antidot configurations are shown schematically in the Fig. 5.3. The step like potentials used

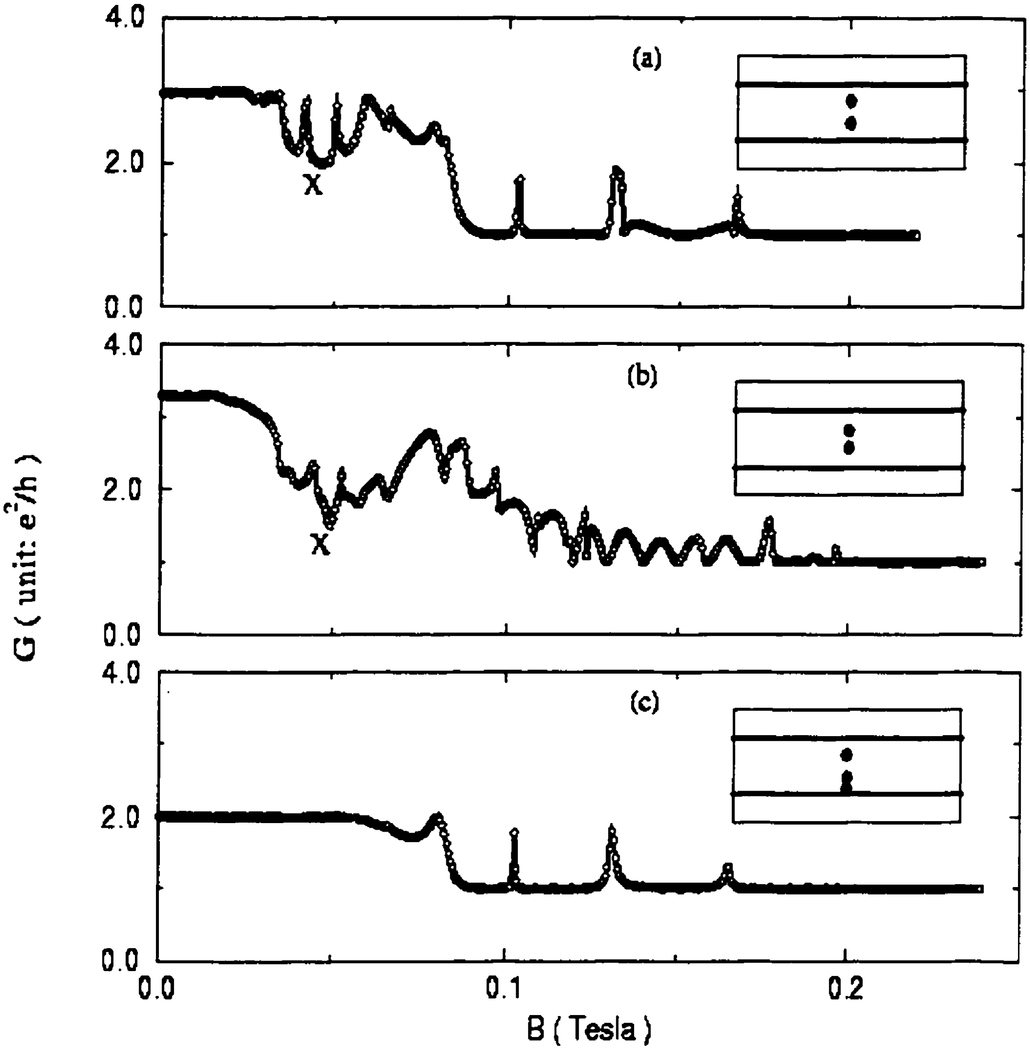

Figure 5.3: Conductance $G(B)$ as a function of the magnetic field. The corresponding arrangements of the antidots are indicated in the insets.

to mimic the confinement due to the wires boundary and the repulsion of the antidots, has a height of 2.8 electron volt (eV). The electron energy is equivalent to a wavelength $\lambda = 2\pi \times \lambda_F^*$. We consider a lower energy in order to minimize the computation time, but this doesn't change the main features of the transport coefficients. In all our calculations, we assume an electron effective mass $m_* = 0.067 m_e$, which is appropriate for *AlGaAs/GaAs* interfaces, where m_e is the bare electron mass. Our numerical results are presented in the form of the magneto conductance $G(B)$ as a function of the magnetic field B. Here, $G(B)$ is related to the transmission amplitudes t_{nm} via the Landauer-Büttiker formula, $G = e^2/h \sum_{n,m} |t_{nm}|^2$.

In the calculation shown in Fig. 5.3(a), the centers of both antidots are placed at a distance of 0.3μ from the nearby boundary, thus three 0.2μ wide QPC's are formed between the boundaries of the confinement and the antidots. The magneto conductance plot show interesting resonance behavior. The valley in conductance marked by the letter X corresponds to the "X" peak, which is experimentally observed in the magneto resistance [1]. The X peak is due to the coupling of the local states caused by cyclotron trapping. This happens when the cyclotron orbit is commensurate with the size of the "molecule" formed by the two antidots. The radius of the cyclotron orbit is estimated by $R_c = \hbar kc/(eB) \approx 0.4\mu$. Assuming that the typical molecular orbit is roughly a constant for different energies, which is reasonable since the molecular orbit is largely fixed by the geometry of the arrangement of antidots inside the wire. This implies the position of the X peak in B found in the experiment should be different than what we find numerically, but the ratio k/B should remain a constant. Since the experimental k_F^* is a factor 2π larger than the wave vector k used in our simulation, we expect that the experimental X peak position be at a higher value of the magnetic field than what we find in our theoretical work, by the same factor. The experimental X peak occurs at about $B = 0.24$ T [1] while our result is at around $B = 0.045$ T. Hence, taking into account of the 2π difference in the k values, good agreement between our numerical simulations and the experiment is found. One source for the small difference of the k/B ratio could be due to the fact that the molecular orbit changes slightly for different energies.

On top of the X peak, there are extra modulations which are due to the Aharonov-Bohm (AB) effect. The peaks showing here are due to the coupling of the local orbits that circumvent both antidots. The modulation period is proportional to the inverse of the area enclosed by the local orbits. The period obtained from our calculation is $\Delta B \approx 8.2$ mT, corresponding to a AB area $\Delta A \approx \pi R_c^2 \approx 0.5\mu^2$, which also agrees reasonably well with the experimental result[1] of 7 mT.

At magnetic field greater than 0.1 T, Fig. 5.3.(a) shows 3 more peaks, which corresponds to the AB oscillations induced by the electron circumventing a single antidot. The distance between the first two peaks is 28 mT, corresponding to a AB area $\Delta A' \approx \pi R_c^2 \approx 0.14\mu^2$, which is again in excellent agreement with experimentally observed AB period of 27 mT in this range of the field strength [1]. Furthermore, one can see that the AB period has a trend of getting larger at higher magnetic field. This effect is also observed in the experiment [1].

In the calculation shown in Fig. 5.3.(b), we move the two antidots closer such that there is now only a 0.1μ gap between them. The other two gaps between the antidots and the boundaries are now 0.25μ wide. It can be seen that in this case the X peak appears at approximately the same position as the situation of Fig. 5.3.(a). However, since the gap between the antidots is now narrower, it is harder for the electron to pass through there. Therefore the AB oscillations due to the single antidot orbit are suppressed. We are left with AB oscillations which are only due to the larger "molecular" orbits, i.e. orbits that circumvent both antidots. As shown in Fig. 5.3.(b), one finds a smaller period oscillations all the way up to 0.2 T. The period found in Fig. 5.3.(b), on average, is about 8 mT, which is consistent with a "molecular" orbit AB effect. It is worth noting that other than the AB peaks, there seems to be some extra resonances in Fig. 5.3.(b). The cause of these extra peaks is likely to be due to quantum resonances caused by the QPC's.

In the device geometry shown in Fig. 5.3.(c), we put an additional antidot in the structure of Fig. 5.3.(a). The additional antidot is placed in between the lower boundary and the lower antidot, so that the lowest gap is effectively closed. Experimentally this situation was established by adjusting the negative potential on the wires boundary which pinches off the lower QPC, as discussed in detail in [1]. For this case the orbits which surround two antidots cannot exist, only those surrounding one antidot remains. Indeed, as shown in Fig. 5.3.(c) the valley that corresponds to the X peak disappears. On the other hand the three AB peaks at B greater than 0.1 Tesla still remains at the same position. This clearly demonstrates that the X peak is caused by the "molecular" orbits that surround the two antidots. The results from Fig. 5.3.(c) agree with those found experimentally when the device has the same configuration [1].

5.4 Conclusion

In order to simulate the experimental situations of [1], we developed an extended transfer matrix technique which solves the full quantum scattering problem in the presence of a magnetic field. The experimental device was used to study the classical and quantum transport features as a function of a uniform magnetic field. The resonance behavior in the magneto conductance, observed experimentally, was reproduced and understood. The peak positions and spacings agree quantitatively with the experimental data. In particular, the classical focusing effect is responsible for the anomalous X peak; and the AB oscillations account for the near regular magnetoconductance peaks at higher magnetic field strength. The simulation results of this work thus confirms the physical picture established by the experimental measurements. In contrast to other model studies [46, 107] our work provides a full quantum mechanical analysis and our results agrees quite well with the measurements.

As discussed in the text, while good quantitative agreement has been obtained between our simulation and the measurements, there do exist slight differences regarding to the precise values of the X peak position and the AB periods: our simulation values are slightly larger. This can be understood in the following way. When comparing numerical results with experimental values, we have assumed that the "molecular" orbit which surrounds the two antidots remain the same for different electron energies. While this is a reasonable assumption for the particular system we have studied (because the electron motion is confined by the walls and QPC's), in reality, the "molecular" orbit size is weakly dependent on the electron energy. We find that the small discrepancy between the numerical values and the experimental data can be accounted for if we assume that the radius of the trapped "molecular" orbit in the numerical study is a few percent smaller than the corresponding experimental one. However, this energy dependence is indeed very weak since the energy chosen for our numerical calculation is a factor $4\pi^2$ smaller than the experimental Fermi energy.

6

Conclusion

In this thesis, we have developed and applied a first principle approach to study emittance and nonlinear conductance fluctuations, in disordered quantum conductors. In particular, we studied quantum transport fluctuations in the Universal Conductance Fluctuations (UCF) regime in a diffusive conductor. We also developed a numerical transfer matrix technique in order to study the magneto conductance of an antidot system which was experimentally realized and reported in Ref.[1]. These developments form the bulk of our work.

To study linear AC and nonlinear DC conductance, Büttiker's quantum transport theory was used. In contrast to the linear DC quantum conductance, the linear AC and the nonlinear DC transport coefficients require internal response terms in order to satisfy gauge invariance and current conservation, essential physical requirements for any realistic theory of quantum transport. The internal response of the emittance and the nonlinear conductance, in the scattering matrix approach, requires the knowledge of the functional derivative of the scattering matrix. To compute this, from first principles, we used Lippmann-Schwinger equation to derive an explicit expression for the functional derivative of the wave function. This result was then used to obtain an expression for the functional derivative of the scattering matrix. This led us to an equation which depends on the wave function and the Greens function. To eliminate the functional derivatives dependence on the Green function we introduced the Generalized Fisher-Lee (GFL) relation, which expresses the wave function in terms of the Green's function. Putting these results together we obtained an equation for the functional derivative of the scattering matrix, which only depends on the scattering wave functions. This eliminated the need to calculate the Green's function, which drastically reduced the computational time required to obtain the functional derivative, and thus $E_{\alpha\beta}$ and $G_{\alpha\beta\gamma}$.

Once the expressions for the transport coefficients were obtained in terms of the scattering matrix and the wave function, we next turned our attention to computing the wave function for a diffusive conductor. We use the same model for disordered conductor as Al'tshuler, Lee, Stone, and Fuckuyama for their study of UCF [38]. The model uses N localized elastic scattering centers of strength γ, represented by delta functions, to generate an impurity potential landscape for the disordered conductor in the diffusive regime. We derived exact expressions for the Green's function and the wave function. Solving Dyson's equation, we obtained an expression for the N-delta impurity Green's function. Then using the Lippmann-Schwinger equation the N-delta impurity wave function was obtained. The final expression for the wave function was expressed in terms of the impurity free Green's function, wave function, and the matrix M_{ij} (see Eq. (4.7)), which contained the information of the localized scattering centers. This exact solution was used to obtain expressions for all the transport coefficients of interest.

With all these theoretical developments, we analyzed the sample-to-sample fluctuations for the linear DC, linear AC, and nonlinear DC conductance coefficients in two dimensional disordered conductors in the diffusive regime. We found that the distribution for G_{21} is a Gaussian like function for values of N and γ away from the insulating regime $G_{21} = 0$. The usual UCF regime was found for a range of values of N and γ, where $\Delta G_{21} \approx 0.86e^2/h$, which is the expected value for UCF in 2D. The boundary of the UCF regime was identified with the accumulation of the tail of the Gaussian distributions against the $G_{21} = 0$ limit, which led to a narrower distribution and thus a reduced value for ΔG_{21}. In contrast to $P(G_{21})$, we found that $P(E_{21})$ is symmetric for small disorder and asymmetric for strong disorder. When the value of N is low, the function $P(E_{21})$ is symmetric and centered around a positive value of E_{21}, which corresponds to an inductive behavior. But when the value of N is high the distribution $P(E_{21})$ becomes asymmetric: the body of the distribution is in the capacitive side $E_{21} < 0$, while having a long tail which extends into the inductive side $E_{21} > 0$. Finally, we also computed the distribution function for G_{111}. At low value for the disorder $P(G_{111})$ is a Gaussian like function, and its width increases in a linear fashion with N. When we have strong disorder, $P(G_{111})$ looks like a symmetric exponential and the width of the distribution increases exponentially with N. This picture is confirmed when plotting ΔG_{111} versus N. Thus, distribution function of the nonlinear conductance depends sensitively on the internal response of the conductor: for small disorder the distribution is symmetric and Gaussian-like, but for strong disorder the distribution is symmetric exponential-like.

The theoretical results that were developed can be applied to a wide range of physical systems. In particular, the linear AC and nonlinear DC quantum conductance through atomic wires can be efficiently computed numerically using our results. Conventionally, one requires the Green's function to compute the emittance and the nonlinear conductance. Computing the Green's function for an atomic system with open boundary conditions can be a very tedious process [72], but computing scattering wave function can often be much easier. Using our results. One only needs the wave function to compute the linear AC and nonlinear DC conductances. Therefore, for example, the second order transport coefficients can now be studied for the first time for atomic and molecular systems using our theoretical formalism. This has not been carried out so far, but will be investigated in the near future. As for our exact solution for the N-delta impurity Green's function and wave function, they can be used to explore the quantum transport in different regimes, one very interesting situation is the the "mixed" regime [108] where both diffusive and ballistic transport characteristics play an important role. Moreover, using the same technique we can obtain exact solutions for the N-magnetic impurity Green's function and wave function (see appendices), which can then be applied to study the so called Giant Magneto Resistance (GMR) phenomenon [109, 110, 111, 112].

Our numerical work on transfer matrices was aimed at simulating the experiment reported in [1]. In this experiment the magneto conductance of a 2D wire with two antidots, with adjustable diameters, was measured. The aim of the measurements was to understand the classical and the quantum transport features in such ballistic systems using a magnetic field. The transfer matrix technique was developed to make full quantum scattering calculations in the presence of a magnetic field. We found that the experimentally observed resonance behavior in the magneto conductance was reproduced and understood. In particular, our numerical results exhibit the classical focusing effect that causes the X-peak to appear. The spacing of the peaks due to AB oscillations were, approximately, in quantitative agreement with the experimental data. Our results confirmed the physical picture which arises from the experimental measurements, and our work provided the first full quantum mechanical approach which gave good quantitative agreement with the experimental results. Finally, we point out that our numerical transfer matrix technique is very useful in its own right: it can be applied to a variety of 2D quantum coherent conductors in the presence of magnetic field. Especially, it can be efficiently applied to systems with irregular potential landscape, and with the more realistic soft device confinement. There have been extensive experimental studies on transport of 2D electrons in semiconductor systems in both low and high magnetic fields [106, 113, 114], our technique is applicable to simulate these measurements.

Appendices

A.1 N-Magnetic Impurity Green's Function

In this appendix we derive an expression for the N-magnetic impurity Green's function using Dyson's equation. In matrix notation Dyson's equation is given by

$$\hat{G}^{(N)}(\mathbf{r},\mathbf{r}') = \hat{G}^{(0)}(\mathbf{r},\mathbf{r}') + \int d\mathbf{r}''\hat{G}^{(0)}(\mathbf{r},\mathbf{r}'')\hat{V}^{(N)}(\mathbf{r}'')\hat{G}^{(N)}(\mathbf{r}'',\mathbf{r}')\,. \tag{A.1}$$

The N-magnetic impurity potential is,

$$\hat{V}^{(N)}(\mathbf{r}) = \sum_{i=1}^{N}\hat{U}_i\delta(\mathbf{r}-\mathbf{r}_i) \tag{A.2}$$

where

$$\hat{U}_i = |\vec{\gamma}_i|\begin{pmatrix} \cos(\theta_i) & \sin(\theta_i)e^{-i\phi_i} \\ \sin(\theta_i)e^{i\phi_i} & -\cos(\theta_i) \end{pmatrix}\ .$$

The angles θ_i and ϕ_i, with the magnitudes $|\vec{\gamma}_i|$, completely characterize the magnetic impurity vectors $\vec{\gamma}_i$. The free Green's function has the general form,

$$\hat{G}^{(0)}(\mathbf{r},\mathbf{r}') = \begin{pmatrix} G^{(0)}_{\uparrow\uparrow}(\mathbf{r},\mathbf{r}')G^{(0)}_{\uparrow\downarrow}(\mathbf{r},\mathbf{r}') \\ G^{(0)}_{\downarrow\uparrow}(\mathbf{r},\mathbf{r}')G^{(0)}_{\downarrow\downarrow}(\mathbf{r},\mathbf{r}') \end{pmatrix}\ .$$

Once we have integrated out the all delta functions Dyson's equation becomes an algebraic equation,

$$\hat{G}^{(N)}(\mathbf{r},\mathbf{r}') = \hat{G}^{(0)}(\mathbf{r},\mathbf{r}') + \sum_{i=1}^{N}\hat{G}^{(0)}(\mathbf{r},\mathbf{r}_i)\hat{U}_i\hat{G}^{(N)}(\mathbf{r}_i,\mathbf{r}')\ . \tag{A.3}$$

Using this equation we generate a system of N matrix equations with N unknowns $\{\hat{G}^{(N)}(r_i,r')\}$:

$$\hat{G}^{(N)}(\mathbf{r}_1,\mathbf{r}') = \hat{G}^{(0)}(\mathbf{r}_1,\mathbf{r}') + \sum_{i=1}^{N}\hat{G}^{(0)}(\mathbf{r}_1,\mathbf{r}_i)\hat{U}_i\hat{G}^{(N)}(\mathbf{r}_i,\mathbf{r}')$$

$$\hat{G}^{(N)}(\mathbf{r}_2,\mathbf{r}') = \hat{G}^{(0)}(\mathbf{r}_2,\mathbf{r}') + \sum_{i=1}^{N} \hat{G}^{(0)}(\mathbf{r}_2,\mathbf{r}_i)\hat{U}_i\hat{G}^{(N)}(\mathbf{r}_i,\mathbf{r}')$$

$$\dots$$

$$\hat{G}^{(N)}(\mathbf{r}_N,\mathbf{r}') = \hat{G}^{(0)}(\mathbf{r}_N,\mathbf{r}') + \sum_{i=1}^{N} \hat{G}^{(0)}(\mathbf{r}_N,\mathbf{r}_i)\hat{U}_i\hat{G}^{(N)}(\mathbf{r}_i,\mathbf{r}')$$

In matrix notation we find:

$$\begin{pmatrix} \hat{G}^{(N)}(\mathbf{r}_1,\mathbf{r}') \\ \hat{G}^{(N)}(\mathbf{r}_2,\mathbf{r}') \\ \\ \dots \\ \\ \hat{G}^{(N)}(\mathbf{r}_N,\mathbf{r}') \end{pmatrix} = \begin{pmatrix} \hat{G}^{(0)}(\mathbf{r}_1,\mathbf{r}') \\ \hat{G}^{(0)}(\mathbf{r}_2,\mathbf{r}') \\ \\ \dots \\ \\ \hat{G}^{(0)}(\mathbf{r}_N,\mathbf{r}') \end{pmatrix} + \begin{pmatrix} \hat{\eta}_{11}\hat{U}_1 & \hat{\eta}_{12}\hat{U}_2 & \dots & \hat{\eta}_{1N}\hat{U}_N \\ \hat{\eta}_{21}\hat{U}_1 & \hat{\eta}_{22}\hat{U}_2 & \dots & \hat{\eta}_{2N}\hat{U}_N \\ & & & \\ \dots & & \dots & \\ & & & \\ \hat{\eta}_{N1}\hat{U}_1 & \hat{\eta}_{N2}\hat{U}_2 & \dots & \hat{\eta}_{NN}\hat{U}_N \end{pmatrix} \begin{pmatrix} \hat{G}^{(N)}(\mathbf{r}_1,\mathbf{r}') \\ \hat{G}^{(N)}(\mathbf{r}_2,\mathbf{r}') \\ \\ \dots \\ \\ \hat{G}^{(N)}(\mathbf{r}_N,\mathbf{r}') \end{pmatrix},$$

where $\hat{\eta}_{ij} = \hat{G}^{(0)}(r_i, r_j)$. The solution to this system of equation is given by

$$\begin{pmatrix} \hat{G}^{(N)}(\mathbf{r}_1,\mathbf{r}') \\ \hat{G}^{(N)}(\mathbf{r}_2,\mathbf{r}') \\ \\ \dots \\ \\ \hat{G}^{(N)}(\mathbf{r}_N,\mathbf{r}') \end{pmatrix} = \begin{pmatrix} \hat{M}_{11} & \hat{M}_{12} & \dots & \hat{M}_{1N} \\ \hat{M}_{21} & \hat{M}_{22} & \dots & \hat{M}_{2N} \\ & & & \\ \dots & & \dots & \\ & & & \\ \hat{M}_{N1} & \hat{M}_{N2} & \dots & \hat{M}_{NN} \end{pmatrix} \cdot \begin{pmatrix} \hat{G}^{(0)}(\mathbf{r}_1,\mathbf{r}') \\ \hat{G}^{(0)}(\mathbf{r}_2,\mathbf{r}') \\ \\ \dots \\ \\ \hat{G}^{(0)}(\mathbf{r}_N,\mathbf{r}') \end{pmatrix}, \tag{A.4}$$

where the matrices $\hat{M}_{ij}$ are defined by,

$$\begin{pmatrix} \hat{M}_{11} & \hat{M}_{12} & \dots & \hat{M}_{1N} \\ \hat{M}_{21} & \hat{M}_{22} & \dots & \hat{M}_{2N} \\ & & & \\ \dots & & \dots & \\ & & & \\ \hat{M}_{N1} & \hat{M}_{N2} & \dots & \hat{M}_{NN} \end{pmatrix} = \begin{pmatrix} \hat{I} - \hat{\eta}_{11}\hat{U}_1 & -\hat{\eta}_{12}\hat{U}_2 & \dots & -\hat{\eta}_{1N}\hat{U}_N \\ -\hat{\eta}_{21}\hat{U}_1 & \hat{I} - \hat{\eta}_{22}\hat{U}_2 & \dots & -\hat{\eta}_{2N}\hat{U}_N \\ & & & \\ \dots & & \dots & \\ & & & \\ -\hat{\eta}_{N1}\hat{U}_1 & -\hat{\eta}_{N2}\hat{U}_2 & \dots & \hat{I} - \hat{\eta}_{NN}\hat{U}_N \end{pmatrix}^{-1}. \tag{A.5}$$

Putting all these results together we find,

$$\hat{G}^{(N)}(\mathbf{r},\mathbf{r}') = \hat{G}^{(0)}(\mathbf{r},\mathbf{r}') + \sum_{i,j=1}^{N} \hat{G}^{(0)}(\mathbf{r},\mathbf{r}_i)\hat{U}_i\hat{M}_{ij}\hat{G}^{(0)}(\mathbf{r}_j,\mathbf{r}'). \tag{A.6}$$

This is an exact expression for the N-magnetic impurity Green's function for any free Green's function $\hat{G}^{(0)}(\mathbf{r},\mathbf{r}')$.

A.2 N-magnetic impurity Wave function

In this appendix we use the Lippmann-Schwinger equation to derive an expression for the N-magnetic impurity scattering wave function. The strategy that was used in the previous appendix will once again be employed. The Lippmann-Schwinger equation is given by

$$\hat{\psi}^{(N)}(\mathbf{r}) = \hat{\psi}^{(0)}(\mathbf{r}) + \int d\mathbf{r}'\hat{G}^{(0)}(\mathbf{r},\mathbf{r}')\hat{V}^{(N)}(\mathbf{r}')\hat{\psi}^{(N)}(\mathbf{r}') \ . \tag{A.7}$$

Integrating out the delta functions we find,

$$\hat{\psi}^{(N)}(\mathbf{r}) = \hat{\psi}^{(0)}(\mathbf{r}) + \sum_{j=1}^{N}\hat{G}^{(0)}(\mathbf{r},\mathbf{r}_j)\hat{U}_j\hat{\psi}^{(N)}(\mathbf{r}_j) \ . \tag{A.8}$$

Using the above equation we generate N matrix equations for the N unknowns $\hat{\psi}^{(N)}(\mathbf{r}_j)$:

$$\hat{\psi}^{(N)}(\mathbf{r}_j) = \hat{\psi}^{(0)}(\mathbf{r}_j) + \sum_{i=1}^{N}\hat{G}^{(0)}(\mathbf{r}_j,\mathbf{r}_i)\hat{U}_i\hat{\psi}^{(N)}(\mathbf{r}_i) \ . \tag{A.9}$$

Following the same mathematical procedure that was used in the previous appendix, we easily find,

$$\hat{\psi}^{(N)}(\mathbf{r}_j) = \sum_{i=1}^{N}\hat{M}_{ji}\hat{\psi}^{(N)}(\mathbf{r}_i) \ . \tag{A.10}$$

Finally, putting this result into Eq. (A.8) we find,

$$\hat{\psi}^{(N)}(\mathbf{r}) = \hat{\psi}^{(0)}(\mathbf{r}) + \sum_{i,j=1}^{N}\hat{G}^{(0)}(\mathbf{r},\mathbf{r}_i)\hat{U}_i\hat{M}_{ij}\hat{\psi}^{(0)}(\mathbf{r}_j) \ . \tag{A.11}$$

This is an exact expression for the N-magnetic impurity wave function for any free wave function $\hat{\psi}^{(0)}(\mathbf{r})$.

BIBLIOGRAPHY

[1] C. Gould, A.S. Sachrajda, M.W. Dharma-wardana, Y. Feng, and P.T. Coleridge. *Phys. Rev. Lett*, 77:5272, 1996.

[2] M.A. Reed and W.P. editors Kirk. *Nanostructure physics and fabrication: Proceedings of the International Symposium.* Academic press, New York, 1989.

[3] B.L. Altshuler, P.A. Lee, and R.A. Webb. *Mesoscopic Phenomena in Solids.* North Holland, Amsterdam, 1991.

[4] C.W.J. Beenakker and H. van Houten. *Solid State Physics*, 44:1, 1991.

[5] S. Datta. *Electronic Transport in Mesoscopic Systems.* Cambridge University Press, New York, 1995.

[6] Y. Imry. *Introduction to Mesoscopic Physics.* Oxford University Press, New York, 1997.

[7] T. Ando, Y. Arakawa, K. Furuya, S. Komiyamam, and H. (Eds.) Nakshima. *Mesoscopic Physics and Electronics.* Springer-Verlag, New York, 1998.

[8] H. van Houten, B.J. van Wees, M.G.J. Heijman, and J.P. Amdre. *Appl. Phys. Lett.*, 49:1781, 1986.

[9] J.T. Thornton, M. Pepper, M. Ahmed, D. Andrews, and G.J. Davies. *Phys. Rev. Lett.*, 56:1198, 1986.

[10] M.A. Reed, J.N. Randall, R.J. Aggarwl, R.J. Matyi, T.M. Moore, and A.E. Wetsel. *Phys. Rev. Lett.*, 60:535, 1988.

[11] P. Delsing, T. Claeson, K.K. Likharev, and L.S. Kuzmin. *Phys. Rev. B*, 42:7439, 1990.

[12] L.P. Kouwenhoven, N.C. van der Vaart, C. Johnson, A.T. Kool, C.J.P.T. Harmans, J.G. Williamson, A.M. Staring, and C.T. Foxon. *Z. Phys. B*, 85:367, 1991.

[13] M. Kastner. *Physics Today*, 46:24, 1993.

[14] Y. Wang, N. Zhu, J. Wang, and H. Guo. *Phys. Rev. B*, 53:16408, 1996.

[15] N.D. Lang. *Phys. Rev. B*, 52:5335, 1995.

[16] A. Yazdani, D.M. Eigler, and N. Lang. *Science*, 272:1921, 1996.

[17] N.D. Lang. *Phys. Rev. B*, 55:4113, 1997.

[18] S.J. Tans, M.H. Devoret, R.M. Alwin, and H. Dai. *Nature*, 386:474, 1997.

[19] M.A. Reed, C. Zhou, and C.J. Muller. *Science*, 278:252, 1997.

[20] C.C. Wan, J.L. Mozos, G. Taraschi, J. Wang, and H. Guo. *Appl. Phys. Lett.*, 71:419, 1997.

[21] W. Tian, S. Datta, S. Hong, R. Reifenberger, J.I. Henderson, and C.P. Kubiak. *J. Chem. Phys.*, 109:2874, 1998.

[22] J.K. Gimzewski and C. Joachim. *Science*, 283:1683, 1999.

[23] J.L. Mozos, C.C. Wan, G. Taraschi, J. Wang, and H. Guo. *Phys. Rev. B*, 56:4351, 1997.

[24] S.J. Tans, J. Verschueren, R.M. Alwin, and C. Dekker. *Nature*, 393:49, 1998.

[25] R. Martel, T. Schmidt, H.R. Shea, T. Hertel, and P. Avouris. *Appl. Phys. Lett.*, 73:2447, 1998.

[26] C. Joachim, J.K. Gimzewski, and H. Tang. *Phys. Rev. B*, 58:16407, 1998.

[27] C. Joachim and J.K. Gimzewski. *Proc. of the IEEE*, 86:184, 1998.

[28] N.G. van Kampen. *Stochastic Processes in Physics and Chemistry.* North-Holland, Amesterdam, 1981.

[29] V.M. Gasparian, T. Christen, and M. Büttiker. *Phys. Rev. A*, 54:4022, 1996.

[30] P. Mohanty, E.M.Q. Jariwala, and R.A. Webb. *Phys. Rev. Lett.*, 78:3366, 1997.

[31] P. Mohanty, E.M.Q. Jariwala, and R.A. Webb. *Phys. Rev. B*, 55:13452, 1997.

[32] T. Ando, A.B. Fowler, and F. Stern. *Rev. of Mod. Phys.*, 54:437, 1982.

[33] J.J. Harris, J.A. Pals, and R. Woltjer. *Rep. Prog. Phys.*, 52:1217, 1989.

[34] B.J. van Wees, H. van Houten, C.W.J. Beenakker, J.G. Williamson, L.P. Kouwenhoven, D. van der Marel, and C.T. Foxon. *Phys. Rev. Lett.*, 60:848, 1988.

[35] B.L. Altshuler. *JETP Lett.*, 41:648, 1985.

[36] B.L. Altshuler and D.E. Khmel'nitskii. *JETP Lett.*, 42:359, 1986.

[37] P.A. Lee and A.D. Stone. *Phys. Rev. Lett.*, 55:1622, 1985.

[38] P.A. Lee and A.D. Stone. *Phys. Rev. B*, 35:1039, 1987.

[39] R. Landauer. *IBM J. Res.. Dev.*, 1:223, 1957.

[40] R. Landauer. *Philosophical Magazine B*, 31:863, 1970.

[41] M. Büttiker, Y. Imry, R. Landauer, and S. Pinhas. *Phys. Rev. B*, 31:6207, 1985.

[42] M. Büttiker. *Phys. Rev. Lett.*, 57:1761, 1986.

[43] N. Zhu. *Conductance Fluctuations in Nanostructures.* PhD thesis, McGill University, 1997.

[44] G. Kirczenow, A.S. Sachrajda, Y. Feng, R.P. Taylor, J. Henning, L. Wang, P. Zawadski, and P.T. Coleridge. *Phys. Rev. Lett*, 78:1952, 1997.

[45] C. Gould, A.S. Sachrajda, Y. Feng, A. Delage, K. Kelly P.J., Leung, and P.T. Coleridge. *Phys. Rev. B*, 51:11213, 1995.

[46] Y. Takagaki. *Phys. Rev. B*, 55:16021, 1997.

[47] S. Washburn, C.P. Umbach, R.B. Laibowitz, and R.A. Webb. *Phys. Rev. B*, 32:4749, 1985.

[48] A.D. Stone. *Phys. Rev. Lett.*, 54:2692, 1985.

[49] C.P. Umbach, S. Washburn, R.B. Laibowitz, and R.A. Webb. *Phys. Rev. B*, 30:4048, 1984.

[50] R.A. Webb, S. Washburn, and C.P. Umbach. *Phys. Rev. B*, 37:8455, 1988.

[51] R.A. Webb, S. Washburn, R.B. Laibowitz, and C.P. Umbach. *Phys. Rev. Lett.*, 54:2696, 1985.

[52] J. Licini, D.J. Bishop, M.A. Kaster, and A. Harstein. *Phys. Rev. Lett.*, 56:2403, 1986.

[53] D.E. Beutler, L. Meisenheimer, and N. Giordano. *Phys. Rev. Lett.*, 58:1240, 1987.

[54] R. Harris and A. Houari. *Philosophical Magazine B*, 65:1131, 1992.

[55] R. Harris and A. Houari. *Phys. Rev. B*, 41:5487, 1990.

[56] R. Harris and A. Houari. *Phys. Rev. B*, 42:7266, 1990.

[57] J. Rammer. *Rev. Mod. Phys.*, 63:781, 1991.

[58] Z. Ma, J. Wang, and H. Guo. *Phys. Rev. Lett*, 82:398, 1999.

[59] O. Yevtusshenko, G. Lütjering, D. Weiss, and K. Richter. *Phys. Rev. Lett.*, 84:542, 2000.

[60] Y. Aharonov and D. Bohm. *Phys. Rev.*, 115:485, 1959.

[61] A.D. Stone. *Phys. Rev. Lett.*, 54:2692, 1985.

[62] A.A. Farajian, K. Esfarjani, and Y. Kawazoe. *Phys. Rev. Lett.*, 82:5084, 1999.

[63] H. Pastawski. *Phys. Rev. B*, 46:4053, 1992.

[64] M. Büttiker. *J. Phys. Condens. Matter*, 5:9361, 1993.

[65] M. Büttiker, A. Pretre, and H. Thomas. *Z. Phys. B*, 94:133, 1994.

[66] M. Büttiker, A. Pretre, and H. Thomas. *Phys. Rev. Lett.*, 70:4114, 1993.

[67] W. Chen, T.P. Smith, M. Büttiker, and M. Shayegan. *Phys. Rev. Lett.*, 73:146, 1994.

[68] J. Wang and H. Guo. *Phys. Rev. B*, 54:11090, 1996.

[69] T. Christen and M. Büttiker. *Euro. Phys. Lett.*, 35:523, 1996.

[70] T. Christen and M. Büttiker. *Phys. Rev. Lett.*, 77:143, 1996.

[71] M. Büttiker, A. Pretre, and H. Thomas. *Phys. Lett. A*, 180:364, 1993.

[72] J. Taylor. PhD thesis, McGill University, 2000.

[73] M. Büttiker. *Phys. Rev. B*, 46:12485, 1992.

[74] T. De Jesus, H. Guo, and J. Wang. *Phys. Rev. B*, 62:10774, 2000.

[75] C.C. Wan, T De Jesus, and H. Guo. *Phys. Rev. B*, 57:11907, 1998.

[76] J. Wang, Q. Zheng, and H. Guo. *Phys. Rev. B*, 55:9763, 1997.

[77] J. Wang, Q. Zheng, and H. Guo. *Phys. Rev. B*, 55:9763, 1997.

[78] P.G.N. de Vegvar. *Phys. Rev. Lett.*, 70:837, 1993.

[79] J.B. Pieper and J.C. Price. *Phys. Rev. Lett.*, 72:3586, 1994.

[80] C. Bruder and H. Schoeller. *Phys. Rev. Lett.*, 72:1076, 1994.

[81] C. Roland, M.B. Nardelli, J. Wang, and H. Guo. *Phys. Rev. Lett.*, 84:2921, 2000.

[82] Z. Ma, J. Wang, and H. Guo. *Phys. Rev. B*, 57:9108, 1998.

[83] Q. Zheng. *Weakly Nonlinear and Low Frequency Quantum Transport in Mesoscopic Systems.* PhD thesis, University of Hong Kong, 1998.

[84] C.C. Wan. *Unpublished*, 1998.

[85] P. Pomorski, H. Guo, and R. Harris. *Phys. Rev. B*, 58:15393, 1998.

[86] D. Pines and P. Nozieres. *The Theory of Quantum Liquids.* Addison-Wesley, New York, 1989.

[87] J. Wang, H. Guo, J.L. Mozos, C.C. Wan, G. Taraschi, and Q. Zheng. *Phys. Rev. Lett.*, 80:4277, 1998.

[88] C.C. Wan, J.L. Mozos, J. Wang, and H. Guo. *Phys. Rev. B*, 55:13393, 1997.

[89] P.A. Lee and D.S. Fisher. *Phys. Rev. B*, 23:6851, 1981.

[90] M.K. Yip, J. Wang, and H. Guo. *Z. Physik B*, 104:463, 1997.

[91] C.P. Collier and *et.al. science*, 289:1172, 2000.

[92] C.P. Collier and *et.al. science*, 285:391, 1999.

[93] J. Chen, M.A. Reed, and A.M. Rawlett. *Science*, 286:1550, 1999.

[94] C. Joachim, J.K. Gimzewski, R.R. Chlitter, and C. Chavy. *Phys. Rev. Lett.*, 74:2102, 1995.

[95] T. Rueckes and *et.al. Science*, 28:94, 2000.

[96] J.W.G. Wildoeer, L.C. Venema, and A.G. Rinzler. *Nature*, 391:59, 1998.

[97] Y. Xue, S. Datta, S. Hong, R. Reifenberger, J.I. Henderson, and C.P. Kubiak. *Phys. Rev. B*, 59:7852, 1999.

[98] Y. Imry. *Europhys. Lett.*, 1:249, 1986.

[99] V.A. Gopar, P. Mello, and M. Büttiker. *Phys. Rev. Lett*, 77:3005, 1996.

[100] Y.V. Fyodorov and H.J. Sommers. *Phys. Rev. Lett*, 76:4709, 1996.

[101] A.M. Jayannavar, G.Y. Vijayagovindan, and N. Kumar. *B. Condens. Matter*, 75:77, 1989.

[102] C. Texier and A. Comtet. *Phys. Rev. Lett.*, 82:4220, 1999.

[103] Y.V. Fyodorov. *Phys. Rev. B*, 61:2444, 2000.

[104] P.W. Brouwder and M. Büttiker. *Euro. Phys. Lett.*, 37:441, 1997.

[105] M. Lei, N. Zhu, and H. Guo. *Phys. Rev. B*, 52:16784, 1995.

[106] R.P. Taylor, R. Newbury, A.S. Sachrajda, Y. Feng, P.T. Coleridge, P.J. Delage, A. Kelly, Z. Wasilewski, N. Zhu, H. Guo, and C. Dettmann. *Phys. Rev. Lett*, 78:1952, 1997.

[107] G. Kirczenow, B.L. Johnson, B.L. Kelly, C. Gould, A.S. Sachrajda, Y. Feng, and A. Delage. *Phys. Rev. B*, 56:7503, 1997.

[108] N. Zhu, H. Guo, and R. Harris. *Phys. Rev. Lett.*, 77:1825, 1996.

[109] K.M. Schep, P.J. Kelly, and G.E.W. Bauer. *Phys. Rev. Lett.*, 74:586, 1995.

[110] J. Barnas and Y. Bruynseraede. *Phys. Rev. B*, 53:5449, 1996.

[111] L. Sheng, Y. Chen, H.Y. Teng, and C.S. Ting. *Phys. Rev. B*, 59:480, 1999.

[112] I. Malajovich, J.M. Kikkawa, D.D. Awschalom, J.J. Berry, and N. Samarth. *Phys. Rev. Lett.*, 84:1015, 2000.

[113] D. Weiss, M.L. Roukes, A. Menschig, P. Grambow, K. von Klitzing, and G. Weimann. *Phys. Rev. Lett*, 66:2790, 1991.

[114] D. Weiss, K. Richter, A. Menschig, R. Bergmann, H. Schweizer, and K. von Klitzing. *Phys. Rev. Lett*, 70:4118, 1993.